UNIVERSITY OF SOUTHAMPTON

FACULTY OF SOCIAL, HUMAN AND MATHEMATICAL SCIENCES

Mathematical Sciences

Hairy black holes, solitons and multi-oscillators

by

Ramon Masachs

May 2019

UNIVERSITY OF SOUTHAMPTON

ABSTRACT

FACULTY OF SOCIAL, HUMAN AND MATHEMATICAL SCIENCES

Mathematical Sciences

HAIRY BLACK HOLES, SOLITONS AND MULTI-OSCILLATORS

by Ramon Masachs

This thesis is centered in the study of new solutions to Einstein's equations. A common property of all new solutions presented in this thesis is that they have a scalar field condensate, independently of having a horizon or not. A key motivation for studying such cases is given by the gauge/gravity duality hence our starting point will be asymptotically AdS spacetimes. However, we will apply some of the intuition gained from this context to asymptotically flat spacetimes. Within this context, there are two main different parts in this thesis:

- The study of linear instabilities of charged black holes and the construction of the endpoint of the instabilities: hairy black holes. Firstly, one considers the linear problem of scalar field perturbations in order to characterise the unstable region as well as determining the onset of the instability. This onset is given by a zero-mode perturbation, hence it is regular in the past and future horizons. This zero-mode signals the possible existence of a new solution. Secondly, we solve the non-linear problem using a perturbative expansion and encounter two new solutions in the system: a soliton, which is a horizonless solution and a hairy black hole which is the endpoint of the linear instabilities. This study is performed in asymptotically AdS spacetimes and in asymptotically flat spacetimes with a box at a finite distance with Dirichlet boundary conditions for the scalar field: the *black hole bomb*.

- The study of the nonlinear instability of AdS. We present new results in the charactersation of the islands of stability of AdS. In particular we study the dependence of the nonlinear instability on the commensurability of the frequency spectrum of the theory by introducing a double trace deformation in AdS. We study these islands of stability by determining the region of existence of multi-oscillators. In addition, we use the construction as intuition to postulate the existence in asymptotically flat spacetimes of an infinite-parameter family of solutions that oscillate on any number of non-commensurate frequencies. A particular solution within this infinite-parameter family is the well-known boson star solution which oscillates in one frequency. We construct numerically two-frequency solutions: double-oscillators.

Table of Contents

List of Figures

Declaration of Authorship

I, Ramon Masachs, declare that the thesis entitled *Hairy black holes, solitons and multi-oscillators* and the work presented in the thesis are both my own, and have been generated by me as the result of my own original research. I confirm that:

- this work was done wholly or mainly while in candidature for a research degree at this University;
- where any part of this thesis has previously been submitted for a degree or any other qualification at this University or any other institution, this has been clearly stated;
- where I have consulted the published work of others, this is always clearly attributed;
- where I have quoted from the work of others, the source is always given. With the exception of such quotations, this thesis is entirely my own work;
- I have acknowledged all main sources of help;
- where the thesis is based on work done by myself jointly with others, I have made clear exactly what was done by others and what I have contributed myself;
- parts of this work have been published as:
  - O. J. C. Dias and R. Masachs, *Hairy black holes and the endpoint of AdS_4 charged superradiance*, `1610.03496`
  - O. J. C. Dias and R. Masachs, *Charged black hole bombs in a Minkowski cavity*, `1801.10176`
  - O. J. C. Dias and R. Masachs, *Evading no-hair theorems: hairy black holes in a Minkowski box*, `1802.01603`
  - M. Choptuik, R. Masachs and B. Way, *Multi-oscillating Boson Stars*, `1904.02168`

Signed: .....

Date: .....

Acknowledgements

First I want to thank Oscar Dias for the constant support, patience, insight and guidance over the almost four years he has been my thesis supervisor. He gave me the opportunity to enter this thesis program despite my unusual background as a civil engineer. I hope I have honoured that confidence.

I also thank Kostas Skenderis and Marika Taylor who have always been willing and helpful. Their vast knowledge was always a motivation and an inspiration. Marika together with Ian Hawke supervised my annual progress each of the first three years. I thank them for their comments and orientation.

At the beginning of my third year I visited the Universidad de Santiago de Compostela. I am in debt to Javier Mas who was incredibly welcoming and who introduced me to the field of time evolutions. I want to thank his student Anxo for his helpful discussions. I also met Anibal, Daniele, Alfonso and Jose who were all supportive and with whom I had pleasant physics discussions.

I would like to thank Benson Way and Matthew Choptuik for giving me the opportunity to visit them at the University of British Columbia. The time I spent there was a very pleasant and productive time. I will always remember spending Thanksgiving at Matthew's. Benson is a master of spectral methods and was incredibly patient teaching me some of his knowledge. Thanks also to Michael and Graham for their help. The string theory group welcomed me to their journal club lunch and seminars that proved to be very interesting.

I would not have started this thesis without the earlier advice and guidance from the people in Barcelona where I began my studies in physics. I learned a lot from Jorge Russo as well as from David, Roberto, Tomeu and Francesc.

Thanks to all the friends and colleagues I met at the University of Southampton. I owe to you a big part of the wonderful experience I had in Southampton. The officemates I had with whom I discussed about everything and also about physics, Stefanos, Aaron, George and Fabian. Also thanks to Ariana, William W., Stas, Elliott, Federico, Paul, Linus, Will C., Alice, Emma, Kostas as well as Gavin, Olga, Francesco, Marco, David and Andy.

We arrived together to Southampton from Barcelona with Joan Garcia. We shared office the first year as well as flat the first two years. Sens dubte la teva amistat ha amenitzat els llargs i humits hiverns anglesos. Desitjo que aquests sentiments hagin estat mutus. Crec que ho haurem aconseguit.

Thanks to my family for their love from the distance, it felt like the strong interaction. Thanks Olga for your love, la distància ha estat dura però crec que ens ha enfortit.

A la memòria de l'avi.

Part I

Introduction

This thesis is centered on the study of general relativity with a timelike boundary which is provided either by the asymptotic behaviour (AdS) or by the presence of a hard box. The main motivation to study such systems is given by the gauge/gravity duality. In this Introduction Part we first give an overview of some important aspects of the duality that help put into context the results in this thesis in Chapter 1.

In Chapter 2 we introduce the specific phenomenological aspects we study related to black hole and spacetime instabilities: superradiance in section 2.1, near-horizon condensation instability in section 2.2, nonlinear instability in section 2.3 and in section we discuss about hairy black holes 2.4 which are the end point of instabilities. Finally, in section 2.5 we give an outline of the thesis.

CHAPTER 1

The holographic principle and gauge/gravity duality

The holographic principle was first proposed by Gerard 't Hooft [5] and later refined into string theory by Leonard Susskind [6] (also see Thorn [7] and Susskind-Klebanov [8]). The idea of the holographic principle arose from the works of Bekenstein [9] and Hawking [10] and the observation that black holes are thermodynamic objects that radiate at temperature proportional to the surface gravity at the horizon and they have an entropy that is proportional to the area of the horizon

$$S_{BH} = \frac{A_H}{4} \tag{1.0.1}$$

in Planck units. Indeed, consider a volume V with surface area A and entropy larger than the black hole entropy of the same area. Assume that the energy inside the volume is smaller than the black hole energy (otherwise gravitational collapse would form a black hole). Add energy into the volume so that the energy density reaches the value at which a black hole would form. Due to our assumption, this final configuration has less entropy than the starting one since $S > S_{BH}$. But this violates the second law of thermodynamics and hence 't Hooft assumed that a black hole is the configuration with the highest entropy per unit volume in a gravitational system. Since in statistical mechanics entropy is a counting of the degrees of freedom of the system, one arrives to the conclusion that in a gravitational system the degrees of freedom are proportional to the area. This is in contrast with local quantum field theory (with a UV cutoff at the Planck scale) where the number of degrees of freedom is proportional to the volume. Since in a d-dimensional spacetime

$[A] = L^{d-2}$ and $[V] = L^{d-1}$, the counting of degrees of freedom suggests that a theory of gravity in d dimensions (bulk) should be dual to a quantum field theory in $d-1$ dimensions ("living" at the boundary). This is the holographic principle.

This idea was put into firm footing when Maldacena in 1997 [11] published the famous paper *The Large N limit of superconformal field theories and supergravity* where he conjectured the first specific example of the holographic principle. His proposal conjectured the equivalence between 10-dimensional Type IIB string theory in $\mathrm{AdS}_5 \times \mathrm{S}^5$ and $\mathcal{N} = 4$ Super Yang-Mills (SYM) in 4 dimensions with gauge group $SU(N)$, which is a conformal field theory (CFT).

The two theories are equivalent for any rank of the gauge group N and Yang-Mills coupling g_{YM} and the equivalence is at the level of partition functions of the two theories [12, 13]

$$Z_{QFT} = Z_{string}. \tag{1.0.2}$$

We will come back to this relation when we describe the dictionary of the duality.

This is the strongest form of the duality. By taking limits to the different parameters one can arrive to more tractable forms where we can treat string theory perturbatively or even consider its low energy limit, supergravity; or where the gauge theory becomes perturbative. Let us first identify the fundamental constants present on both sides and identify a correspondence between them. On the quantum field theory side there is the rank of the gauge group N and the coupling constant g_{YM}. It is however more convenient to work with the rank of the gauge group N and the 't Hooft coupling $\lambda = g_{YM}^2 N$. On the gravity side there is the string coupling g_s, the AdS radius L and the string length l_s. Notice that the last two are dimensionful constants hence, one can construct two adimensional constants that characterize the theory in the bulk. Let us point out without explicitly showing, that the radius of the S^5 in the bulk is precisely given by the AdS radius L [11].

The correspondence, we will see in the following sections, establishes that physical quantities on both sides of the duality can be identified. It is thus crucial to find first an identification between the parameteres of both sides. These identifications will constitute the first main ingredients of the holographic dictionary that we will further discuss in the following sections. The relation between the parameters on both sides is:

$$g_s = \frac{1}{4\pi}\frac{\lambda}{N}, \qquad \lambda = \left(\frac{L}{l_s}\right)^4. \tag{1.0.3}$$

Notice that one could also use Newton's constant as a parameter in the bulk through the

relation

$$G = 8\pi^6 g_s^2 l_s^8. \tag{1.0.4}$$

Taking limits on the parameters one can achieve limits of the correspondence where the theories become perturbative and thus more tractable. Indeed, the correspondence is a strong-weak duality, hence achieving a perturbative limit of the theory on one side implies that the theory on the other side is strongly coupled. Indeed, take the large N limit while holding λ fixed. In this case, by the first equality in equation (1.0.3), the string coupling becomes perturbative as $g_s \to 0$. The theory in the bulk is perturbative string theory. One can go even further by then taking the large λ limit, i. e. $\lambda \to \infty$ in the second equality in equation (1.0.3). Then the bulk theory becomes supergravity, since this implies that the AdS radius is much larger than the string length $L \gg l_s$. Notice that this limit works the other way as well. Take the perturbative limit in the quantum field theory side, $\lambda \to 0$. The string length becomes large compared to the AdS radius and thus the bulk is described by string theory and not just supergravity.

After this example, others have been established from different compactifications of string theory such as D1-D5 system and ABJM [11, 14]. These dualities have been obtained following the route known as top-down construction. Top-down models are obtained from low-energy dynamics of brane configurations of string theory or M-theory. It provides with a specific holographic duality where, in principle, one knows the field content both in the string theory and gauge theory sides. However, it is quite an involved procedure and one has little flexibility.

Alternatively one can follow a bottom-up approach. It makes use of the broad concept of holography. One postulates an asymptotically locally AdS spacetime (AlAdS) with a set of fields which are dual to a set of operators in the field theory. In this case the dual theory is not known, but only its operator content, and one studies properties expected to hold generally in strongly coupled quantum field theories[1]. Typically, it has been used to gain insight into QCD and in particular to the quark-gluon plasma that is produced in experiments at CERN [17]. It is also the general approach used within the gauge/gravity duality applied to condensed matter [18, 19]. This approach makes use of the AdS/CFT dictionary which is a map relating the quantum field theory operators and symmetries to the supergravity fields. Within the bottom-up approach one can also follow the inverse path. One can postulate operators or correlation functions of general quantum field theories and infer behaviours of the quantum gravity systems. This path has been followed in particular for the study of inflation in cosmological models [20, 21].

[1] This is for example the case for the celebrated shear viscosity to entropy ratio [15, 16].

Gauge/gravity correspondence is most understood between asymptotically AdS spacetimes and quantum field theories that flow to a UV fixed point (CFT). This thesis is motivated by this duality but only discusses the gravity side. Thus in the following we will introduce the concepts of asymptotically AdS spacetimes as well as the holographic dictionary. The aim is not to give an exhaustive nor a complete review. There are in the literature numerous publications reviewing these topics (e.g. [22, 17]).

1.1 Asymptotically AdS spacetimes

The gauge/gravity duality is the main motivation why one studies general relativity in asymptotically AdS spacetimes. In addition, the gravitational phenomenology is much richer in AdS spacetimes, as the existence of a timelike boundary allows for fields to scatter-off infinity leading to new solutions that in asymptotically flat or de Sitter spacetimes do not exist. It is thus a good laboratory to study properties of gravity.

AdS is a maximally symmetric solution to Einstein's equations with negative cosmological constant [2]. It solves the equation[3]

$$R_{\mu\nu} - \frac{1}{2}\left(R - 2\Lambda\right) g_{\mu\nu} = 0. \tag{1.1.1}$$

The metric of global AdS is given by

$$\mathrm{d}s^2 = -\left(1 + \frac{r^2}{L^2}\right)\mathrm{d}t^2 + \frac{\mathrm{d}r^2}{1 + \frac{r^2}{L^2}} + r^2\mathrm{d}\Omega_{d-2}^2, \tag{1.1.2}$$

where L is the AdS radius and $\Lambda = \frac{(d-2)(d-1)}{2L^2}$ is the cosmological constant, and $\mathrm{d}\Omega_{d-2}^2$ is the metric of the sphere S^{d-2}. One can compactify the radial direction by introducing the change of coordinate $r = L\tan^2 x$ and $t = L\tau$, and the metric becomes

$$\mathrm{d}s^2 = \frac{L^2}{\cos^2 x}\left(-\mathrm{d}\tau^2 + \mathrm{d}x^2 + \sin^2 x\mathrm{d}\Omega_{d-2}^2\right), \tag{1.1.3}$$

where $x \in [0, \pi/2)$. In these coordinates we can see that there is a second order pole at $x = \pi/2$.

This leads to the definition of a conformally compact metric: Given a manifold with boundary $\bar{M}$, the boundary given by ∂M and the interior by M; a metric g_{ab}, like for example (1.1.3), is conformally compact if it has a second order pole in ∂M and there exists a function r, called defining function, such that the metric $\hat{g}_{ab} = r^2 g_{ab}$ extends

[2] A spacetime is maximally symmetric if and only if it has the maximum number of Killing vector fields given by $\frac{d(d+1)}{2}$ in d dimensions.

[3] In this section we follow closely [23, 24, 25].

smoothly to ∂M and is non-degenerate. The defining function r is such that it is positive in M, it has a first order pole in ∂M and $\mathrm{d}r \neq 0$ in ∂M.

In fact, the metric g_{ab} only defines a conformal class of metrics in ∂M since for a given defining function r, any function re^{ω}, with ω a function with no zeros or poles, is also a defining function extending the metric g_{ab} to ∂M.

We are now ready to define asymptotically locally AdS spacetimes. We say that a manifold M equipped with metric g_{ab} is AlAdS if

- (M, g_{ab}) is conformally compact,
- g_{ab} satisfies Einstein's equations with a negative cosmological constant.

In order to compute charges and apply the AdS/CFT dictionary it is useful to introduce a new set of coordinates known as Fefferman-Graham coordinates. We introduce the new coordinates z, τ defined as $r = \frac{L\left(z^2-1\right)}{2z}$ and $\tau = Lt$. Then the AdS metric (1.1.2) becomes

$$\mathrm{d}s^2 = \frac{L^2}{z^2}\left(\mathrm{d}z^2 + \frac{\left(-\mathrm{d}\tau^2 + \mathrm{d}\Omega_{d-2}^2\right)}{4} - \frac{z^2}{2}\left(\mathrm{d}\tau^2 + \mathrm{d}\Omega_{d-2}^2\right)\right). \tag{1.1.4}$$

In this coordinate system the boundary is at $z = 0$. The structure of this metric is of the form

$$\mathrm{d}s^2 = \frac{L^2}{z^2}\left(\mathrm{d}z^2 + g_{ij}\mathrm{d}x^i\mathrm{d}x^j\right) \tag{1.1.5}$$

where x^i refers to any coordinate but z.

Any AlAdS metric can always be brought, near the boundary, to the form (1.1.5) with

$$g = g_{(0)} + zg_{(1)} + z^{d-1}g_{(d-1)} + \cdots + z^{d-1}h_{(d-1)}\log z^2 + \ldots \tag{1.1.6}$$

For even d the $h_{(d)}$ term vanishes. We will come back to this form of the metric in section 1.2.

In this thesis we have worked with asymptotically global AdS spacetimes in Chapters 4 and 5 where we have used metric ansatz that asymptote to (1.1.2) and also in Chapter 9 where we have made use of the coordinate system (1.1.3).

1.2 Holographic dictionary

According to the gauge/gravity correspondence, both the QFT side and the gravity side describe the same physics. Consequently, both theories should have some identification between their symmetries and degrees of freedom as well as their dynamics. We present here some of these identifications that constitute a subset of the dictionary identifying the correspondence.

1.2.1 Symmetries

The isometry group of AdS spacetime is $SO(d-1,2)$. This is more easily seen by the embedding of AdS in d dimensions to $\mathbb{R}^{d-1,2}$. The result is a hyperboloid satisfying the constraint[4]:

$$-X_0^2 + X_1^2 + \cdots + X_{d-1}^2 - X_d^2 = -L^2. \tag{1.2.1}$$

The group $SO(d-1,2)$ is isomorphic to the conformal group in $(d-2,1)$ dimensions. It is also common within the correspondence to work in the Poincaré patch of AdS. In that case, rather than asymptotically having a sphere, one has a plane and the dual quantum field theory lives in $\mathbb{R}^{d-2,1}$. In such case the metric of AdS can be written as

$$\mathrm{d}s^2 = -\frac{r^2}{L^2}\mathrm{d}t^2 + \frac{L^2}{r^2}\mathrm{d}r^2 + \frac{r^2}{L^2}\mathrm{d}\vec{x}^2. \tag{1.2.2}$$

The conformal metric at the boundary is then that of $\mathbb{R}^{d-2,1}$, and we have identified the isometries of the CFT and those of the normal directions to the radial direction in AdS. This brings us naturally to the meaning of this radial direction r.

Among the global symmetries in AdS, there is in particular a scaling symmetry whereby one can make the transformation $t \to \lambda t$ and $r \to r/\lambda$ and $\vec{x} \to \lambda\vec{x}$ in (1.2.2) or $t \to \lambda t$ and $z \to \lambda z$ in (1.1.5) and the metric remains unchanged. This symmetry is to be compared with the same scaling symmetry in the CFT. One can redefine $x^\mu \to \lambda x^\mu$ with $x^\mu = (t, \vec{x})$. This induces a rescaling of the energy as $E \to E/\lambda$. This establishes the correspondence as a UV/IR duality. Indeed, large energies in the field theory correspond to small z distances in the bulk, or equivalently large distances r in the bulk. This is a geometrization in the bulk side of the renormalization group (RG) flow in the field theory . This has led to the

[4] In order to recover the AdS metric (1.1.2) we can use the transformation $X_0 = L\cosh\rho\cos\tau$ and $X_{d-1} = L\cosh\rho\sin\tau$; $r = \sinh\rho$ and $\tau = t/L$ while choosing some polar transformation for the other $X_i = rx_i$ such that the x_i parametrise the sphere.

identification

$$E \leftrightarrow 1/z. \tag{1.2.3}$$

This is deeper than just a mere identification for it also establishes the correspondence as a UV/IR duality. Indeed, large energies in the field theory correspond to small z distances in the bulk, or equivalently large distances r in the bulk.

1.2.2 Field identifications

As commented around (1.1.5) one can always write the asymptotic behaviour of the metric field in the Fefferman-Graham form (1.1.5)-(1.1.6). The independent fall-offs of the expansion are $g_{(0)}$ and $g_{(d-1)}$. All the terms $g_{(i)}$ with $i < d-1$ can be determined via a Frobenius analysis at the boundary of the equations of motion as a function of $g_{(0)}$ whereas the terms with $i > d-1$ by both $g_{(0)}$ and $g_{(d-1)}$.

Both $g_{(0)}$ and $g_{(d-1)}$ have a dual field theory meaning. As implicitly explained in the discussion about the global symmetries after (1.2.1), $g_{(0)}$ corresponds to the induced metric in the field theory side. From the $g_{(d-1)}$ term one can read off the 1-point function of the stress energy tensor in the field theory [26, 27, 28]. In addition, in odd dimensions the Fefferman-Graham expansion has the logarithmic term $h_{(d-1)}$ in (1.1.5). This term gives the anomaly present in even dimensions in the computation of the 1-point function in the field theory side [29].

In the bottom-up approach the minimum ingredients one considers in the bulk Lagrangian are

$$S = \int \mathrm{d}^d x \sqrt{g} \left(R - 2\Lambda\right), \tag{1.2.4}$$

which is also a consistent truncation of supergravity in a top-down approach. This action only contains gravity fields. We can also have matter fields. In this thesis we have worked with scalar fields and gauge fields in asymptotically AdS spacetimes and with a bottom-up approach. We have added the terms

$$S = \int \mathrm{d}^d x \sqrt{g} \left(-\frac{1}{2} F_{\mu\nu} F^{\mu\nu} - 2 D_\mu \phi (D^\mu \phi)^\dagger + m|\phi|^2\right), \tag{1.2.5}$$

where $F = dA$ with A being a gauge potential, $D_\mu \phi = \nabla_\mu \phi - iqA_\mu \phi$ is the associated gauge covariant derivative and m is the mass of the charged scalar field ϕ.

The scalar field has two independent fall-offs $\Delta_\pm$ at the boundary. In the Fefferman-

Graham expansion the asymptotic expression for the scalar field is

$$\phi(x,z)|_{z\to 0} = z^{\Delta_-}\left(\phi_{(0)}(x)+\mathcal{O}(z)\right)+z^{\Delta_+}\left(\phi_{(d-1)}(x)+\mathcal{O}(z)\right). \tag{1.2.6}$$

where $x \equiv x^\mu$ refers to all coordinates except z. $\Delta_\pm$ are given by the solutions to the equation

$$\Delta\left(\Delta(d-1)+1\right) = m^2L^2 \implies \Delta_\pm = \frac{d-1}{2} \pm \sqrt{\frac{(d-1)^2}{4}+m^2L^2}. \tag{1.2.7}$$

Scalar fields are dual to scalar operators. We identify two particular values for the decays: $\Delta_{BF} = \frac{d-1}{2}$ and $\Delta_* = \frac{d-3}{2}$. If $\Delta \geq \Delta_{BF}$ then the only normalizable decay is precisely Δ_+ which is identified with the 1-point function of the dual operator (vev) and Δ_- is identified with the source. If $\Delta_* < \Delta < \Delta_{BF}$ then both modes are normalizable and $\Delta_+ = (d-1)-\Delta_-$.

In general a Dirichlet boundary condition on the scalar consists in fixing the value of $\phi_{(0)}(x)$ whereas one would call a Neumann boundary condition fixing $\phi_{(d-1)}(x)$. Both Dirichlet and Neumann boundary conditions on the scalar field imply no flux of energy across the timelike boundary [30].

There are two particular bounds on the mass of the scalar field that have an important impact on the discussion of the asymptotic behaviour. These are the Breitenlohner-Freedman bound $m^2_{BF} = -\frac{d-1}{2L^2}$ [31, 32] and the unitary bound $m^2_* = \frac{1}{L^2} + m^2_{BF}$. Consequently we distinguish the following three different cases:

- $m^2_* < m^2$: Normalisability requires we set $\phi_{(0)}(x) = 0$. This will be the case in all AdS discussions in Part II.

- $m^2_{BF} < m^2 \leq m^2_*$: Both decays give normalisable solutions. Both Dirichlet and Neumann boundary conditions as well as mixed boundary conditions give normalisable solutions which are related to multitrace deformations of the CFT [33, 34]. The particular case of Dirichlet boundary condition is known as canonical quantisation whereas Neumann boundary conditions as alternate quantisation. We will use masses in this region in Chapter 9.

- $m^2 < m^2_{BF}$: Masses in this region cannot exist in a well-defined quantum field theory in AdS as the Euclidean on-shell action would not be finite[5].

Finally, in the action (1.2.5) we also have a gauge field. We can also write an expansion of

[5]The case $m^2 = m^2_{BF}$ has a double root and a the asymptotic expansion has logarithms. This case is not considered in this thesis. It was studied in [35, 36].

the field near the boundary as

$$A_\mu|_{z\to 0} = A_{(0),\mu} + \cdots + A_{(d-3),\mu} z^{d-3} + z^{d-3} a_{(d-3)} \log(z^2) + \dots \tag{1.2.8}$$

with no A_z component. In the gauge/gravity correspondence, gauge fields in the bulk give rise to global symmetries in the boundary field theory. In the particular cases we have considered, the gauge field in the bulk is a $U(1)$ gauge field leading to a global $U(1)$ symmetry in the boundary. Fields, such as the scalar field, that are charged under the local $U(1)$ in the bulk are charged under the global symmetry in the QFT side. The term $A_{(d-3)}$ gives the 1-point function of the current of the global symmetry whereas the leading term of the expansion (1.2.8), $A_{(0)}$ corresponds to a source for the current. Throughout the thesis we have worked in spherical symmetry and we have taken a gauge for the gauge field such that $A_\mu \mathrm{d}x^\mu = A_t \mathrm{d}t$. In this case the expansion (1.2.8) becomes

$$A_t|_{z\to 0} = \mu + \cdots + J_t z^{d-3} + \dots \tag{1.2.9}$$

where μ is the chemical potential and J_t the electric flux which is proportional to the electric charge, and the log terms appear as in the metric analysis.

Until now we have analysed the asymptotic behaviour of the fields that will be treated in this thesis (1.2.4)-(1.2.5) and their corresponding dual interpretation. The typical equations of motion obtained from the action are second order differential equations (see (3.0.6) and (3.0.7)). Consequently, boundary conditions at the conformal boundary are not enough to uniquely solve the equations of motion. Additionally, one has to include some boundary conditions in the interior of the spacetime, also referred to as the IR. In the interior region of the spacetime one always requires regularity of the fields.

When in the interior region one has a horizon one may specify different regularity boundary conditions. In Lorentzian time in QFT, one may have retarded, advanced and other types of correlators and this is explicitly seen by the insersion of the $i\varepsilon$ term in the correlators. It was first postulated in [37] that regularity at the horizon in ingoing Eddington-Finkelstein coordinates for matter fields will correspond to retarded Green's functions in the field theory. However a systematic holographic prescription to deal with the $i\varepsilon$ insertion in holography was given in [38, 39]. It computes real-time holography, inspired by the Schwinger-Keldysh formalism in quantum field theory, by patching Euclidean and Lorentzian asymptotically AdS spacetimes corresponding to imaginary time and real time in the Schwinger-Keldysh formalism, respectively [40]. In addition, it was shown in [41] for the case of scalar fields, that using this real-time holographic prescription, the study of retarded Green's functions actually corresponds to regularity at the horizon in ingoing Eddington-Finkelstein coordinates. This is the approach we will follow in Chapter 4 when we compute quasinormal modes of asymptotically AdS Reissner-Nordström black holes.

Thus the bulk partition function in (1.0.2) will be a functional of the sources. In the large N limit and large 't Hooft coupling, the partition function will become

$$Z_{string}[g_{(0)}, \phi_{(0)}, A_{(0)}, \dots] \approx e^{-S^{SUGRA}_{on-shell}[g_{(0)}, \phi_{(0)}, A_{(0)}, \dots]} \tag{1.2.10}$$

and we will use $\Phi_{(0)}$ to refer to $g_{(0)}, \phi_{(0)}, A_{(0)}, \dots$, the boundary conditions on the field. The partition function of the field theory depends on the sources and operators

$$Z_{CFT} = e^{W[f_0, \mathcal{O}]}, \tag{1.2.11}$$

where W is the generating function of connected n-point diagrams. f_0 refers generically to sources coupled to operators $\mathcal{O}$.

In order to compute n-point functions one subtracts from the action the term $\int \mathrm{d}^{d-1}x f_0 \mathcal{O}$. Then, $W = S - \int \mathrm{d}^{d-1}x f_0 \mathcal{O}$, and taking functional derivatives with respect to f_0 then setting $f_0 = 0$, gives the n-point functions:

$$\langle \mathcal{O}_1 \dots \mathcal{O}_n \rangle = (-1)^{n+1} \frac{\delta^n W}{\delta f_0(x_1) \dots \delta f_0(x_n)} \Big|_{f_0=0} \tag{1.2.12}$$

Thus the correspondence establishes that to compute n-point correlation functions in the field theory, one can use the supergravity on-shell action since:

$$S^{SUGRA}_{on-shell}[\Phi_{(0)}] \approx -W[\mathcal{O}]. \tag{1.2.13}$$

Hence we have that

$$\langle \mathcal{O}_1 \dots \mathcal{O}_n \rangle = (-1)^{n+1} \frac{\delta^n S^{SUGRA}_{on-shell}}{\delta \Phi_0(x_1) \dots \delta \Phi_0(x_n)} \Big|_{\Phi_0=0}. \tag{1.2.14}$$

1.2.3 Holographic renormalization

The previous equation (1.2.13) is a bare equality as both sides suffer from infinite divergences. The field theory typically suffers from UV type divergences whereas the gravity theory from IR divergences related to the infinite volume of AdS. This is not a striking fact since as we saw in (1.2.3) the gauge/gravity duality is a UV/IR duality. To covariantly deal with the IR divergences of the gravity side the method of holographic renormalization was developed in [27, 28, 42, 43, 24, 44].

The procedure consists in the following parts [24]:

- Asymptotic solution of the fields which has already been sketched previously in this section (in general using Fefferman-Graham gauge).

- Regularization of the action. One introduces a cutoff $\epsilon > 0$ and restricts the integration of the radial coordinate to $z \geq \epsilon$.

- Identification of ϵ divergent terms in the on-shell action that determine the counterterms.

- Inversion of the asymptotic series of the fields to express boundary counterterms as a function of bulk fields.

- Renormalized action by adding the regularized and counterterm actions and taking the limit $\epsilon \to 0$, which is finite.

In this thesis this procedure has been used to compute the 1-point function of the stress energy tensor from which one can read off the energy of the bulk solutions. Closed expressions in terms of the asymptotic expansions of the fields were given in [27, 24] for Dirichlet boundary conditions and for scalar and metric fields.

CHAPTER 2

Black holes and instabilities

In section 1.1 we saw that in asymptotically AdS spacetimes the presence of the timelike boundary has deep implications for the phenomenology of stationary solutions to Einstein's equations. Indeed, whereas different forms of uniqueness and no-hair theorems [45, 46, 47] vastly restrict the possible types of solutions to Einstein-Maxwell theory in 4-dimensional asymptotically flat spacetimes and their instabilities [48, 49, 50], in asymptotically AdS spacetimes there exist more known solutions with matter fields floating outside the horizon. The easiest way of searching for new solutions is to study stability of already known black hole solutions. In this thesis we will often use this approach so in this section we review some known facts on instabilities and associated hairy black holes.

In a linear mode study of a black hole one may encounter zero-modes that connect stable with unstable modes. These zero-modes have vanishing frequency [1]. This implies that both the future and past horizon are regular and hence a new solution may branch off. Early examples of asymptotically AdS black holes with scalar hair that branch-off from a zero-mode are the supercondutor black holes of [18, 19] and the superradiant hairy black holes of [51, 52, 53]. A linear mode analysis of black holes within the Kerr-Newman-AdS family has led to the identification of two different mechanisms that lead to the appearance of unstable modes: superradiance [54, 55] and near-horizon condensation [56]. We will review them in the following.

[1] This statement is gauge-dependent and will be made clearer later in the section

The new hairy solutions found have had an important impact within the gauge/gravity community giving rise to the study of strongly coupled condensed matter systems using holographic methods [18] coined AdS/CMT. As discussed in the previous section the aim is to obtain general properties of strongly coupled field theories usually following a bottom-up approach with only the minimal set of matter fields that contain the necessary ingredients to study the desired physics.

Going beyond the applications to the gauge gravity correspondence, AdS spacetime introduces an infinite potential on the matter fields that can reflect them back to the interior. One can thus use intuition from AdS to infer properties of systems in asymptotically flat spacetimes that also have a similar potential wall. This is the case of enclosing a scalar field inside a box in an asymptotically flat spacetime as was first envisaged by Press and Teukolsky [57], or the effect of the mass or other types of interactions for scalar fields [58, 59, 60].

Finally, unlike Minkowski and de Sitter spacetimes for which nonlinear stability has been established [61, 62], AdS spacetimes with reflecting boundary conditions have been found to allow for an arbitrary small fluctuation to lead to the formation of black holes [63]. A first numerical simulation was performed by Bizon and Rostworowski [64]. We will review this nonlinear instability and some of its properties in section 2.3, and some new results related to it in Part III.

In this Chapter we discuss linear instabilites: superradiance in section 2.1 and the near-horizon condensation in section 2.2; as well as the nonlinear instability in section 2.3. We discuss about hairy black holes that are the endpoint of the instabilities in section 2.4.

2.1 Superradiance

Superradiance is the amplification of waves during the scattering process with an absorbing object [30]. In the case of a rotating object it was shown by Zel'dovich [65] that for a monochromatic wave of frequency ω, the condition for superradiance is $0 < \omega < m_\varphi \Omega$ with m_φ the azimuthal number and Ω the angular velocity of the object. A Kerr black hole is effectively a rotating perfectly absorbing object, and as such it was shown to induce superradiance on bosonic waves as long as the condition

$$0 < \omega < m_\varphi \Omega_H \tag{2.1.1}$$

is satisfied [66, 67], with Ω_H the angular velocity at the horizon radius. In the case of black holes, the existence of an ergoregion is a crucial point for a superradiant scattering. An ergoregion is the region outside the event horizon and inside the ergosurface where

negative energy states with respect to an observer at infinity can exist. Consider the time translation Killing vector k_t which is the unique Killing vector that approaches a unit timelike vector at spatial infinity. Consider also the azimuthal Killing vector k_ϕ. Any linear combination of the two Killing vectors is also a Killing vector, hence k_t and k_ϕ are the two generators of Killing vectors of axisymmetric black hole spacetimes. The ergosurface is an infinite redshift surface defined by the locus where $g_{ab}k_t^a k_t^b = 0$. Outside the ergosruface $g_{ab}k_t^a k_t^b < 0$ and in the ergoregion $g_{ab}k_t^a k_t^b > 0$. An ergosurface always exists in a smooth stationary axisymmetric black hole spacetime. This can be shown by continuity: at the horizon of the black hole, r_+, the following condition is satisfied

$$g_{ab}\left(k_t^a + \Omega_H k_\phi^a\right)\left(k_t^b + \Omega_H k_\phi^b\right) = 0. \tag{2.1.2}$$

Since te horizon is a null 3-surface that is invariant, this also gives a definition of Ω_H. Thus at the horizon we have that $g_{ab}k_t^a k_t^b \geq 0$. Asymptotically one has $g_{ab}k_t^a k_t^b = -1$. Thus continuity implies the existence of a surface where $g_{tt} = 0$.

The existence of a superradiant scattering can be inferred from black hole thermodynamics. A Kerr black hole with angular momentum J, mass M and angular velocity Ω_H obeys the first law of black hole mechanics

$$\mathrm{d}M = T_H \mathrm{d}S + \Omega_H \mathrm{d}J \tag{2.1.3}$$

where $T_H = \frac{\kappa}{2\pi} \geq 0$ is the temperature at the horizon (κ is the surface gravity) and $S = \frac{A_H}{4}$ is the entropy which is a quarter of the horizon area. The second law of black hole mechanics establishes that in classical processes, and with matter obeying the null energy condition, the area of the horizon can only increase thus $\mathrm{d}S \geq 0$. Hence one has that

$$T_H \mathrm{d}S = \frac{\mathrm{d}M}{\omega}\left(\omega - m_\varphi \Omega_H\right) \geq 0, \tag{2.1.4}$$

where we have used $\frac{\mathrm{d}J}{\mathrm{d}M} = \frac{m_\varphi}{\omega}$ for a bosonic wave in a stationary axisymmetric spacetime. We see that when the condition for superradiance (2.1.1) is satisfied, necessarily $\mathrm{d}M \leq 0$ and the black hole loses energy. Conservation of energy implies that the reflected wave is amplified $-\mathrm{d}M \geq 0$.

In the case of Einstein-Maxwell theory, for charged static black holes a similar effect occurs when the bosonic wave being scattered is also charged. In this case the first law is

$$\mathrm{d}M = T_H \mathrm{d}S + \mu \mathrm{d}Q \tag{2.1.5}$$

with μ the electrostatic potential and Q the charge of the black hole. Equation (2.1.4)

becomes for charged black holes [2]

$$T_H \mathrm{d}S = \frac{\mathrm{d}M}{\omega}\left(\omega - q\mu\right) \geq 0, \tag{2.1.6}$$

where we used $\frac{\mathrm{d}Q}{\mathrm{d}M} = \frac{q}{\omega}$ for a bosonic field with charge q. The condition for superradiance in the charged case is

$$\mathrm{Re}\omega < \mathrm{q}\mu. \tag{2.1.7}$$

When the system wave-black hole is confined in a spacetime that has a timelike boundary with reflecting boundary conditions the process can occur repeatedly leading to an instability. This is the case in an asymptotic AdS black hole with specified boundary metric [68, 69, 55, 70, 30] that in the asymptotically AdS cases treated in this thesis will be the static Einstein Universe

$$\mathrm{d}s^2|_{bdry} = -\mathrm{d}t^2 + \mathrm{d}\Omega^2_{d-2}. \tag{2.1.8}$$

The timelike boundary of AdS with reflecting boundary onditions reflects back the scattered bosonic wave and the energy extraction process occurs repeatedly leading to an instability. It is also the case when confining the system in a box in an asymptotically flat spacetime. This system was first envisaged for a rotating black hole by Press and Teukolsky and was coined *black hole bomb* [57]. A further case is provided by massive fields, where the mass acts as a confining potential (although of finite height) as initially proposed in [58, 59].

Explicit mode computations of the onset of the instability as well as numerical computations of the frequencies are done in Chapter 4 for RN black holes both in asymptotically AdS and asymptotically flat backgrounds with a box.

2.2 Near-horizon condensation

In 2008, Gubser [56] showed the existence of a new mechanism that can trigger a linear instability in asymptotically AdS spacetimes involving near extremal black holes and scalar fields. This instability has been coined the near-horizon scalar condensation instability and has been a main focus of research in the AdS/CFT community as an application of this correspondence to condensed matter. As reviewed in previous section 1.2.2, in asymptotically AdS spacetimes scalar fields can be stable whilst having a negative mass [31]. There is indeed a bound on how negative this mass can be to still have a unitary

[2] Note that we can make, as we will typically do in this thesis, the gauge choice $A(r_+) = 0$ where A is the electromagnetic gauge vector. In this case the criterion for instability reads instead $\mathrm{Re}(\omega) < 0$.

theory [71]: it is the Breitenlöhner Freedman (BF) bound that establishes that theories in asymptotically AdS spacetimes with scalar fields with masses below

$$m_{BF}^2 L^2 = -\frac{(d-1)^2}{4} \tag{2.2.1}$$

do not have positive definite Euclidean action. The key heuristic observation that led to the discovery of the instability is the fact that extremal black holes develop a near horizon structure which is of the form of an $AdS_2 \times \mathcal{M}$ spacetime, with $\mathcal{M}$ a manifold that is usually S^2 for static global AdS spacetimes or $\mathbb{R}^2$ in the Poincaré patch. AdS_2 spacetimes have a bigger BF bound than higher dimensional AdS spacetimes. Hence while a scalar field can be stable in the UV (asymptotic AdS boundary) as it has a mass above the BF bound of the d-dimensional spacetime, it may be unstable in the IR (near the horizon) if the effective mass of the system as seen by a near horizon AdS_2 oberver is below its BF bound $m^2L^2 < -1/4$.

In fact, for charged scalar fields, masses above the AdS_2 bound can still lead to instabilities. In this case, it is the charge, coupling the scalar field to a $U(1)$ gauge field, that induces an effective mass which is below the AdS_2 BF bound. This is the case that will be encountered in this thesis. Whereas in discussions about the near horizon instability in sections 4.2.4 and 4.3.3 we have kept a generic mass m for the scalar field, the specific examples have considered massless scalar fields, thus they lie above the AdS_2 BF bound.

The above arguments suggesting the existence of a near horizon instability are not restricted to the original planar RN BH considered originally by Gubser. Actually, such a near horizon instability is present for any black hole system with asymptotically reflecting boundary conditions that has an extremal configuration ($T = 0$) whose near horizon is of the form $AdS_2 \times \mathcal{M}$ [19, 72, 73] [3]. It follows that such a near horizon instability should also be present in the original black hole bomb of Press and Teukolsky although it was not discussed in the original study [57] (only the superradiant instability was discussed). In section 4.3.3 we will confirm that these expectations are correct: asymptotically flat RN BHs with a cavity have the near horizon instability in addition to the superradiant one. In particular we will compute unstable modes of the system that show that the AdS_2 BF bound analysis above yields quantitative bounds that are sharp and agree with our exact numerical results.

Both superradiance and the near horizon instability are linear mode instabilities, hence they are in general intimately entangled. However, consider L either the radius of the box in the black hole bomb case or the radius of AdS. An important observation is that whereas a perturbative estimate of the superradiant frequencies can be performed for small black holes ($r_+ \ll L$), the near-horizon bound is enhanced for large black holes ($r_+ \gg L$)

[3] The Kerr geometry is not of this type but rather a fibration over AdS_2. We will not deal with this case in this thesis but the conclusions are similar as shown in [72].

and suppressed for small ones. This property is the one that best illustrates the different physical nature of the two instabilities. In this sense both constructions allow for analytic estimates in very differentiated regions of parameter space. This is best seen, in the case of the black hole bomb, in figure 4.3.2 and in figure 4.2.1 for the AdS_4 case.

2.3 Nonlinear instability

The non-globally hyperbolic structure of AdS is the key feature when determining its stability. Studying stability properties of AdS is always intrinsically related to the boundary conditions one imposes at timelike infinity. The most widely used boundary conditions for asymptotically global AdS spacetimes are motivated by holography and we have already introduced them in (1.1.4), (1.1.6) and (2.1.8). These boundary conditions have zero flux hence they prevent fields to escape from the spacetime, but rather confine them inside. This property will ultimately allow global AdS to be unstable unlike Minkowski and de Sitter where nonlinear stability has been proved [62, 61]. Howevere, arguments suggesting that global AdS should be nonlinearly unstable were presented in [63]. In 2011 Bizon and Rostworowski published a numerical study that gives strong evidence that global AdS is indeed nonlinearly unstable [64]. They showed through a numerical evolution that initial data consisting of a Gaussian distributed scalar field would always form a black hole regardless of the inital energy. In addition they showed how the time for black hole formation was related with break down of perturbation theory.

The work in [64] restricts to the spherically symmetric sector. Thus it could be reasonable to expect that the associated nonlinear instability was a fine-tuned process restricted to spherically symmetric evolutions. More generically, once we allowed spherical symmetry to be broken, the intuition would suggest that the instability might halt: centrifugal effects could balance the gravitational collapse into a black hole. However, soon after [64] it was shown that this naive intuition is not correct: the nonlinear instability is also present for gravitational perturbations which necessarily break spherical symmetry [74]. Thus nonlinear instability is expected to be present for general bosonic fields. A key ingredient for the appearance of the nonlinear instability is that the normal mode frequencies of the spacetime are *commensurable*. This occurs when given the spectrum of frequencies $\{\omega\}_{n\geq 0}$, there exist frequencies ω_{j_i} with $i = 1, 2, 3$ such that the frequency

$$\omega_J = \omega_{j_1} + \omega_{j_2} - \omega_{j_3} \tag{2.3.1}$$

also belongs to the spectrum.

Even though there is substantial numerical evidence (as well as perturbative results) that support that AdS is nonlinearly unstable, there does not exist, up to date, a rigorous

mathematical proof. Important progress was done, though, in this direction with the proof of nonlinear instability in the simpler Einstein-Vlasov system [75, 76, 77].

Despite all the evidence in favour of AdS being nonlinearly unstable, there are sets of initial data that do not lead to black hole formation [78, 79, 80, 81, 82, 83, 84, 85, 86, 87]. These sets of initial data leading to stable non-collapsing states are said to lie within the *islands of stability* [78].

It is by now unclear the frontier between collapsing and non-collapsing initial data, but evidence shows that both are of non-null measure in the set of initial data, in the sense that parametrising initial data by ε there is an interval $\varepsilon \in [0, \delta]$ with $\delta > 0$, for which one can have non-collapsing initial data [87]. A useful perturbative method to study islands of stability is the two-time formalism (TTF). It was introduced and developed in [83, 88, 89, 90]. The main idea is to introduce a new slow-time dependence $\tau = \epsilon^2 t$ and allow functions to depend both in t and τ as well as spatial coordinates. This allows for a resummation of the secular terms that would otherwise signal the break down of perturbation theory. This type of analysis is known in the mathematical numerical literature as multi-scale methods in time or homogeneisation in space dimensions.

An example of non-collapsing initial data is the one-mode initial data. In that case the resummation procedure of perturbation theory outlined in section 9.3 is enough to ensure that perturbation theory can be applied at any order leading to the constructon of a stable non-collapsing solution. These solutions are called oscillons for real-valued initial data and are periodic AAdS solutions. One can also have complex-valued solutions which lead to boson stars that are constructed in this thesis and are related to superradiance (see 5.4). From the TTF and the numerical studies [83, 88, 89, 90] it is seen that initial data leading to periodic stable solutions are non-collapsing. Small deviations seem to also be non-collapsing as there is no transmission to higher modes, but rather the evolution of the system gets restricted to the first modes in a mode expansion of the solution [85].

Another way of studying islands of stability aside from numerical time simulations and the TTF, consists in finding numerically, solutions to the equations of motion. This is the path followed in [87] with the objective of charting the islands of stability. It is also the path we follow in Chapter 9 where we will vary the boundary conditions of the scalar field at the boundary of AdS in order to study the dependence of the nonlinear instability on the commensurability of the frequency spectrum. Indeed, there seems to be enough evidence suggesting that two-mode-equal-amplitude initial data always collapses to a black hole[4]. Thus we will study scalar field asymptotically AdS double-oscillator solutions with boundary conditions that depend on a parameter κ. We will study these solutions as a function of the value of κ starting from Dirichlet boundary conditions and flowing to Neumann

[4]See Chapter 9 for details on the precise meaning of two-mode-equal-amplitude.

boundary conditions. Unsurprisingly, such double-oscillators do not exist for Dirichlet boundary conditions as this case has been deeply studied in the literature and has been found to always lead to black hole formation. As the parameter shifts away from Dirichlet boundary conditions, the region of existence of double-oscillators expands. Interestingly, we will encounter that the behaviour in the Neumann case (which also has a commensurate frequency spectrum) is different from the Dirichlet case and thus unexpected.

The construction of double-oscillators to chart islands of stability in asymptotically AdS spacetime worked as an inspiration to also find double-oscillator solutions in asymptotically flat spacetime. Indeed, in asymptotically flat spacetime there exist (as in AdS) boson stars that are compact self-gravitating objects made of a massive complex scalar field. They were first introduced by Kaub and also Ruffini and Bonazzola in the late 1960's [91, 92] (see [93] for a review.). We propose in Chapter 10 and in the publication produced [4] that boson stars are a particular single-oscillating solution among an infinite parameter family of multi-oscillating solutions. These are solutions that oscillate in a number of non-commensurable frequencies and we explicitly compute the double-oscillator family. These solutions can be found at the perturbative level from the normal modes of boson stars. Thus double-oscillators are solutions that also expand away from the perturbative regime to fully nonlinear solutions. We discuss these solutions and some of their properties in Chapter 10.

2.4 Hairy black holes

The existence of the linear instabilities of sections 2.1 and 2.2 naturally raises the question of the end-point of those instabilities. The answer depends crucially on the system one is considering.

Indeed, for the rotating case, finding the properties and endpoint of the instability requires a non-trivial (3+1)-dimensional numerical simulation not yet available. Although important progress was done in an impressive recent time evolution [94]. Valuable insights on the possible evolution can be obtained without solving the actual initial value problem. Indeed, it was found that the zero mode (i.e. onset) of the instability signals the existence of a new branch of black hole solutions with scalar hair [95, 96, 53, 97] or even gravitational hair [98]. *Per se* the existence of these hairy black holes is interesting for two main reasons: 1) it immediately rules out any attempts of proving no-hair theorems (under non-restrictive assumptions), and 2) these hairy black holes have a single Killing vector field that is also the horizon generator, thus showing that the assumptions of Hawking's rigidity theorem can be evaded [53, 98, 50]. Of relevance for the initial value problem, it turns out that, given a mass and angular momentum, these hairy black holes always

have higher entropy than the Kerr-AdS black hole. This property and the fact that they are connected to the onset of superradiance suggest that these black holes could be the endpoint of rotational superradiance. However, this is not the case because all of those constructed to date have $\Omega_H L > 1$ (where L is the AdS radius) and are thus still superradiantly unstable [53, 98, 99], this time to superradiant modes with higher azimuthal number m. This, together with other observations that can be found in the original articles, led the authors of [53, 98, 100] to conjecture that the superradiant instability might evolve into one of two possibilities: 1) the endpoint is a singular solution reached in finite time which implies cosmic censorship violation, or 2) the time evolution develops higher and higher m_φ structure (with increasing entropy) and the system never settles down. In the latter case quantum gravity effects would become relevant at some point and cosmic censorship would also be violated, at least in spirit. In either case, we would have an explicit example of cosmic censorship violation in four dimensions and in a system that can be formed by gravitational collapse. This would show that the violation found in [101, 102, 103, 104, 105] can also occur in a four-dimensional geometry. The time evolution [94] seems to be consistent with this conjectured scenario, yet it needs to be extended to even later times for stronger confirmation.

In the case of charged superradiance the problem simplifies considerably as one can have spherical symmetry and thus the numerical evolution simulation is only (1+1) dimensional [106, 107]. This can be the charged partner of Press-Teukolsky's system − a Reissner-Nordström black hole placed inside a box with a complex scalar field [108, 109, 110, 111, 112, 113, 107, 114, 115, 116, 117, 118, 119, 120, 121, 122, 123, 124]− or a Reissner-Nordström black hole in global AdS [125, 51, 126, 127, 128]. These charged systems are interesting on their own and because they can provide insights for the endpoint of the rotating superradiant instability.[5] In such cases, the endpoint of the superradiant instability is either known or we have already good hints of what it might be. Indeed, in global AdS, the time simulations of [106, 131] confirmed that the endpoint of charged superradiance is one of the hairy black holes of [51, 126, 127, 1]. Similarly, for charged superradiance on Reissner-Nordström black holes with a mirror, recent time simulations indicate that the endpoint is again a charged hairy black hole of Einstein-Maxwell theory [107, 117, 118].

For a given energy and charge, the hairy solutions of [51, 125, 126, 128] have higher entropy than the AdS_5 Reissner-Nordström black hole. Therefore, unless the phase diagram of the theory contains a solution with even higher entropy, these hairy black holes should be the endpoint of charged superradiance. Unlike the rotating case, this is a robust statement

[5] In spite of the close connection between the rotating and static-charged superradiant systems there is also a fundamental distinction. In the latter case, q is fixed once we choose the theory and thus the associated hairy black holes are not further unstable to superradiance (except if we introduce a second scalar field with charge q_2). On the other hand, the hairy black holes that emerge from the onset of the rotating superradiant instability have a particular m and are still unstable to superradiant modes with higher m [129] with timescales that can be extremely large [130].

since q is fixed once we choose the theory and thus the hairy black holes are not unstable to superradiance. This is where the charged superradiant system becomes a less interesting toy-model to discuss the endpoint of rotating superradiance.

Hairy black holes do not only appear as the endpoint of linear instabilities of black holes arising from a zero mode. Horizonless initial data may also evolve into the formation of hairy black holes. The nonlinear instability of the previous section 2.3 provides such an example: perturbing AdS with a neutral scalar field results in the formation of a Schwarzschild black hole. However a charged scalar field perturbation with initial data such that the would-be Reissner-Nordström black hole is unstable should evolve to a stable configuration that has higher entropy, thus it should naturally evolve to a hairy black hole [131]. Similarly initial data in a non-spherically symmetric configuration should evolve into black resonators and follow the same fate as the superradiant instability in the rotating case [98].

In Part II, in addition to determining the linear instabilities of Reissner-Nordström black holes, we will construct static charged hairy black holes that are the endpoint of linear and nonlinear instabilities discussed in previous sections. We will construct these black holes both in the AdS_4 and in the asymptotically flat with a box cases.

2.5 Outline of this thesis

This thesis is divided into two main Parts: Part II dedicated to the study of black hole instabilities and hairy black holes, and Part III dedicated to multi-oscillator solutions.

Part II is divided into five Chapters. In the first, Chapter 3 we introduce the theory and the action that will be studied throughout the Part. We describe the symmetries and give the equations of motion that will be solved in the following Chapters. We study the linear instabilities of charged black holes in AdS_4 and in flat spacetime with a box in Chapter 4. We give analytical bounds corresponding to superradiance and the near-horizon condensation instability for both cases. We give numerical onset curves for the instabilities in the AdS_4 case in section 4.2.5. For the case of flat spacetime with a box we provide a more detailed numerical study of the instabilities and we describe onset curves as well as frequency curves in section 4.3.4. At the end of the Chapter we describe a non-interacting model for the construction of hairy black holes that in the following Chapters we confirm gives the correct leading order thermodynamic quantities.

In the two following Chapters 5 and 6 we solve the nonlinear equations of motion presented in the setup Chapter 3 for asymptotically AdS_4 and asymptotically flat with a box spacetimes respectively. In both cases we use a perturbative expansion as well as a matched

asymptotic expansion in order to solve the equations. In addition, for the boxed case we use Israel junction conditions to relate the region inside the box with the region outside. After solving the equations order by order in a perturbative expansion we present the final thermodynamic quantities in equations (5.5.6) for AdS_4 and (6.6.8) for the boxed case. Finally we study the phase diagram of both cases in the microcanonical ensemble in sections 5.6.2 and 6.7.2 respectively. In the boxed case we also give the Israel stress energy tensor of the box.

Finally, Chapter 7, the last of this Part, gives a summary of the results obained.

Part III is divided into four Chapters. As in the previous Part, in the first Chapter 8 we introduce the theory as well as the common technical elements that will be used in the following Chapters. In Chapter 9 we use multi-oscillators to discuss the nonlinear instability of AdS_4 to scalar field perturbations with double-trace deformation boundary conditions. We study the region of existence of equal-amplitude double-oscillators starting with Dirichlet boundary conditions. Then we introduce the double-trace deformation resulting in Robin boundary conditions and finally arriving to Neumann boundary conditions. Interestingly, we find unexpected differences between the two commensurate limits of Dirichlet and Neumann boundary conditions. Thus to further study the multi-oscillating solutions in the Neumann case, we perform a time evolution simulation in section 9.5.

In Chapter 10 we find multi-oscillator solutions in asymptotically flat spacetime. In particular we consider the backreactions of the perturbations of asymptotically flat spacetimes to postulate the existence of an infinite parameter family of multi-oscillator solutions. To show this construction we compute the family of double-oscillators that merge with the lowest energy asymptotically flat boson star. We study some of the physical properties of double-oscillators and in particular we make the observation that for a given energy, double-oscillators are wider than the corresponding boson star.

Chapter 11, the last of this Part, is presents a summary and discussion of results.

This thesis also has Appendix A where we discuss some of the numerical methods that have been used to solve the projects in the thesis.

Part II

Charged superradiance and hairy black holes

In this Part we will consider both the linear and nonlinear effects of scalar field perturbations in static backgrounds. We will consider two different types of spacetimes: asymptotically AdS_4 with cosmological constant $\Lambda = -\frac{3}{L^2}$ and asymptotically flat ($\Lambda = 0$) with a box of radius L that encloses the scalar field inside it. Notice the use of L as both the radius of the box and the characteristic inverse curvature of AdS. We will see that due to scaling symmetries, in both cases, we can express all dimensionful quantities in units of L. This part is organised as follows: First in Chapter 3 we will consider the general setup that is common throughout this part. Then in Chapter 4 we will consider the linear case of non-backreacting scalar fields and find the scalar field normal and quasinormal mode spectrum. Finally in Chapters 5 and 6 we will consider the non-linear problems in asymptotically AdS_4 and $flat$ respectively and construct hairy black holes.

This part is mostly contained in the three publications [1], [2] and [3] that are co-authored with my PhD supervisor Oscar Dias.

CHAPTER 3

General setup

We consider 4-dimensional Einstein-Maxwell gravity minimally coupled to a charged complex scalar field ϕ with charge q. The associated action is

$$S = \frac{1}{16\pi G_4}\int \mathrm{d}^4x\sqrt{-g}\left[R - 2\Lambda - \frac{1}{2}F_{\mu\nu}F^{\mu\nu} - 2D_\mu\phi(D^\mu\phi)^\dagger + 2V(|\phi|)\right], \tag{3.0.1}$$

where R is the Ricci scalar, $F = dA$ with A being a gauge potential and $D_\mu\phi = \nabla_\mu\phi - iqA_\mu\phi$ is the associated gauge covariant derivative and as commented before Λ is the cosmological constant. We consider a potential $V(|\phi|) = m^2\phi\phi^*$, with m being the mass of the scalar field and fix Newton's constant as $G_4 = 1$.

We are interested in solitonic and black hole solutions of (3.0.1) that are static and spherically symmetric. We can use reparametrization of the time t and radial coordinates r, $r \to \tilde{r}(r)$ and $t \to \tilde{t} = t + H(t, r)$ to fix the gauge to be such that the radius of a round S^2 is r and there is no cross term $dtdr$ (this is often called the radial or Schwarzschild gauge)[1]. A field ansatz that accommodates the desired symmetries is

$$\mathrm{d}s^2 = -f(r)\mathrm{d}t^2 + g(r)\mathrm{d}r^2 + r^2\mathrm{d}\Omega^2_{(2)}, \qquad A_\mu\mathrm{d}x^\mu = A(r)\mathrm{d}t, \qquad \phi = \phi^\dagger = \phi(r). \tag{3.0.2}$$

where $\mathrm{d}\Omega^2_{(2)}$ describes the line element of a unit radius S^2 (parametrized by $\{\theta, \psi\}$, say or $x = \cos\theta$).

[1] In this gauge, the horizon radius r_+, if present, is also a gauge invariant quantity since it is proportional to the entropy $r_+ = \sqrt{S/4\pi}$.

Once a static solution is found we can always use a $U(1)$ gauge transformation, $\varphi \to \varphi + q\,\chi\,, A_t \to A_t + \nabla_t \chi$ to rewrite a scalar field $\phi = |\phi| e^{i\varphi}$ in a gauge where the scalar field oscillates with a frequency ω, $\phi = |\phi| e^{-i\omega t}$. However, since the energy-momentum tensor of the scalar field only depends on $\phi\phi^\dagger$ and $\partial\phi(\partial\phi)^\dagger$, the gravitational and Maxwell fields are always invariant under the action of the Killing vector field ∂_t. In this gauge, the equations of motion require that $A\big|_{r_+} = \omega/q$.

At this point we have fixed almost all the diffeomorphic and $U(1)$ gauge freedom to simplify our field ansatz. However, our systems still have two scaling symmetries that we can use for further simplifications [2]. The first scaling symmetry is

$$\begin{aligned} &\{t, r, \theta, \psi\} \to \{\lambda_1 t, \lambda_1 r, \theta, \psi\}, \quad \{f, g, A, \phi\} \to \{f, g, A, \phi\}, \\ &\{q, L, r_+\} \to \left\{ \frac{q}{\lambda_1}, \lambda_1 L, \lambda r_+ \right\}, \end{aligned} \tag{3.0.3}$$

which leaves the equations of motion invariant and rescales the line element and the gauge field 1-form as $\mathrm{d}s^2 \to \lambda_1^2 \mathrm{d}s^2$ and $A\mathrm{d}t \to \lambda_1\, A\mathrm{d}t$. We use this scaling symmetry to work with dimensionless coordinates and measure our thermodynamic quantities in units of L (this amounts to setting $L \equiv 1$). The second scaling symmetry is

$$\{t, r, \theta, \psi\} \to \{\lambda_2 t, r, \theta, \psi\}, \quad \{f, g, A, \phi\} \to \{\lambda_2^{-2} f, g, \lambda_2^{-1} A, \phi\}, \quad \{q, L, r_+\} \to \{q, L, r_+\}. \tag{3.0.4}$$

We use the scaling symmetry (3.0.4) to require that g approaches $1/f$ as $r \to \infty$, i.e. to fix $c_0 \equiv 1$. This choice can also be motivated by the following observation (see e.g. [19]). In the context of the $\mathrm{AdS}_4/\mathrm{CFT}_3$ duality, AdS_4 black holes are dual to thermal states on the boundary CFT. The choice $g = \frac{1}{f}$ as $r \to \infty$ fixes the normalization of the time coordinate with respect to the gravitational redshift normalization of the radial coordinate to be such that the Hawking temperature of the black hole in the bulk matches the temperature of the dual CFT on the boundary. Using both symmetries we will make the following redefinitions:

$$\{t, r, r_+, m, q, \omega, L\} \to \{TL, RL, R_+ L, M/L, e/L, \Omega/L, 1\}. \tag{3.0.5}$$

Variation of (3.0.1) yields the equations of motion for the fields f, g, A and ϕ:

[2] For planar AdS solutions there is a third scaling symmetry that allows to set the Poincaré horizon at $r = r_+ \equiv 1$ (see e.g. [19]). This is the reason why we can have small and large black holes in global AdS but not in planar AdS.

$$\phi''(R)+\frac{\phi'(R)}{R}\left(1-\frac{R^2A'(R)^2}{2f(R)}+g(R)(1-R^2\Lambda)\right)+\phi(R)g(R)\left(\frac{e^2A(R)^2}{f(R)}-M^2\right)=0, \tag{3.0.6a}$$

$$A''(R)+\frac{A'(R)}{R}\left(2-\frac{e^2R^2A(R)^2\phi(R)^2g(R)}{f(R)}-R^2\phi'(R)^2\right)-2e^2\phi(R)^2g(R)A(R)=0, \tag{3.0.6b}$$

$$f'(R)+\frac{f(R)}{R}\left(1-g(R)\left(1-R^2\Lambda\right)-R^2\phi'(R)^2\right)+\frac{R}{2}\left(A'(R)^2-2e^2A(R)^2\phi(R)^2g(R)\right)=0, \tag{3.0.6c}$$

$$g'(R)-\frac{g(R)}{R}\left(1+\frac{R^2A'(R)^2}{2f(R)}+R^2\phi'(R)^2\right)+\frac{g(R)^2}{R}\left(1-R^2\Lambda-\frac{e^2R^2A(R)^2\phi(R)^2}{f(R)}\right)=0. \tag{3.0.6d}$$

We can use (3.0.6c) to get an algebraic relation for g in terms of the other fields and their first order derivatives:

$$g(R)=\frac{2f(R)\left(1-R^2\phi'(R)^2\right)+R\left(RA'(R)^2+2f'(R)\right)}{2\left(e^2R^2A(R)^2\phi(R)^2+f(R)\left(1-R^2\Lambda\right)\right)}. \tag{3.0.7}$$

This algebraic relation can be inserted into (3.0.6a), (3.0.6b) and (3.0.6d) to obtain a coupled system of three second order ODE's that constitue the system of independent equations of motion of the problem we are considering in this part. Onwards, these are the three equations of motion that we will solve to find the three fields $\{f, A, \phi\}$ (and thus also g).

When we consider the linear problem we are only interested in the Klein Gordon equation which is (3.0.6a). However in the previous analysis we have considered a spherically symmetric scalar field. The reason is that, in order to have a static spherically symmetric geometry taking into account the scalar field backreaction on it, the scalar field itself must also be spherically symmetric. This is no longer necessary when we only consider the linear problem.

The electrovacuum background is time independent and axisymmetric. Therefore, we can Fourier expand our massive scalar field perturbation along the Killing directions T and φ. This introduces the adimensional frequency $\Omega=\omega L$ and the azimuthal quantum number m_φ. Moreover, in a linear mode analysis, we assume a separation *ansatz* for the radial and polar angle dependence:

$$\phi(T,R,x,\varphi)=e^{-i\,\Omega\,T}e^{i\,m_\varphi\varphi}P_\ell^{m_\varphi}(x)\,\psi(R)\,, \tag{3.0.8}$$

where $P_\ell^{m_\varphi}(x)$ refers to the Legendre polynomials (ℓ essentially gives the number of zeros

of the eigenfunction along the polar direction). We thus obtain the following Klein Gordon equation:

$$\partial_R \left(R^2 f \, \partial_R \psi \right) + \left(\frac{R^2}{f} \left(\Omega + eA \right)^2 - \ell(\ell+1) \right) \psi = 0, \tag{3.0.9}$$

where we have considered $g(R) = f(R)^{-1}$ as justified by the scaling symmetries in (3.0.4).

CHAPTER 4

Linear mode analysis

In this Chapter we compute the frequencies of charged scalar fields in an asymptotically flat Reissner-Nordström black hole (RN BH) background inside a confining box and in an asymptotically AdS_4 RN BH. The box system was first proposed for rotating black holes by Press and Teukolsky and is known as black hole bomb [57]. Our main goal is to perform a detailed study of the linear mode instability problem. In particular we find two analytical expressions for the onset of instabilities in different regions of parameter space that emerge from the superradiant instability and near horizon condensation instability. We also compute numerically onset charges and frequencies in a wide range of parameter space.

4.1 Summary of results

Previous literature already addressed several aspects of the linear mode stability problem (and even its nonlinear evolution) [108, 109, 110, 111, 112, 113, 107, 114, 115, 116, 117, 118, 119, 120, 106]. The aim is to complement and complete these studies in three main directions. First, to point out that the system is unstable to superradiance but also to the near-horizon scalar condensation instability [56, 18, 72] (section 4.3.2). The latter source of instability seems to have been missed in previous studies of the black hole bomb mirror system. Essentially, this instability is present because a scalar field can violate the

Breitenlöhner-Freedman [31] bound associated with the $AdS_2 \times S^2$ near-horizon geometry of the extremal RN BH configuration[1]. These two instabilities are typically entangled. However, there are two limits (which we will identify) where they disentangle and expose their different nature: in units of L, *large* RN BH have the near-horizon instability, while *small* RN BH are unstable to superradiance.

Built on these considerations, the second main aim is to find the onset surface for instability and key properties of it. To begin, we find the critical scalar field charge, as a function of the horizon radius and chemical potential, above which the system is unstable. The exact identification of this onset surface proves useful, for example, to identify good initial data for time evolution simulations. Our results are exact and considerably sharpen (and testify) the analytical bounds necessary for the existence of instability given in [108, 119]. RN BH are parametrized by two parameters, *e.g.* the (dimensionless) horizon radius R_+ and the chemical potential μ. The extremality condition $\mu = \mu_{ext}$ determines a 1-parameter family of RN BH that have zero temperature. The onset curve $e_{onset}(R_+)$ − to be displayed in Figs. 4.2.1 and 4.3.2 − describes the minimal scalar field electric charge above which nearly-extremal RN BH are unstable (non-extremal black holes are unstable above even higher charges $e_{onset}(R_+, \mu)$ that are also identified). For the box case we also study exhaustively the frequency spectrum of the instability. In particular, we show that the most unstable modes are those described by a spherical harmonic with angular quantum number $\ell = 0$, in agreement with the time domain analysis of [110] (note that the frequency-domain study of [108] just considered the $\ell = 1$ harmonic).

The third goal is to use the properties of the linear instability problem to infer the existence and properties of hairy black holes that should bifurcate (in a phase diagram of solutions of the theory) from the RN family at the onset of the instability (section 4.4). Without the box, no-hair theorems forbid the existence of regular asymptotically flat solitons and black holes [46, 132, 47, 133, 134, 135]. Essentially, this is because a linearized scalar field that extends all the way up to asymptotic infinity, when back-reacted on the gravitoelectric fields, sources terms that diverge logarithmically as the radius grows large (see [2]). However, this no-hair theorem can be evaded if we confine the scalar field inside a box. In these conditions it should be possible to have asymptotically flat solutions that are regular everywhere. Then both cases (box and AdS_4) should have a hairy charged soliton (aka boson star) that is the back-reaction of a normal mode in a box. Assuming this, we can use a simple *non*-interacting thermodynamic model [51, 53, 126, 30, 98] to predict the *leading* order thermodynamics (in a small mass and charge expansion) of the hairy black holes. Interestingly, the leading order expansions of RN BH in R_+ are equivalent for the box and AdS_4 case, thus the same expressions apply to both cases. This thermodynamic model assumes that the hairy black hole can be constructed by placing a small RN BH on

[1]This is the very same instability that ignited the holographic AdS/condensed matter correspondence programme [56, 18, 72].

top of the soliton of the theory, subject to the condition that they have the same chemical potential. The soliton is just a regular horizonless solution with scalar hair that results from the back-reaction of a scalar field normal mode. Interestingly, this thermodynamic model does *not* make use of the equations of motion. Yet, it does yield the correct leading order thermodynamics of the charged hairy black hole. This will be explicitly confirmed in Chapters 5 and 6 where we find the charged hairy black holes solving explicitly the equations of motion.

4.2 Asymptotically AdS_4

4.2.1 AdS_4 and its normal modes

The simplest asymptotically AdS solution to the equations of motion (3.0.6) is AdS_4 itself. This takes the form

$$f(R) = g(R)^{-1} = 1 + R^2, \qquad A(R) = \mu, \qquad \phi(R) = 0. \tag{4.2.1}$$

Consider a scalar field with mass m and charge q in an asymptotically AdS_4 background and its Klein Gordon (KG) equation (3.0.9). A Frobenius analysis at the asymptotic boundary yields the two independent solutions

$$\phi(R) \simeq \frac{\sigma}{R^{\Delta_-}} + \cdots + \frac{\varepsilon}{R^{\Delta_+}} + \cdots, \quad \text{with} \quad \Delta_\pm = \frac{3}{2} \pm \sqrt{\frac{9}{4} + m^2 L^2}\,. \tag{4.2.2}$$

Breitenlöhner and Freedman (BF) found that a scalar field in AdS_4 is normalizable, i.e. it has finite energy, as long as its mass obeys the AdS_4 BF bound [31],

$$m^2 \geq m^2_{\rm BF} \equiv -\frac{9}{4}\frac{1}{L^2}. \tag{4.2.3}$$

When this is the case we can have asymptotically AdS_4 solutions that are stable *in the UV* region. Notice that when $m^2L^2 < -5/4$ both behaviors (σ and ϵ) are normalisable. This is the unitarity bound for the scalar field mass. Throughout this chapter we will consider scalar field masses that are above the unitarity bound. It follows that only the mode ε/r^{Δ_+} with faster fall-off is normalisable (since it has finite canonical energy) and σ/r^{Δ_-} is a non-normalisable mode [31, 136]. We thus choose the BC $\sigma = 0$. According to the AdS/CFT dictionary, the boundary CFT is then not sourced and the scalar field amplitude ε is proportional to the expectation value $\langle\mathcal{O}\rangle$ of the boundary operator $\mathcal{O}$ that has dimension $\Delta_+ = 3$ [71].

In the AdS_4 background (4.2.1) and with the boundary condition $\sigma = 0$, the only solution

to the KG equation is

$$\psi(R) = \frac{\varepsilon R^{\Xi_+ - \Delta_+}}{(R^2+1)^{\frac{1}{2}\Xi_+}}\, {}_2F_1\left[\frac{1}{2}\left(\Xi_+ - e\mu - \omega\right), \frac{1}{2}\left(\Xi_+ + e\mu + \omega\right), \Delta_+ - \frac{1}{2}; \frac{1}{1+R^2}\right], \quad (4.2.4)$$

where Δ_+ is defined in (4.2.2) and $\Xi_+ = \Delta_+ + \ell$, ε is an arbitrary amplitude and ${}_2F_1$ is the hypergeometric function.

To have a regular solution at the origin, the frequency spectrum must be quantized as[2]

$$\omega_n = \Xi_+ + 2n - e\mu, \quad (4.2.5)$$

where the non-negative integer n is the radial overtone that relates to the radial zeros of $\psi(R)$. Equations (4.2.4) and (4.2.5) give, respectively, the eigenvectors and eigenvalues of the KG equation (3.0.9) in AdS_4. Note however that we can use the $U(1)$ gauge transformation of the system to choose the gauge potential to be such that, e.g. $\mu = (\Xi_+ + 2n)/e$ and the normal mode frequency (i.e. for a given n) vanishes, $\omega_n = 0$.

In our current study, we are interested in the case $\ell = 0$ and if $m = 0$, we have that $\Xi_+ = \Delta_+ = 3$. Onwards we choose to work with the solution that has the lowest frequency (and thus energy), namely we set $n = 0$. Then, (4.2.5) reads

$$\omega_0 = 3 - e\mu\,. \quad (4.2.6)$$

4.2.2 AdS_4 – Reissner-Nördstrom black holes

When the scalar field vanishes, global AdS_4 – Reissner-Nördstrom black hole (RN-AdS_4 BH) is another known solution of (3.0.6). This is a 2-parameter family of solutions, that we can take to be the horizon radius R_+ and the chemical potential μ. It is described by ansatz (3.0.2) with

$$\begin{aligned} f(R) &= \frac{1}{g(R)} = 1 + R^2 - \frac{R_+}{R}\left[1 + R_+^2 + \frac{\mu^2}{2}\left(1 - \frac{R_+}{R}\right)\right], \\ A(R) &= \mu\left[1 - \frac{R_+}{R}\right], \\ \phi(R) &= 0. \end{aligned} \quad (4.2.7)$$

Alternatively, we can parametrize RN-AdS_4 with R_+ and the temperature T in which case the chemical potential is given by

$$\mu = \sqrt{2}\sqrt{1 + 3R_+^2 - 4\pi R_+ T}. \quad (4.2.8)$$

[2]This follows from the Gamma function property $\Gamma[-n] = \infty$ for $n = 0, 1, 2, \cdots$

It follows that regular RN-AdS_4 black holes exist if their chemical potential satisfies

$$\mu \leq \sqrt{2}\sqrt{1+3R_+^2}. \tag{4.2.9}$$

When $\mu = 0$ one recovers the AdS_4-Schwarzschild solution while the upper bound of (4.2.9) occurs for the extremal configuration ($T = 0$) where the entropy is finite but the temperature vanishes.

The mass, charge, entropy and temperature expressed as a function of R_+ and μ are

$$\begin{aligned} M_{RN}/L &= \frac{R_+}{2}\left(1+\frac{\mu^2}{2}+R_+^2\right), \qquad Q_{RN}/L = \frac{1}{2}\,\mu\, R_+\,, \\ S_{RN}/L^2 &= \pi R_+^2, \qquad T_{RN}L = \frac{1}{8\pi R_+}\left(2-\mu^2+6R_+^2\right). \end{aligned} \tag{4.2.10}$$

In section 4.4, we will find the leading order thermodynamics of hairy black holes assuming that they can be described as a non-interacting mixture of a soliton and a small RN-AdS_4 BH. To complete that analysis, we will only consider the leading order (in the R_+ expansion) thermodynamics. For future reference they are:

$$\begin{aligned} M_{RN}/L &\simeq \frac{R_+}{2}\left(1+\frac{\mu^2}{2}\right)+\mathcal{O}(R_+^3), \qquad Q_{RN}/L = \frac{1}{2}\,\mu\, R_+\,, \\ S_{RN}/L^2 &= \pi R_+^2, \qquad T_{RN}L \simeq \frac{1}{8\pi R_+}\left(2-\mu^2\right)+\mathcal{O}(R_+). \end{aligned} \tag{4.2.11}$$

When perturbed by an infinitesimal scalar field perturbation, global RN-AdS_4 BHs can develop two types of linear instabilities that have different physical nature. One is the near-horizon scalar condensation instability and the other is the superradiant instability. The former is already present in planar RN-AdS_4 BHs (where it was first found) while the latter is only present in asymptotically global AdS. The zero mode of these instabilities is closely connected to the existence of hairy black hole solutions. Therefore, in the following we discuss the main properties of these two instabilities with some detail.

4.2.3 Superradiant instability of small black holes and matched asymptotic expansion method

In the present subsection we consider a massless scalar field and we set $\ell = 0$ and show that small RN-AdS_4 BHs are unstable to the superradiant instability. For that we solve the KG equation for a massless scalar field perturbation with charge $e \geq \frac{3}{\sqrt{2}}$,

$$\phi(T,R) = e^{-i\Omega T}\phi(R) \tag{4.2.12}$$

around RN-AdS$_4$ in a perturbative expansion in the horizon radius R_+. We will find that the imaginary part of the perturbation frequency Ω is positive, and thus the system is unstable when $\mu \geq \frac{3}{e}$.

To impose smoothness of the perturbations at the horizon boundary it is convenient to work in ingoing Eddington-Finkelstein coordinate

$$v = T + \int \frac{1}{f(R)} \mathrm{d}R. \tag{4.2.13}$$

The KG equation cannot be solved analytically at each order. To circumvent this limitation, we consider small black holes, $R_+ \ll 1$, and use a matched asymptotic expansion method to solve the resulting KG equation at each order in R_+. Namely, we consider two different regions: the far region, $R \gg R_+$, and the near region, $R \ll 1$ which have an overlapping region $R_+ \ll R \ll 1$ since we are assuming $R_+ \ll 1$. In the near and far regions, certain contributions in the KG equation are sub-dominant and can be discarded. We are left with ODEs with a source term that depends on the previous order solutions and their derivatives which can be solved analytically. At each order, the near and far region solutions are matched in the overlapping region. In the following we explicitly show the method of matched asymptotic expansion which will be used throughout this Part.

Both in the far (superscript ^{out}) and in the near (superscript ^{in}) regions, we write the perturbative expansion in R_+ of $\phi(R)$ and Ω as:

$$\begin{aligned} &\phi^{out}(R) = \sum_{k\geq 0} R_+^k \, \phi_k^{out}(R), \qquad \phi^{in}(R) = \sum_{k\geq 0} R_+^k \, \phi_k^{in}(R), \\ &\Omega = \sum_{k\geq 0} R_+^k \, \Omega_k \quad \text{with} \;\; \Omega_0 = 3 - \mu e, \end{aligned} \tag{4.2.14}$$

and solve the KG equation order by order. The choice of Ω_0 is justified because the perturbation mode of RN-AdS$_4$ with lowest frequency reduces to the lowest normal mode of AdS (4.2.6) in the limit $R_+ \to 0$. At any order $k \geq 1$ we have five parameters to determine: two integration constants from $\phi_k^{out}(R)$, two integration constants from $\phi_k^{in}(R)$, and the frequency coefficient Ω_k. For our purposes, it is enough to present the results up to order $k = 2$: this is the order at which the frequency acquires an imaginary contribution.

`Far region analysis:`

In the far region, $R \gg R_+$, the KG equation for $\phi^{out}(R)$ around the RN-AdS$_4$ BH (4.2.7) effectively describes linearized perturbations around global AdS. Indeed at each order in the R_+ expansion it reads,

$$\bar{D}^\mu \bar{D}_\mu \phi_k^{out} = S_k^{out}\left(\phi_{j<k}^{out}, \partial\phi_{j<k}^{out}\right), \tag{4.2.15}$$

where $\bar{D}_\mu = \bar{\nabla}_\mu - ieA_\mu$ is the gauge covariant derivative of the global AdS background $\bar{g}$ with a gauge potential $A = \mu dt$, and the RHS is a source term that depends on the lower order fields $\phi^{out}_{j<k}$ and their derivatives. As justified when discussing (4.2.2), at any expansion order, in the far region we impose the Dirichlet boundary condition:

$$\phi^{out}\big|_{R\to\infty} = \frac{\varepsilon}{R^3} + \mathcal{O}(1/R^5). \tag{4.2.16}$$

The KG equation (3.0.9) is a linear eigenvalue equation, this implies that given a solution $\{\phi(R), \Omega\}$, the pair $\{K\phi(R), \Omega\}$ is also a solution with K a constant number. Equation (4.2.16) tells us that we fix the leading behaviour of the field at the boundary to be ε. Hence any correction of order $\mathcal{O}(R_+)$ or higher in our expansion must only contribute in the behaviour of the scalar field at the boundary as $\mathcal{O}(1/R^5)$.

At leading order the far region reduces to the AdS case:

$$\phi^{out}_0(R) = \frac{3\alpha_0 R + \tilde{\alpha}_0\left(R^4 + 6R^2 - 3\right)}{3R\left(R^2+1\right)^{3/2}} e^{-i(\mu e - 3)\arctan R}. \tag{4.2.17}$$

The boundary condition (4.2.16) requires we set $\tilde{\alpha}_0 = 0$ and $\alpha_0 \equiv 1$. (4.2.16) and (4.2.17) fix the amplitude of the scalar field to be $\varepsilon = -ie^{-\frac{1}{2}i\pi e\mu}$.

For higher orders, $k \geq 1$, the boundary condition (4.2.16) always fixes the two integration constants α_k and $\tilde{\alpha}_k$ but leaves the frequency coefficient Ω_k undetermined. It is fixed by matching the far region with the near region. The final far region solutions ϕ^{out}_k for $k = 0, 1, 2$, after imposing the boundary condition (4.2.16) and fixing the frequency coefficients, are listed in equation $(A1)$ of Appendix A in [1].

`Near region analysis:`

In the near region $R \ll 1$, it is convenient to work with the rescaled variable $y = \frac{R}{R_+}$. The reason for this rescaling will become fully clear in the discussion associated to (5.5.3) and (5.5.4): In the near region the perturbation problem simplifies since, for $R_+ \ll 1$, the electric field is *weak* and the perturbation system reduces to a small perturbation around the neutral solution. After this rescaling, the KG equation at each order for $\phi^{in}(y)$ around RN-AdS_4 BH reads

$$\bar{D}^\mu \bar{D}_\mu \phi^{in}_k = S^{in}_k\left(\phi^{in}_{j<k}, \partial\phi^{in}_{j<k}\right), \tag{4.2.18}$$

where $\bar{D}_\mu$ is the leading order part of the gauge covariant derivative of the rescaled coordinate in the RN-AdS_4 BH[3], and the RHS is a source term that depends on the lower order fields $\phi^{in}_{j<k}$ and their derivatives. At each order, we solve (4.2.18) subject to the boundary condition that the solution is regular at the horizon in Eddington-Finkelstein coordinates.

[3] In (4.2.18), the gauge covariant derivatives $\bar{D}_\mu$ are covariant derivatives $\bar{\nabla}_\mu$, since the electric field makes no contribution at this leading order.

At leading order the near region solution is

$$\phi_0^{in}(y) = \beta_0 - \frac{\tilde{\beta}_0}{\mu^2 - 2}\left[\log(y-1) - \log\left(2y - \mu^2\right)\right], \tag{4.2.19}$$

and smoothness requires that we set $\tilde{\beta}_0 = 0$.

At any order $k \geq 1$, the boundary condition at the horizon always fixes one of the integration constants, say $\tilde{\beta}_k$, but the other is left undetermined until we do the matching of the near and far regions. The final near region solutions ϕ_k^{in} for $k = 0, 1, 2$, after imposing the boundary condition and fixing the integration constants, are listed in equation $(A2)$ of Appendix A in [1].

`Matching the near and far region solutions:`

At this stage we have two undetermined parameters at each order $k \geq 1$: the near region integration constant β_k and the frequency coefficient Ω_k. They are fixed by requiring that the large radius expansion of the near solution ϕ^{in} matches the small radius expansion of the far solution ϕ^{out}. In these expansions we keep only terms that will not receive contributions from higher orders.

Let us illustrate this matching at leading order, $k = 0$. The small R limit of ϕ_0^{out} and the large R limit of ϕ_0^{in} yield

$$\begin{aligned} &\phi_0^{out}(R) \simeq 1 + \mathcal{O}(R), \\ &\phi_0^{in}(R) = \beta_0. \end{aligned} \tag{4.2.20}$$

Matching requires that we set $\beta_0 = 1$. A similar matching procedure can be done for higher orders.

After doing this procedure for the fields up to order R_+^2, we find that the frequency coefficients in (4.2.14) are:

$$\begin{aligned} \Omega_0 =& 3 - \mu e\,, \\ \Omega_1 =& -\frac{4\left(3\mu^2 - 4\mu e + 6\right)}{3\pi}, \\ \Omega_2 =& \, i\,(\mu e - 3)\frac{16}{3\pi} + \frac{1}{96}\left[\mu\left(-264\left(\mu^2+2\right)e + 9\mu\left(3\mu^2+52\right) + 224\mu e^2\right) + 108\right] \\ &- \frac{4}{27\pi^2}\left(45\mu^2 - 52\mu e + 90\right)\left(3\mu^2 - 4\mu e + 6\right). \end{aligned} \tag{4.2.21}$$

The property in (4.2.21) to be highlighted is that at order $k = 2$ the frequency acquires an imaginary part proportional to $\mu e - 3$. This is negative whenever $\mu \leq \frac{3}{e}$, which signals

exponential damping, but it becomes positive for $\mu > \frac{3}{e}$. The latter case describes the superradiant instability of RN-AdS_4 BHs. Further properties of RN-AdS_4 superradiant modes beyond the perturbative analysis done here can be found in [137, 138].

The above analysis shows that global RN-AdS_4 BHs are unstable to superradiance in the small horizon radius regime, $R_+ \ll 1$. We can also infer the onset of the instability. Indeed, in the gauge the computation has been performed, the onset is at $Re(\Omega) = Im(\Omega) = 0$. We conclude that superradiance will occur for charges obeying

$$e \geq \frac{3}{\mu} + \frac{4\left(2-\mu^2\right)R_+}{\pi\mu} + \frac{\left(\mu^2-2\right)\left(256-640\mu^2+9\pi^2\left(\mu^2-10\right)\right)R_+^2}{32\pi^2\mu} + \mathcal{O}(R_+^3). \quad (4.2.22)$$

4.2.4 Near horizon scalar condensation instability of large black holes

In section 4.2.1 we considered the asymptotic behaviour of the scalar field, to obtain the BF bound for the mass of the scalar field. But this analysis is blind to the behaviour of the scalar field in the interior of the spacetime. In particular, the properties of the scalar field in the IR region of a particular spacetime might drive the system unstable. This is indeed the case: as first found in the context of holographic superconductors [56, 18, 19], planar AdS black holes can be unstable to a near horizon scalar condensation mechanism [56]. The zero mode of this instability signals a second order phase transition to planar hairy black holes that are dual to holographic superconductors [18, 19]. It was later understood that the near horizon scalar condensation instability is quite universal and present for any asymptotically AdS background that has a black hole with an extremal (zero temperature) configuration [19, 72] (this includes even some systems with neutral black holes and uncharged scalar fields)[4]. The criterion for this instability is the following. Start with a scalar field whose mass obeys the UV BF bound (4.2.3). When it violates the AdS_2 BF bound

$$m^2_{\mathrm{BF}_2}L^2 \equiv -\frac{1}{4}, \quad (4.2.23)$$

the system, although asymptotically stable, is unstable in its near-horizon region. We might then expect the system to evolve into a hairy black hole with the same UV asymptotics but different IR behaviour.

We can work out in more detail the consequences of this instability for our current system, following the original analysis in [72] and [126]. Global RN-AdS_4 BHs described by (3.0.2) and (4.2.7) have an extremal configuration when the bound (4.2.9) is saturated, $\mu = \sqrt{2}\sqrt{1+3\frac{R_+^2}{L^2}}$. Take the near-horizon limit of this extremal RN-AdS_4 BH by introducing

[4]The asymptoic AdS condition can be dropped if we consider scalar fields trapped by a potential or by a reflecting box at a finite distance from the black hole as we will show later in section 4.3.

the new coordinates $\{\tau, \tilde{\rho}\}$,

$$t = L^2_{AdS_2}\,\frac{\tau}{\lambda}, \qquad r = r_+ + \lambda\tilde{\rho}, \tag{4.2.24}$$

and lettting $\lambda \to 0$. Setting,

$$L_{AdS_2} \equiv \frac{L\, r_+}{\sqrt{L^2 + 6r_+^2}} \tag{4.2.25}$$

this procedure yields the solution of (3.0.6),

$$\begin{aligned} \mathrm{d}s^2 &= L^2_{AdS_2}\left(-\tilde{\rho}^2\mathrm{d}\tau^2 + \frac{\mathrm{d}\tilde{\rho}^2}{\tilde{\rho}^2}\right) + r_+^2\mathrm{d}\Omega^2_{(2)}, \\ A_\mu \mathrm{d}x^\mu &= \alpha\,\tilde{\rho}\,\mathrm{d}t \qquad \text{with } \alpha \equiv \frac{L_{AdS_2}}{r_+}\sqrt{r_+^2 + L^2_{AdS_2}}. \end{aligned} \tag{4.2.26}$$

So, the near-horizon limit of extremal RN-AdS$_4$ is the direct product of AdS$_2$ with a sphere S^2. Applying this near-horizon limit to the KG equation that describes a perturbation $\delta\phi(t,r) = e^{-i\omega t}R(r)$ of a scalar field (with mass m and charge q) about the extremal RN-AdS$_4$ black hole yields

$$\partial_{\tilde{\rho}}\left(\tilde{\rho}^2\partial_{\tilde{\rho}}R\right) + \left(\frac{(\omega + q\,\alpha\,\tilde{\rho})^2}{\tilde{\rho}^2} - m^2L^2_{AdS_2}\right)R = 0, \tag{4.2.27}$$

which, not surprisingly, is the KG equation for a scalar field around AdS$_2$ with an electromagnetic potential $A_\tau = \alpha\,\tilde{\rho}$. A Taylor expansion of (4.2.27) yields

$$R\big|_{\tilde{\rho}\to\infty} \simeq a\,\tilde{\rho}^{\,-\widetilde{\Delta}_-} + \cdots + + b\,\tilde{\rho}^{\,-\widetilde{\Delta}_+} + \cdots, \quad \text{with} \quad \widetilde{\Delta}_\pm = \frac{1}{2} \pm \frac{1}{2}\sqrt{1 + m^2_{eff}L^2_{AdS_2}}\,, \tag{4.2.28}$$

which dictates the effective mass of the scalar field from the perspective of a near-horizon observer,

$$\begin{aligned} m^2_{eff}L^2_{AdS_2} &\equiv m^2L^2_{AdS_2} - q^2\,\alpha^2 \\ &= m^2L^2_{AdS_2} - 2e^2R_+^2\frac{1 + 3R_+^2}{\left(1 + 6R_+^2\right)^2}, \end{aligned} \tag{4.2.29}$$

where in the second line we re-introduced the dimensionless quantities $R_+ = r_+/L$ and $e = qL$.

A scalar field with mass (4.2.29) in AdS$_2$ is unstable if it violates the AdS$_2$ BF bound (4.2.23). It follows that extremal RN-AdS$_4$ BHs are unstable whenever the charge of the scalar field obeys

$$e^2 \geq \left(1 + 4m^2L^2\frac{R_+^2}{1 + 6R_+^2}\right)\frac{\left(1 + 6R_+^2\right)^2}{8R_+^2\left(1 + 3R_+^2\right)}\,. \tag{4.2.30}$$

Taking the large R_+ expansion, this yields

$$e^2 \geq \left(\frac{3}{2} + m^2L^2\right) - \frac{m^2L^2}{6}\frac{1}{R_+^2} + \left(1 + \frac{4}{3}m^2L^2\right)\frac{1}{24\,R_+^4} + \mathcal{O}(1/R_+^6). \tag{4.2.31}$$

In the strict limit $R_+ \to \infty$, we recover the known result for planar RN-AdS_4 BHs, $e^2 \geq \left(\frac{3}{2} + m^2L^2\right)$ [56, 18, 19]. Global RN-AdS_4 BHs are unstable for larger values of the scalar field charge.

In the opposite $R_+ \to 0$ limit, an expansion of (4.2.30) yields

$$e^2 \geq \frac{1}{8R_+^2} + \mathcal{O}(1), \tag{4.2.32}$$

which indicates that the near-horizon scalar condensation instability is suppressed for small (global) RN-AdS_4 BHs. This is to be contrasted with the superradiant instability bound (discussed in the previous subsection) which is valid for small black holes.

The near-horizon instability criterion that we have been discussing applies strictly to extremal black holes. Continuity indicates that this instability should extend to near-extremal black holes. Thus large, near extremal RN-AdS_4 black holes are unstable to condensation of the scalar field when condition (4.2.30) is satisfied. This statement is verified numerically in the next subsection.

4.2.5 Onset of linear instabilities

There is a large amount of publications on quasinormal modes in asymptotically AdS backgrounds, largely due to the fact that according to the gauge/gravity correspondence quasinormal modes are dual to timescales for thermalisation of the dual thermal quantum field theory (see section 1.2). However, for self-consistency we compute numerically the onsets of instability of scalar fields in RN-AdS_4 BH. To this end we solve equation (3.0.9) in the background (4.2.7). The equation has two parameters in addition to the scalar field charge and mass: the chemical potential μ and the horizon radius R_+. We found the onsets for two different scalar field masses: $mL = 0$ (left panel of Fig. 4.2.1) and $mL = 2$ (right panel of Fig. 4.2.1). For each mass we calculated the onset charges as a function of the horizon radius for different values of the chemical potential that we choose to have the form $\mu = \mu_{ext}(1 - 10^{-x})$.

The dashed red line is the near-horizon bound (4.2.30). In the left panel the dashed blue line is the superradiant bound (4.2.22). The numerical curves correspond to values $x = 2, 3, 6, 15$ from top to bottom. Both bounds are sharp and complement each other very well. In fact, the near-horizon bound reproduces the curve corresponding to $\mu = \mu_{ext}(1 - 10^{-15})$

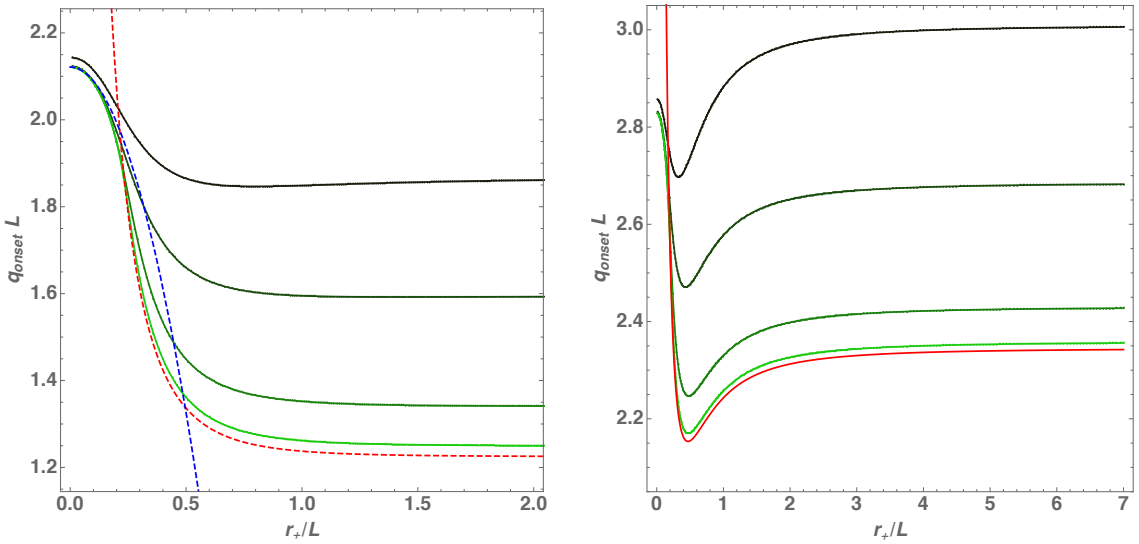

Figure 4.2.1: Onset scalar field charge as a function of the horizon radius for chemical potential $\mu = \mu_{ext}(1 - 10^{-x})$ with $x = 2, 3, 6, 15$ (from top to bottom on the right). The left panel corresponds to massless scalar fields, the right panel to masses $mL = 2$. The red dashed line is the near-horizon condensation analytic bound (4.2.30). In addition, in the left panel we have the dashed blue line which is the superradiant bound (4.2.22).

very accurately in most of the displayed region, that is, for not very small horizon radius. Conveniently, the superradiant bound describes very accurately the small horizon radius region.

4.3 BH bomb in a Minkowski cavity

4.3.1 Reissner-Nordström black hole bomb system

Another solution, in addition to Minkowski, to the equations of motion (3.0.6) when $\Lambda = 0$ is the Reissner-Nordström black hole family of solutions which is a two-parameter family that we can take to be the horizon radius r_+ and the chemical potential $\mu = A(\infty) - A(r_+)$. In the gauge where $A(r_+) = 0$ this solution is described by

$$f(r) = 1 - \frac{r_+}{r}\frac{2+\mu^2}{2} + \frac{r_+^2}{r^2}\frac{\mu^2}{2}, \qquad g(r) = \frac{1}{f(r)}, \qquad A(r) = \mu\left(1 - \frac{r_+}{r}\right). \tag{4.3.1}$$

The ADM mass, electric charge, entropy, and temperature of the RN BH are

$$M = \frac{1}{4}(2+\mu^2)r_+\,, \qquad Q = \frac{1}{2}\,\mu\, r_+\,, \qquad S_H = \pi r_+^2\,, \qquad T_H = \frac{1}{8\pi r_+}(2-\mu^2)\,. \tag{4.3.2}$$

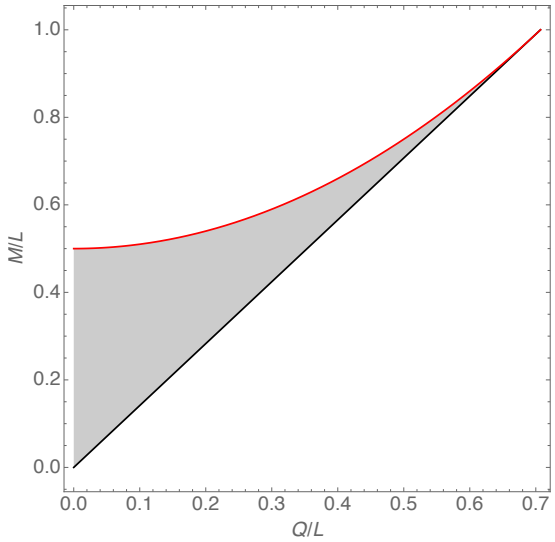

Figure 4.3.1: Region of existence of RN BH inside the box in a phase diagram that plots the dimensionless ADM mass M/L *vs* the dimensionless ADM electric charge Q/L. The lower black line corresponds to extremal RN BHs, and non-extremal RN BHs exist in all the region above this line. The upper red line describes RN BHs that have horizon radius equal to the radius of the box, $r_+ = L$. Thus, the RN BHs that can fit inside the box are those in the shaded area limited by the two lines.

Extremal RN BHs ($T_H = 0$) have $\mu = \sqrt{2}$, so RN BHs exist for $\mu \leq \sqrt{2}$.

RN BHs are known to be linear mode stable to gravitoelectromagnetic perturbations but also to scalar field perturbations [139]. However, we will be interested in placing an asymptotically flat RN BH inside a box Σ of radius $L > r_+$. In this case, a test scalar field ϕ with charge q and mass m can drive the system unstable. In units of the box radius, the condition that the BH is inside the box constrains the dimensionless horizon radius to be $R_+ < 1$. In terms of the dimensionless ADM mass and electric charge, RN BHs with $R_+ < 1$ and $0 \leq \mu \leq \sqrt{2}$ are those in the shaded region of Fig. 4.3.1. The lower black line corresponds to extremality ($\mu = \sqrt{2}$) and the upper red line has $R_+ = 1$.

We require the scalar field to vanish at the box location Σ and outside it, $\phi(R \geq 1) = 0$. This implies we impose the outer boundary condition

$$\phi\big|_{R=1} = 0\,, \tag{4.3.3}$$

and we define the amplitude of the scalar field to be given by the value of its normal derivative at the box, $\phi'^{in}\big|_{R=1^-} \equiv \varepsilon$.

At the inner boundary, $R = R_+$, the scalar field must be regular in Eddington-Finkelstein coordinates (which are appropriate to extend the background solution across the horizon).

In section 4.4, we will find the leading order thermodynamics of hairy black holes assuming

that they can be described as a non-interacting mixture of a soliton and a small RN BH. To complete that analysis, we will only consider the leading order (in the R_+ expansion) thermodynamics of RN black hole. For future reference they are:

$$\begin{aligned} M_{RN}/L &\simeq \frac{R_+}{2}\left(1+\frac{\mu^2}{2}\right)+\mathcal{O}(R_+^3), \qquad Q_{RN}/L = \frac{1}{2}\,\mu\, R_+\,, \\ S_{RN}/L^2 &= \pi R_+^2, \qquad T_{RN}L \simeq \frac{1}{8\pi R_+}\left(2-\mu^2\right)+\mathcal{O}(R_+). \end{aligned} \tag{4.3.4}$$

Notice that they are equivalent to (4.2.11). This is to be expected since taking a small $R_+ \equiv r_+/L$ expansion is equivalent to taking a large L expansion keeping r_+ fixed and effectively discarding the effect of the asymptotic region.

4.3.2 Superradiant instability of a boxed RN

As we did in the asymptotically AdS case, we first consider the case where we have a charged scalar field perturbation confined inside a box Σ in Minkowski space with a constant Maxwell field. Naturally, this confinement condition, $\phi(R \geq 1) = 0$, and regularity at the origin quantize the frequency spectrum of the scalar perturbations.

Using ansatz (3.0.8), we can solve the KG equation (3.0.9) in Minkowski spacetime with gauge field $A = \mu\, \mathrm{d}T$. The most general solution is

$$\begin{aligned} \psi(R) = \frac{\left[(\Omega+e\mu)^2-m_\phi^2\right]^{-\frac{1}{4}}}{\sqrt{R}}\Bigg[&\beta_1 J_{\ell+\frac{1}{2}}\left(R\sqrt{(\Omega+e\mu)^2-M^2}\right)+ \\ &\beta_2 Y_{\ell+\frac{1}{2}}\left(R\sqrt{(\Omega+e\mu)^2-M^2}\right)\Bigg], \end{aligned} \tag{4.3.5}$$

where $J_\nu(z)$ and $Y_\nu(z)$ are the Bessel functions of the first and second kind, respectively, and β_1, β_2 are arbitrary constants. We now have to impose the boundary conditions. Regularity of the solution at the origin, $R = 0$, requires that we set $\beta_2 = 0$ to avoid a divergence of the type $R^{-\ell-1}$and the requirement that the scalar field vanish at the box quanitzes the frequency; see (4.3.3). For $\nu \in \mathbb{R}$, the Bessel function $J_\nu(z)$ has an infinite number of simple zeros that we denote by $j_{\nu,n}$, *i.e.* $n \in \mathbb{N}$ identifies the particular zero we look at. The frequency spectrum is given by

$$\Omega_{\ell,n} = \sqrt{j^2_{\ell+\frac{1}{2},n}+M^2}-e\mu\,, \quad n = 1,2,3,\cdots. \tag{4.3.6}$$

Onwards we consider the solution with lowest frequency (*i.e.*with lowest energy) which amounts to consider the first simple zero *i.e.* $n = 1$. For massless scalar field, $m = 0$ we

obtain that the frequencies become

$$\Omega_{0,1} = j_{\frac{1}{2},1} - e\mu = \pi - e\mu\,. \tag{4.3.7}$$

Condition (4.3.7) gives the lowest frequency for a scalar field that can fit inside a box in Minkowski spacetime. If this box is placed instead in a RN black hole background, the frequency spectrum will change. However, if the black hole is small, $R_+ \ll 1$, the frequency can be approximated by a series expansion in R_+ with the leading order term being (4.3.7). Borrowing results from the scalar field in AdS of the previous section and in [51, 1] we expect that, at higher orders in the R_+ expansion, the frequency correction receives an imaginary contribution. We further expect this imaginary contribution to be proportional to $\Omega_{0,1}$. Therefore the system should be unstable to superradiance for $\Omega_{0,1} < 0$ (*i.e.* for $e \geq \pi/\mu$). In particular, for an extremal RN BH the chemical potential is $\mu = \sqrt{2}$. It then follows that a small extremal RN BH should be unstable to superradiance for scalar field charges that obey the bound

$$e \geq \frac{\pi}{\sqrt{2}} \sim 2.221. \tag{4.3.8}$$

This bound can be expanded in a series expansion in R_+ and away from extremality. This procedure is equivalent to the one done in section 4.2.3 before, where we used a matched asymptotic expansion to solve the KG equation (3.0.9) in an expansion in R_+. Rather than presenting the procedure again, we display the final results for the frequencies. The procedure can also be found in the publication [2] which this research produced. In this case we did the computation up to order R_+ since we did a much more thorough numerical analysis.

$$\begin{aligned}\Omega_0 &= \pi - e\mu \\ \Omega_1 &= \left(\mu e - \frac{1}{2}\pi\left(\mu^2+2\right)\right)\left[\gamma - \mathrm{Ci}(2\pi) + \log(2\pi)\right] + \frac{1}{4}\pi\left(\mu^2+2\right),\end{aligned} \tag{4.3.9}$$

where $\gamma \sim 0.577216$ is Euler's constant and $\mathrm{Ci}(x) = -\int_x^\infty \frac{\cos z}{z}\mathrm{d}z$ is the cosine integral function.

Again, the onset of superradiance occurs when $\Omega = 0$, in the gauge we work. We can thus use the condition $\Omega_0 + \Omega_1 R_+ + \mathcal{O}\left(R_+^k\right) = 0$ to find the electric charge of the scalar field, e_{onset} as a function of the horizon radius and chemical potential, above which the system is unstable to superradiance. This gives:

$$e_{onset} = \frac{\pi}{\mu} - R_+\frac{\pi}{2\mu}\left[\mu^2\left(\gamma + \log(2\pi) - \mathrm{Ci}(2\pi) - \frac{1}{2}\right) - 1\right] + \mathcal{O}\left(R_+^2\right). \tag{4.3.10}$$

In section 4.3.4 we will solve numerically the linearised KG equation to find the linear instabilities of a RN BH in a box. With a numerical analysis we will confirm that, in the

small horizon radius limit and for RN black holes near extremality, the system becomes unstable if (4.3.8) and (4.3.10) are obeyed. In particular, in Fig. 4.3.2, the green dashed straight line is given by (4.3.10) when we set the chemical potential to its extreme value, $\mu = \sqrt{2}$.

4.3.3 The origin of the near-horizon instability of RN black holes in a box

Since a box in asymptotically flat spacetime has reflecting boundary conditions similar to those of asymptotically AdS spacetime, it is natural to ask whether the near horizon instability is also present in the setup we are considering. This section is similar to section 4.2.4. We show again in detail the procedure since it is the first time it is applied to asymptotically flat spacetimes.

To address this question in generic conditions, consider a scalar field with mass m and charge q (we find it convenient to restore the dimensionful quantities in this discussion). Stability conditions in flat spacetime require the mass m to be non-negative, $m \geq 0$. We introduce the new coordinates $\{\tau, \tilde{\rho}\}$ as in (4.2.24) and take the near horizon limit. At leading order the metric takes the form

$$\begin{aligned} \mathrm{d}s^2 &= L_{AdS_2}^2 \left(-\tilde{\rho}^2 \mathrm{d}\tau^2 + \frac{\mathrm{d}\tilde{\rho}^2}{\tilde{\rho}^2} \right) + r_+^2 \mathrm{d}\Omega_{(2)}^2, \\ A_\mu \mathrm{d}x^\mu &= \alpha\, \tilde{\rho}\, \mathrm{d}t \qquad \text{with} \;\; L_{AdS_2} = r_+ \;\; \text{and} \;\; \alpha \equiv \sqrt{2} L_{AdS_2}. \end{aligned} \tag{4.3.11}$$

Thus the near horizon geometry is the direct product of an AdS_2 geometry with an S^2 just as in the asymptotically AdS case. This is still a solution of Einstein-Maxwell theory[5].

We introduce the new coordinates $\{\tau, \tilde{\rho}\}$ into the KG equation (3.0.9) and take the limit $\lambda \to 0$ directly in the equation. To capture the time dependence information, the frequency $\tilde{\omega}$ in the near-horizon geometry is related to ω as:

$$\omega = \tilde{\omega} \frac{\lambda}{L_{AdS_2}^2}. \tag{4.3.12}$$

which follows from the identification $e^{-i\omega t} \equiv e^{-i\tilde{\omega}\tau}$.

Then the KG equation in the near horizon limit becomes

$$\partial_{\tilde{\rho}} \Big(\tilde{\rho}^2\, \partial_{\tilde{\rho}} \psi(\tilde{\rho}) \Big) + \left(\frac{\left(\tilde{\omega} + q\,\alpha\,\tilde{\rho}\right)^2}{\tilde{\rho}^2} - m^2 L_{AdS_2}^2 - \ell(\ell+1) \right) \psi(\tilde{\rho}) = 0. \tag{4.3.13}$$

[5] On the other hand the AdS_2 orbit space is a solution of 2-dimensional Einstein-AdS theory whose equation of motion, in the trace reversed form, reads $R_{ij} + L_{AdS_2}^{-2} g_{ij} = 0$.

A Taylor expansion of this equation at large $\tilde{\rho}$ yields

$$\psi\big|_{\tilde{\rho}\to\infty} \simeq a\,\tilde{\rho}^{\,-\widetilde{\Delta}_-} + \cdots + b\,\tilde{\rho}^{\,-\widetilde{\Delta}_+} + \cdots\,, \quad \text{with} \quad \widetilde{\Delta}_\pm = \frac{1}{2} \pm \frac{1}{2}\sqrt{1 + 4m^2_{eff}L^2_{AdS_2}}\,, \tag{4.3.14}$$

with an effective mass for the scalar field given by

$$\begin{aligned} m^2_{eff}L^2_{AdS_2} &\equiv m^2L^2_{AdS_2} + \ell(\ell+1) - q^2\,\alpha^2 \\ &= m^2L^2_{AdS_2} + \ell(\ell+1) - 2q^2r_+^2. \end{aligned} \tag{4.3.15}$$

A scalar field in AdS_2 is unstable if it violates the AdS_2 Breitenlöhner-Freedman bound (4.2.23). Therefore, it is natural to expect that extremal RN BHs confined in a box might be unstable to scalar condensation when their scalar field charge is large enough, namely when

$$q \geq \frac{\sqrt{(2\ell+1)^2 + 4m^2L^2_{AdS_2}}}{2\sqrt{2}r_+} = \frac{\sqrt{(2\ell+1)^2 + 4m^2r_+^2}}{2\sqrt{2}r_+}. \tag{4.3.16}$$

Now we reintroduce the dimensionless quantities $R_+ = r_+/L$, $e = qL$ and $M = mL$. For large black holes inside the box, a Taylor expansion of (4.3.16) about $R_+ \sim 1$ yields

$$e \geq \frac{\sqrt{(2\ell+1)^2 + 4M^2}}{2\sqrt{2}} + \frac{(2\ell+1)^2}{2\sqrt{2}\sqrt{1 + 4(M^2 + l(l+1))}}(1 - R_+) + \mathcal{O}\Big((1-R_+)^2\Big). \tag{4.3.17}$$

On the other hand, for small black holes (4.3.16) has the expansion,

$$e \geq \frac{2\ell+1}{2\sqrt{2}}\,\frac{1}{R_+} + \mathcal{O}(R_+^1). \tag{4.3.18}$$

Thus, for small black holes $R_+ \ll 1$, we see that the near horizon instability is suppressed. However, near horizon condensation is certainly present for large black holes (when compared with the box radius).

In the next section we will compute numerically the timescales of linear instabilities of a RN BH in a box. We will find that as the system approaches extremality and $R_+ \to 1$, the instability indeed has a near horizon condensation origin since its onset will be given by (4.3.16) (see the right panel of Fig. 4.3.2).

4.3.4 Timescale for superradiant and near-horizon instabilities

In this section we compute numerically the frequencies of a massless scalar field confined inside a box in a RN background. In particular, we find the scalar field charge above which linear mode instabilities appear. This problem was already addressed in previous literature for particular values of the parameters involved in the problem. However, here we want to complement these available results with sharper statements about the region in phase space where the solutions are unstable. For example, for a given scalar field mass[6] we want to identify the critical scalar field charge $e_{onset}(R_+, \mu)$ above which instabilities are present. More importantly, we want to point out that RN BHs are linearly unstable not only to the superradiant instability but also to the near-horizon scalar condensation instability. Previous studies missed the existence of the latter instability. The two instabilities are usually highly entangled (which justifies why previous numerical studies missed identifying the existence of the near-horizon instability) but near extremality they disentangle. In this regime, we can explicitly check that the numerical onset curve $e_{onset}(R_+, \mu)$ approaches the analytical expression for superradiance (4.3.8) and the analytical expression (4.3.16) for the near-horizon instability in the appropriate limits, namely for small and large horizon radius R_+, respectively (see the right panel of Fig. 4.3.2).

Consider the KG equation (3.0.9) in the RN spacetime (3.0.2)-(4.3.1). We restrict to the most unstable mode which happens to be the one with $\ell = 0$ that preserves the spherical symmetry. This case was studied in the time domain in [110]. In [2] we also studied the $\ell = 1$ and $\ell = 2$ and confirmed the $\ell = 0$ is more unstable. We do not reproduce those results here.

The equation has to be solved subject to appropriate boundary conditions. A Taylor expansion of the KG equation about the horizon yields the two linearly independent solutions:

$$\psi(R)\big|_{R\to R_+} \sim \beta_{in}(R-R_+)^{-\frac{i\Omega}{4\pi T_H L}} + \beta_{out}(R-R_+)^{\frac{i\Omega}{4\pi T_H L}} + \cdots . \tag{4.3.19}$$

Regularity of the perturbation in Eddington-Finkelstein coordinates requires that we choose the boundary condition $\beta_{out} = 0$ (this effectively discards outgoing modes and keeps the ingoing waves).

On the other hand, a Taylor expansion around the location $R = 1$ of the box yields:

$$\psi(R)\big|_{R\to 1} \sim \psi_0 + \psi_1(R-1) + \cdots . \tag{4.3.20}$$

[6]For concreteness, in the presentation of our results, we will fix the scalar field mass to zero, but the computation can be repeated for different masses m. In all cases, the onset curve $e_{onset}(R_+, \mu; m)$ for the instability approaches the analytical limiting values (4.3.8) and (4.3.16), see the numerical results in our publication [2].

We want the scalar field to vanish at the location of the box so we impose the Dirichlet boundary condition $\psi_0 = 0$.

In order to solve numerically equation (3.0.9) we introduce the new function $p(R)$ as

$$\psi(R) = (R - R_+)^{-\frac{i\Omega}{4\pi T_H L}} (1 - R)\, p(R). \tag{4.3.21}$$

In addition, we find it convenient (it yields a Neumann boundary condition at the horizon) to work with the new radial variable

$$y = \left(\frac{R - R_+}{1 - R_+}\right)^{\frac{1}{2}}. \tag{4.3.22}$$

Coordinate y ranges between $y = 0$ ($R = R_+$) and $y = 1$ ($R = 1$). In terms of the new function $p(y)$, the boundary conditions read

$$p'(0) = 0\,, \qquad p'(1) + \left(\frac{\left(\mu^2 + 2\right) R_+ - 4}{\mu^2 R_+ - 2} - \frac{4 i R_+ \Omega}{2 - \mu^2}\right) p(1) = 0. \tag{4.3.23}$$

The ODE (3.0.9) and the boundary conditions (4.3.23) yield a quadratic eigenvalue problem in the frequency Ω, for a given e. Interestingly, if we we want to find the onset of an instability (which has $\Omega = 0$), it is also a quadratic eigenvalue problem in the electric scalar field charge e. We will explore both perspectives in our analysis.

For the numerical discretization scheme of $y \in [0, 1]$ we use pseudo-spectral methods with a Chebyshev grid (see details in [50] and Appendix A). We solve for the eigenvalue and associated eigenfunction using one of two methods. In one method, we make use of the fact that the equation at hand is a quadratic eigenvalue problem, which can thus be solved using *Mathematica*'s built-in routine *Eigensystem* (see *e.g.* [52, 50] and section A.2 in Appendix A for details). The second method is based on an application of the Newton-Raphson root-finding algorithm, and is detailed in [30, 50] and in section A.3 of Appendix A.

We can now discuss the results. The system is unstable when the imaginary part of the frequency $\Omega = \omega L$ is positive. An indication of the onset of the instability is given when we encounter what are called the zero-modes which correspond, in our gauge choice, to $\Omega = 0$: $\mathrm{Re}\,\Omega = 0 = \mathrm{Im}\,\Omega$. We find it enlightening to present the results by picking different values of the chemical potential μ and plotting the dependence of the onset charge e_{onset} as a function of the horizon radius R_+. This plot is shown in the left panel of Fig. 4.3.2. The curves with the dots describe the onset charge e_{onset} as a function of the horizon radius for a given choice of chemical potential μ. More concretely, we consider 5 values for μ. We set $\mu = \sqrt{2}(1 - 10^{-n})$ and from the top (black curve) to the bottom (red curve) the 5 curves

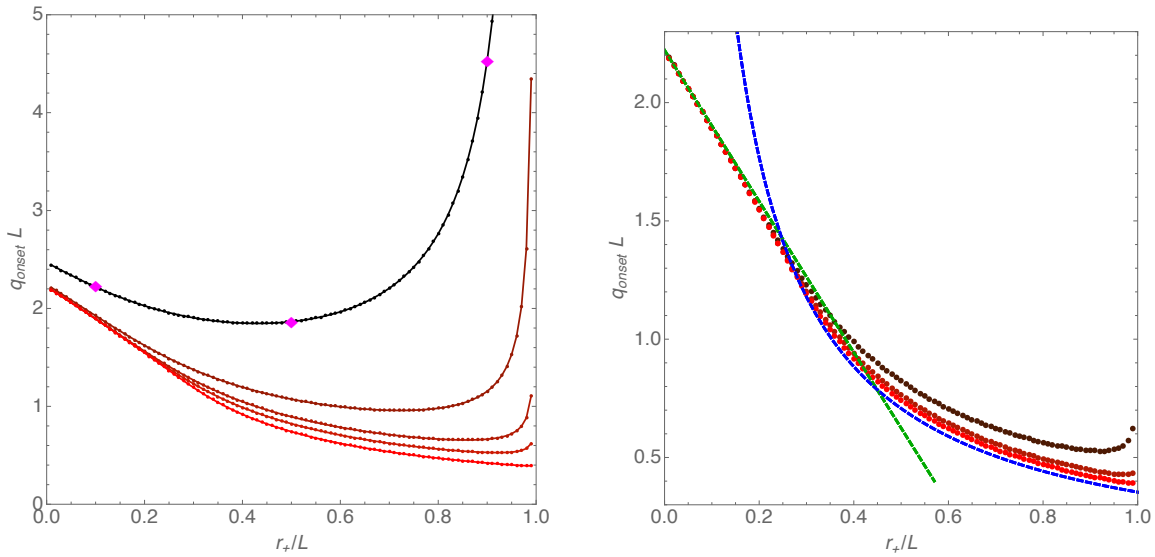

Figure 4.3.2: **Left panel:** Electric charge $e_{onset} = Lq_{onset}$ of the scalar field that signals the onset of instabilities for RN BHs in a box as a function of the horizon radius $R_+ = r_+/L$, and for 5 constant values of the chemical potential $\mu = \sqrt{2}(1 - 10^{-n})$ with $n = 1, 2, 3, 4, 8$ from top (black) to bottom (red). Above these lines, RN BH are unstable as the imaginary part of the frequency Ω is positive. The magenta diamonds pinpoint three particular RN BHs: in the right panel of Fig. 4.3.3 we explicitly show that $\mathrm{Im}\,\Omega$ changes sign precisely at $e = e_{onset}$ identified in this figure. **Right panel:** Similar to left panel but this time we plot the onset curves (dots) with $\mu = \sqrt{2}(1 - 10^{-n})$ with $n = 4, 6, 8$ to see the approach to extremality (which occurs when $\mu = \sqrt{2}$), and we add the analytical curves (4.3.10) (dashed green straight line with negative slope) and (4.3.16) (dashed blue curve).

have $n = 1, 2, 3, 4, 8$.

To further interpret the left panel of Fig. 4.3.2, note that, previously in the literature (first for a scalar field in a Kerr box [140, 141] and then for a charged scalar field in a RN box [108, 119]) it was found that, for a given scalar field charge, there is a minimum critical radius where the mirror can be placed to have an instability. If the mirror is placed below this critical radius there is no instability, that is to say, would-be unstable modes cannot fit inside the box. The superradiant condition allows a straightforward interpretation of this result: in the gauge where the gauge potential vanishes asymptotically, superradiant modes have a maximum frequency, $\mathrm{Re}\,\widetilde{\omega} < q\mu$. Superradiant modes thus have a minimum wavelength and the mirror must be placed at a radius larger than this wavelength if we want to have unstable modes. Now, in our study we use a scaling symmetry of the system to fix the mirror at the dimensionless radius $R = 1$. It follows that the above conclusion restates as follows: for a given RN BH (i.e. for a given $\{R_+, \mu\}$) unstable modes are present if and only if the scalar field charge is above a critical value $e > e_{onset}(R_+, \mu)$. Fig. 4.3.2 precisely displays these critical curves $e_{onset}(R_+, \mu)$ for selected values of μ. These curves are exact (for $M = 0$) and sharpen onset bounds given previously in [108, 119].

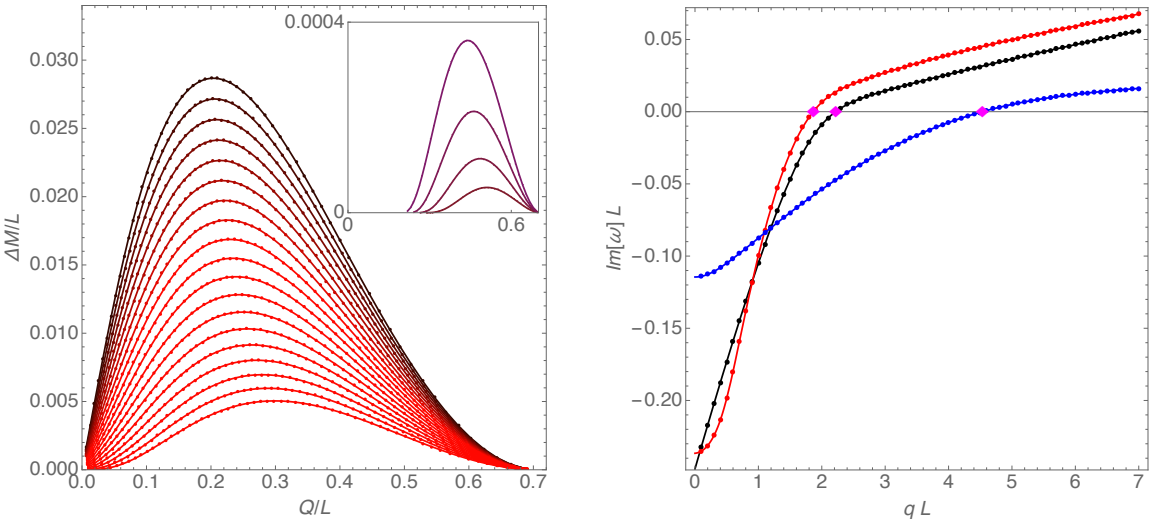

Figure 4.3.3: **Left panel:** Onset curves in a phase diagram that plots the RN electric charge Q/L as a function of the mass difference $\Delta M/L$ w.r.t. the extremal RN with same Q/L. The several curves have different constant scalar field charge: $e_{onset} = 4$ (upper curve) all the way down (in steps of -0.1) to $e_{onset} = 2.2$ (bottom curve). The curves in the inset plot correspond to scalar field charges $e_{onset} = 1.3$ (top) down to $e_{onset} = 1$, in steps of -0.1. **Right panel:** Imaginary part of the dimensionless frequency $\mathrm{Im}\,(\omega L)$ as a function of the dimensionless scalar field charge $e = qL$ at constant chemical potential $\mu = \sqrt{2}(1 - 10^{-1})$ and constant horizon radius: $R_+ = 0.1$ (black), $R_+ = 0.5$ (red) and $R_+ = 0.9$ (blue). The magenta diamonds correspond precisely to the onset charge $e = e_{onset}$ already identified in Fig. (4.3.2).

In the left panel of Fig. 4.3.2, the lowest numerical (red) curve has $\mu = \sqrt{2}(1-10^{-8})$ i.e. it is extremely close to the extremal RN solution which has $\mu = \sqrt{2}$. This curve is particularly enlightening to understand the underlying physical nature of the unstable modes, and how the origin of the instability changes as we go from small to large radius black holes (in units of the mirror radius). For this discussion, in the right panel of 4.3.2 we take the bottom curve of the left panel with $\mu = \sqrt{2}(1 - 10^{-8})$ (as well as as $\mu = \sqrt{2}(1 - 10^{-4})$ and $\mu = \sqrt{2}(1 - 10^{-6})$) and we add two analytical curves. The dashed green straight line with negative slope (starting at $R_+ = 0$ and $e_{onset} = \pi/\sqrt{2} \sim 2.22$) is the superradiant instability curve (4.3.10), which is valid for small R_+. On the other hand, the blue dashed curve (starting on the right at $R_+ = 1$ and $e_{onset} = \frac{1}{2\sqrt{2}} \sim 0.354$) corresponds to the near-horizon instability curve (4.3.16) with $M = 0$, $e_{onset} = (2\sqrt{2}R_+)^{-1}$. We conclude that as extremality ($\mu = \sqrt{2}$) is reached, the onset curve approaches the critical values predicted by the analytical expressions (4.3.10) and (4.3.16) (with $M = 0$ and $\mu = \mu_{ext} = \sqrt{2}$). This is a check of our numerical results. More importantly, it clearly demonstrates one of our main results: RN BHs in a box are not only afflicted by the superradiant instability (as studied in previous literature) but also by the near-horizon scalar condensation instability. For a generic RN BH these two instabilities are entangled but in the RN extremal limit they disentangle and their different nature unravels: the superradiant instability is present for small black holes while the near-horizon instability has the opposite behavior (it is

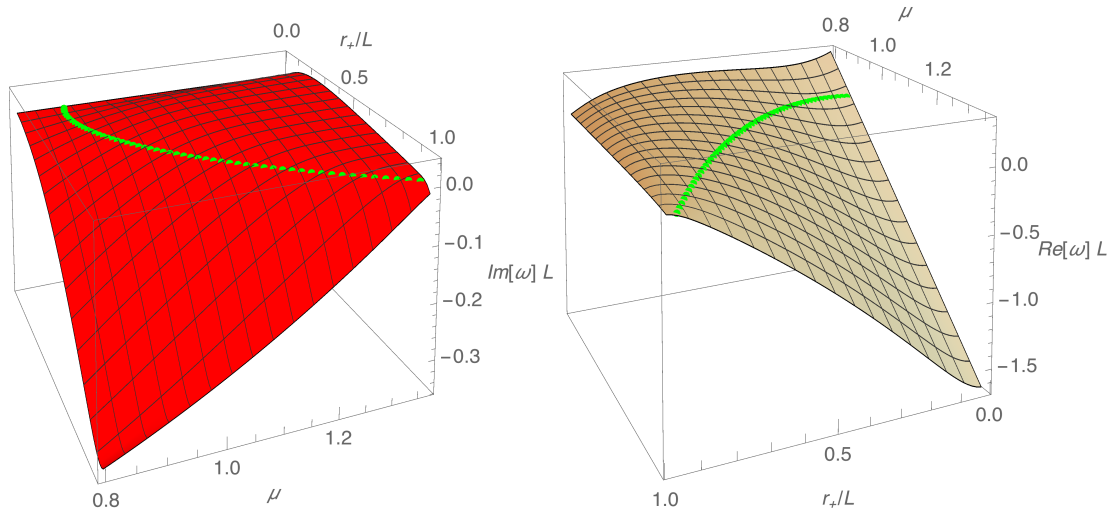

Figure 4.3.4: The imaginary part (**left panel**) and real part (**right panel**) of the frequencies as a function of the chemical potential μ and the horizon radius r_+ for $e = qL = 3.5$. The dotted green curve is the onset curve with $\mathrm{Re}(\omega L) = 0$ and $\mathrm{Im}(\omega L) = 0$.

supressed for small black holes as indicated by (4.3.18)).

The information in Fig. 4.3.2 is complemented by Fig. 4.3.3. In the left panel, on the horizontal axis we have the dimensionless ADM charge Q/L of the RN BH. On the vertical axis, we have the mass difference $\Delta M/L = (M - M_{ext})/L$ between a RN BH and the extremal RN BH that has the same electric charge Q/L. Hence extremal RN BHs are represented by the horizontal line with $\Delta M = 0$. We display several curves in the main left panel plot. Each curve corresponds to a fixed value for the onset charge e_{onset} (a horizontal line in Fig. 4.3.2): the top curve starts with $e_{onset} = 4$ and then we go down in steps of $\delta e_{onset} = -0.1$ to the curve in the bottom that has $e_{onset} = 2.2$. For each e_{onset} curve, RN BHs below the onset curve are unstable. We see that, starting from $Q = 0$, as Q grows so does the region that is unstable: black holes with larger M/L that are further away from extremality become unstable. However, for each e_{onset} curve, $\Delta M/L$ attains a maximum around $Q/L \sim 0.2$. For larger Q/L, $\Delta M/L$ starts decreasing monotonically and approaches zero as Q/L approaches its maximum value ~ 0.7, which corresponds to $R_+ \to 1$.

It is often stated that a RN in a Minkowski box resembles a RN in global anti-de Sitter (AdS) spacetime: reflecting boundary conditions at the timelike boundary of AdS mean that AdS effectively behaves as a box with AdS radius L (set by the cosmological constant $\Lambda = -3/L^2$). Although this statement is generically correct, there are also important differences between the two systems. Notably, the box in the RN BH is at a finite proper distance from the horizon, while in AdS the asymptotic timelike boundary is at an infinite proper distance. This key difference manifests in properties of the instabilities. This is particularly clear when we compare the behaviour displayed in Fig. 4.3.3 with its AdS

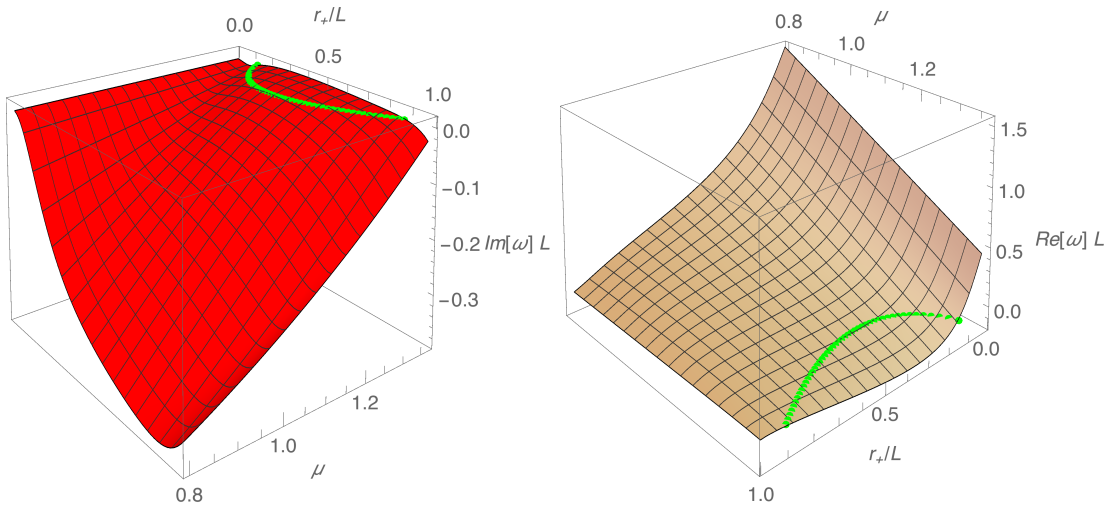

Figure 4.3.5: Similar to Fig. 4.3.4 but this time for a scalar field charge of $e = 1.9$. The dotted green curve is the onset curve with $\mathrm{Re}(\omega L) = 0$ and $\mathrm{Im}(\omega L) = 0$.

counterpart. In AdS, all onset curves e_{onset} are monotonic: larger Q/L corresponds to larger $\Delta M/L$ (below which the system is unstable) and there is no bound for the electric charge Q/M (neither for M/L); see [126] for the corresponding plot for RN-AdS$_5$ BHs. For small RN BHs inside a box, the system behaves similarly to the AdS one only for small Q/L: initially $\Delta M/L$ of the onset curve indeed increases as Q/L grows. However, unlike in AdS, here the e_{onset} curve has a maximum $\Delta M/L$ and, for larger RN charge, Q/L itself also has a maximum value where $\Delta M/L \to 0$. So above $Q/L \sim 0.2$ (say), the box at finite proper distance induces an effect that differs from the behaviour in AdS. This behaviour can be understood from Fig. 4.3.1: as we increase the charge Q/L and the mass M/L, the region of existence of RN BHs inside a box becomes smaller and shrinks to zero as one approaches $Q/L \sim 0.7$. This is not the case in global AdS: unstable RN-AdS BHs exist for arbitrarily large charge and mass.

Still in the left panel of Fig. 4.3.3, in the inset plot we show similar curves for scalar field charges $e_{onset} = \{1.3, 1.2, 1.1, 1\}$ which are all below $\frac{\pi}{\sqrt{2}} \sim 2.22$. We see that for $e \leq \frac{\pi}{\sqrt{2}}$ the onset does not extend to all values of the charge Q/L and mass M/L since these e's lie in the region $\frac{1}{2\sqrt{2}} \leq e \leq \frac{\pi}{\sqrt{2}}$ (see Fig. 4.3.2). Indeed, one can use the bottom curve in the Fig. 4.3.2, since $\mu = \sqrt{2}(1 - 10^{-8})$ is very near extremality, as a good estimative of the extremal curve. The curves in the inset plot of the right panel of Fig. 4.3.3 correspond to horizontal lines in Fig. 4.3.2 with $\frac{1}{2\sqrt{2}} \leq e \leq \frac{\pi}{\sqrt{2}}$ that start at the extremal curve.

To check independently that the onset curves (surface) in Fig. 4.3.2 indeed signal the onset of the instability we have computed the quasinormal mode frequencies $\Omega = \omega L$: above the onset surface the imaginary part of Ω becomes positive. For a simple check, we chose specific values of the horizon radius R_+ and chemical potential μ and compute the imaginary part of the frequency $\mathrm{Im}\,\Omega$ as a function of the scalar field charge $e = qL$.

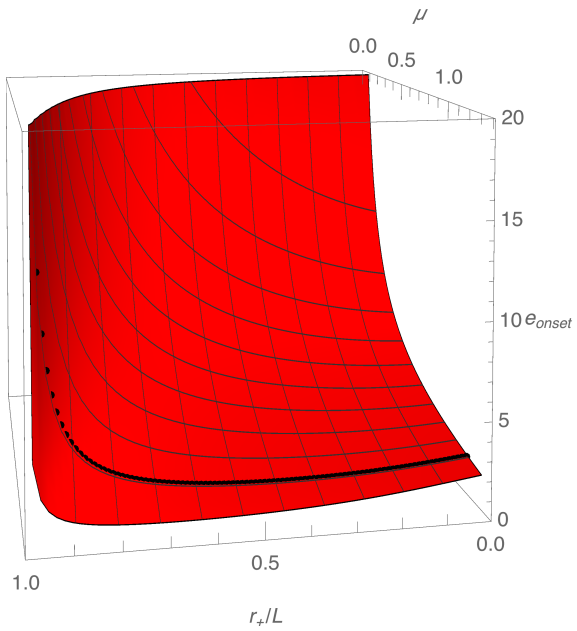

Figure 4.3.6: Critical onset charge e_{onset} as a function of the horizon radius R_+, and of the chemical potential μ. For reference, the black dots represent the curve with $\mu = \sqrt{2}(1-10^{-1})$ already plotted in the top of the left panel of Fig. 4.3.2.

We show three of these curves in the right panel of Fig. 4.3.3. All these curves have $\mu = \sqrt{2}(1-10^{-1})$ but different horizon radius, $R_+ = \{0.1, 0.5, 0.9\}$. These particular RN BHs correspond to the magenta diamonds pinpointed in the upper curve of the left panel of Fig. 4.3.2. That is to say, at the value $e = e_{onset}$ identified in the left plot of Fig. 4.3.2 the imaginary part of the frequency becomes zero in Fig. 4.3.3 (magenta dots in each curve) which is a check to our numerics as these are two independent computations.

For completeness, in Fig. 4.3.4 we fix the scalar field charge $e = 3.5$ and we show a complete 3D plot of both the imaginary and real parts of the dimensionless frequency $\Omega = \omega L$ as a function of the horizon radius R_+ and chemical potential μ. The instability is present when $\mathrm{Im}\,\Omega > 0$. As a non-trivial test of our computations we have checked that the instability onset curve for $e_{onset} = 3.5$ in the left panel of Fig. 4.3.3 coincides with the onset curve in this 3D plot: dotted green curves with $\mathrm{Im}\,\Omega = 0$ and $\mathrm{Re}\,\Omega = 0$. Values of e above $\pi/\sqrt{2} \sim 2.221$ − see (4.3.10) and Fig. 4.3.2− typically give plots qualitatively similar to those of Fig. 4.3.4. Namely, the instability is present from $R_+ = 0$ all the way up to a maximum $R_+ < 1$, as long as we are sufficiently close to extremality.

On the other hand, scalar field charges in the range $\pi/\sqrt{2} < e < 1/(2\sqrt{2}) \sim 0.354$ − see (4.3.10), (4.3.16) and Fig. 4.3.2− give plots qualitatively similar to those in Fig. 4.3.5. In this figure, we fix $e = 1.9$ and plot the imaginary and real parts of the frequency as a function of the horizon radius R_+ and chemical potential μ. For this range of e, the instability is present only in a window of R_+ (starting at $R_+ > 0$), and when we are close

to extremality.

Fig. 4.3.6 complements Fig. 4.3.2 since it shows the evolution of the onset charge e_{onset} with R_+ for a larger range of the chemical potential μ. Namely, for $\mu \leq \sqrt{2}\left(1-\frac{1}{61}\right)$ (for larger μ see Fig. 4.3.2). We see that as we move away from extremality and as the box approaches the horizon, it becomes considerably more difficult to drive the system unstable. In the sense that a higher $e > e_{onset}$ is required to make the system unstable.

4.4 Non-interacting thermodynamic model for hairy black holes

In the previous sections we have seen that RN BH both in AdS_4 and confined inside a box are linearly unstable to the superradiant and near-horizon scalar condensation instabilities. Thus one expects these BHs should evolve to a different configuration that should have scalar hair floating above the horizon (as shown in [51, 125, 126, 107, 118]). This new configuration is stable to the original mechanisms that drive RN BH unstable. In the limit where the amplitude of the scalar hair vanishes, such hairy black hole should merge with the RN family at the onset of the instability.

On the other hand, a scalar field in AdS_4 and inside a box in Minkowski space has its linear spectrum of frequencies quantized as we saw in (4.2.5) and (4.3.6). Borrowing ideas from similar AdS and massive systems with confined potentials, it is natural to expect that such normal modes of the scalar field can be back-reacted to higher order in perturbation theory (with the expansion parameter being the amplitude of the scalar field). That is to say, beyond linear order, the scalar field sources the gravitoelectric field but it should be possible to do so while keeping the solution regular everywhere (in particular, at the origin) and obeying the boundary conditions. This should then yield a new horizonless solution of Einstein-Maxwell-scalar theory (with the confinement condition imposed) that is a boson star oscillating with frequency $\tilde{\omega}$ (if we work in a gauge where the scalar field is complex with time dependence $e^{i\tilde{\omega}t}$) or, equivalently after a gauge transformation, a static soliton (with no time dependence and chemical potential $\mu = \tilde{\omega}/q$).

Again borrowing ideas from similar confined systems, it is also natural to expect that we can place a standard RN BH on top of this soliton to generate a hairy black hole. This hairy black hole family whose zero-horizon radius is the soliton of the theory should then be the same hairy black hole that connects (in a phase diagram of solutions) to the RN BH family at the onset of the instability discussed above.

Such hairy solitons and black holes would have a charged scalar condensate floating above

the origin/horizon, with the electromagnetic repulsion balancing the gravitational collapse of the scalar condensate. For these ideas to be correct, in the case of the hairy black hole, we further expect that hairy black holes have higher entropy than the RN BH with the same mass and electric charge (when they coexist).

To prove these ideas correct, we have to solve the Einstein-Maxwell-scalar equations of motion and find the proposed hairy black hole solutions. We will do this in sections 5 and 6. However, here we want to derive heuristically the *leading order* thermodynamic properties of such hairy solutions using a simple non-interacting thermodynamic model that does *not* make use of the equations of motion. This model proved to capture the correct leading order physics of charged and rotating AdS systems [51, 53, 126, 30, 98, 125, 128].

At leading order, a charged soliton (boson star) is just a normal mode of the ambient background (whose frequency $\tilde{\omega}$ is then corrected as we climb the perturbation expansion ladder). This is a 1-parameter family of solutions with mass $\mathcal{M}_{sol} = \mu\,\mathcal{Q}_{sol} + \mathcal{O}(\mathcal{Q}^2)$ with $\mu = \frac{\tilde{\omega}}{q}$ (we are interested in the soliton with lowest energy which has $\mu = 3/e$ in the AdS case and $\mu = \pi/e$ in the box case). This soliton further obeys the first law, $d\mathcal{M}_{sol} = \mu\, d\mathcal{Q}_{sol}$.

The non-interacting thermodynamic model of [51, 53, 126, 30, 98, 125, 128] assumes that we can place a small RN BH on top of this soliton to get a 2-parameter family of hairy BHs (the parameters being the mass and the charge). It further assumes that, at leading order (and certainly only at this order), the system can be considered as a *non*-interacting mixture of a soliton and a RN BH at its core in the sense that the mass and the charge of the hairy BH are given by the direct sum of the mass and charge of the RN BH and the soliton,

$$\mathcal{M} = \mathcal{M}_{sol} + \mathcal{M}_{RN} \quad \text{and} \quad \mathcal{Q} = \mathcal{Q}_{sol} + \mathcal{Q}_{RN}. \tag{4.4.1}$$

The soliton carries no entropy, so the entropy S of the hairy BH simply reads

$$S = S_{RN}(\mathcal{M}_{RN}, \mathcal{Q}_{RN}) + S_{sol}(\mathcal{M}_{sol}, \mathcal{Q}_{sol}) = S_{RN}(\mathcal{M} - \mathcal{M}_{sol}, \mathcal{Q} - \mathcal{Q}_{sol}). \tag{4.4.2}$$

The hairy BH can partition its charge $\mathcal{Q}$ and mass $\mathcal{M}$ between the RN BH and soliton components. On physical grounds one expects this distribution to be such that, for fixed mass $\mathcal{M}$ and charge $\mathcal{Q}$, the entropy S is maximised, $dS = dS_{RN} = 0$, while respecting the first law of thermodynamics $\mathrm{d}\mathcal{M} = T_H \mathrm{d}S + \mu \mathrm{d}\mathcal{Q}$. The maximisation of the entropy turns out to imply [126]

$$\mu_{RN} = \mu_{sol} \equiv \mu \quad \text{and} \quad T_{RN} \equiv T_H, \tag{4.4.3}$$

not surprisingly, the two mixed constituents must be in thermodynamic equilibrium to

yield a hairy BH.

The mass and charge of the soliton are related by $\mathcal{M}_{sol} = \mu\mathcal{Q}_{sol}$, while the mass and charge of the RN BH are given in (4.2.10) and (4.3.2) (recall that both cases have the same leading terms in an expansion in R_+) . Using these relations together with the non-interacting relation (4.4.1) and equilibrium conditions (4.4.3), we can express the leading order thermodynamic quantities of the hairy black hole (and of its two constituents) in terms of its mass $\mathcal{M}$, charge $\mathcal{Q}$ and chemical potential μ:

$$\begin{aligned}
R_+ &= \frac{4}{2-\mu^2}(\mathcal{M}-\mu\mathcal{Q}) + \mathcal{O}\left(\mathcal{M}^2,\mathcal{Q}^2,\mathcal{M}\mathcal{Q}\right),\\
TL &= \frac{\left(2-\mu^2\right)^2}{32\pi(\mathcal{M}-\mu\mathcal{Q})} + \mathcal{O}\left(\mathcal{M}^2,\mathcal{Q}^2,\mathcal{M}\mathcal{Q}\right),\\
S/L^2 &= \frac{16\pi}{\left(2-\mu^2\right)^2}(\mathcal{M}-\mu\mathcal{Q})^2 + \mathcal{O}\left(\mathcal{M}^3,\mathcal{Q}^3,\mathcal{M}^2\mathcal{Q},\mathcal{M}\mathcal{Q}^2\right);\\
\mathcal{M}_{RN} &= \frac{\left(2+\mu^2\right)}{2-\mu^2}(\mathcal{M}-\mu\mathcal{Q}) + \mathcal{O}\left(\mathcal{M}^2,\mathcal{Q}^2,\mathcal{M}\mathcal{Q}\right),\\
\mathcal{M}_{sol} &= \frac{\mu\left(2+\mu^2\right)\mathcal{Q}-2\mu^2\mathcal{M}}{2-\mu^2} + \mathcal{O}\left(\mathcal{M}^2,\mathcal{Q}^2,\mathcal{M}\mathcal{Q}\right),\\
\mathcal{Q}_{RN} &= \frac{2\mu}{2-\mu^2}(\mathcal{M}-\mu\mathcal{Q}) + \mathcal{O}\left(\mathcal{M}^2,\mathcal{Q}^2,\mathcal{M}\mathcal{Q}\right),\\
\mathcal{Q}_{sol} &= \frac{\left(2+\mu^2\right)\mathcal{Q}-2\mu\mathcal{M}}{2-\mu^2} + \mathcal{O}\left(\mathcal{M}^2,\mathcal{Q}^2,\mathcal{M}\mathcal{Q}\right).
\end{aligned} \tag{4.4.4}$$

The domain of existence of the hairy black hole can be inferred from this analysis. In one extremum, the soliton constituent is absent and all the mass and charge of the hairy BH is carried by the RN component. This describes the hairy BH that merges with the RN BH at the zero-mode of its linear instability. On the opposite extremum configuration, the RN BH constituent is absent and the soliton component carries all the mass and charge of the solution. This is the zero-radius or zero-entropy limit of the hairy black hole. It follows that the hairy black hole mass must be within these two boundaries:

$$\mu\mathcal{Q}+\mathcal{O}(\mathcal{Q}^2) \leq \mathcal{M} \leq \frac{\mu^2+2}{2\mu}\mathcal{Q}+\mathcal{O}(\mathcal{Q}^2). \tag{4.4.5}$$

Equating the two extrema configurations, yields an interval of existence for the chemical potential:

$$\mu \leq \frac{\mu^2+2}{2\mu} \quad \Rightarrow \quad \mu \leq \sqrt{2} \quad \Longrightarrow\ e \geq \frac{\omega_0}{\sqrt{2}}, \tag{4.4.6}$$

where in the last relation we used that for the ground state solution the leading order potential is $\mu = \tilde{\omega}/e = \omega_0/e + \mathcal{O}(R_+)$ and $\omega_0 = 3$ or π for the AdS and box case respectively. The lower bound for e in (4.4.6) is precisely the leading term in (4.2.22) and (4.3.10) when

we set the chemical potential to its extreme value, $\mu = \sqrt{2} + \mathcal{O}(R_+^2)$.

The above leading order thermodynamic analysis must be considered with a few grains of salt. Indeed, first note that a theory can have hairy black holes that do not have a zero-radius limit, *i.e.* a solitonic limit (see *e.g.* [126]). Second, there is no reason why the non-interacting mixture assumption (4.4.1) should hold, even at leading order. Nevertheless, in Chapters 5 and 6, we will solve the equations of motion to find the hairy BHs and we will confirm that the thermodynamic model indeed captures the correct leading order thermodynamics (4.4.4)-(4.4.6) of the system.

A final important observation is in order for the boxed case. To keep the scalar field of the asymptotically flat hairy black hole confined inside the box ($\phi(R \geq 1) = 0$), the latter must have a certain Lanczos-Darmois-Israel surface stress tensor [142, 143, 144, 145]. That is to say, the induced gravitoelectric fields are continuous at the thin layer surface that confines the scalar hair but the extrinsic curvature is discontinuous. The above thermodynamic model is completely blind to this information. It is too simple for that; yet it yields the correct leading thermodynamics. In Chapter 6, we will emphasize the importance of using the Brown-York quasilocal formalism [146] to appropriately discuss hairy black holes contained inside a box, for the difference between the Brown-York tensor outside and inside the box surface layer yields precisely the Lanczos-Darmois-Israel surface stress tensor [142, 143, 144, 145] that describes the energy-momentum content of the box [146].

CHAPTER 5

Small hairy black holes in AdS_4

In this Chapter we construct perturbatively hairy black holes that are the end-point of the superradiant instability discussed in the previous Chapter. We analyse the microcanonical ensemble in order to determine the dominating phases.

5.1 Summary of results

The superradiant instability studied in the previous Chapter is present in small AdS-Reissner-Nordström black holes. This implies that the associated hairy black holes can be constructed perturbatively around global AdS as a small expansion in the horizon radius and in the scalar condensate amplitude [51, 125, 126]. In fact, one can construct perturbatively, in the scalar condensate amplitude, horizonless solutions by considering the backreaction of the normal modes computed in (4.2.5). These solutions constitute the solitons 5.4 of the theory and as seen in the non-interacting thermodynamic model of 4.4, they form at linear level the hair of hairy black holes.

In the case of hairy black holes, the double expansion in the horizon radius and the scalar field amplitude is not enough to exactly solve the equations of motion of the system (3.0.6). We make use of a standard matching asymptotic expansion procedure (see e.g. [51, 125, 126, 53, 97] and section 4.2.3) in which one considers a near region $\frac{r_+}{L} \leq \frac{r}{L} \ll 1$ and a

far region $r \gg r_+$ which overlap in the region $\frac{r_+}{L} \ll \frac{r}{L} \ll 1$ if we consider small black holes, $\frac{r_+}{L} \ll 1$. The resulting thermodynamic quantities of the hairy black hole − energy, charge, chemical potential, temperature and entropy − are then computed in (5.5.6) and obey the first law of thermodynamics. Confirming the rationale beyond their construction, hairy black holes merge with the RN-AdS$_4$ family at the onset of superradiance and their zero-horizon radius limit is a soliton.

The hairy black holes and solitons of the theory add new competitions in the phase diagram. It turns out that, as summarized in the phase diagrams of Fig. 5.6.1, in the microcanonical ensemble hairy black holes are always the dominant thermal phase.

Summarizing our results, the phase diagram of AdS$_4$-Einstein-Maxwell theory with a complex scalar field depends on the window of the dimensionless scalar field charge e that we consider. There are three cases:

- $e^2 < \frac{3}{2}$: in this case RN-AdS$_4$ is stable both against superradiance and the near-horizon scalar condensation instability. Thus, there are no hairy black hole solutions. We do have a 1-parameter soliton family.

- $\frac{3}{2} \leq e^2 \leq \frac{9}{2}$: the near horizon instability takes place near extremality for large RN-AdS$_4$ black holes, i.e. only above a critical mass and charge. Consequently, the associated *large* hairy black hole solutions cannot be constructed perturbatively and would require a full non-linear numerical construction.

- $e^2 \geq \frac{9}{2}$: Small RN-AdS$_4$ black holes are unstable to the superradiant instability and the associated hairy black holes can be constructed perturbatively for small mass and charge (see section 5.5). They are a 2-parameter family of solutions that in a phase diagram span an area bounded by the onset of superradiance (where they merge with RN-AdS$_4$) and, at their zero-horizon radius limit, the soliton (see Fig. 5.6.1). These hairy black holes always have higher entropy than the RN-AdS$_4$ black hole in the window of energy and charge where the two phases co-exist. Interestingly, in the phase diagram of solutions of the theory, the hairy black holes connect the onset of the (linear) superradiant instability with the key player − the soliton − of the non-linear weakly turbulent instability of AdS$_4$. Indeed, at the simplest but fundamental level, this non-linear instability follows from the appearance of irremovable secular resonances when two or more solitons are taken as initial data and collide [64, 78, 147].

The Chapter is structured as follows: In section 5.2 we introduce the boundary conditions for the elliptic problem, and describe how the thermodynamic quantities can be computed in 5.3. The soliton (boson star) of the theory is constructed perturbatively in section 5.4. In section 5.5, hairy black hole solutions are constructed perturbatively using a matched

asymptotic expansion analysis. The thermodynamical and physical properties of the hairy solutions are analysed in detail in the microcanonical ensemble in section 5.6. The expressions for the field coefficients that appear in the perturbative expansions of the soliton construction of section 5.4 and of the hairy black hole of section 5.5 can be found in Appendix B and C of [1] respectively.

5.2 Boundary conditions

We consider the theory described by (3.0.1) with cosmological constant $\Lambda = -\frac{3}{L^2}$, and solutions to the theory of the form (3.0.2). The set of equations of motion of the theory are given in (3.0.6). In this Chapter we are restricting to massless scalar fields.

The most notable solution of (3.0.1) is global AdS_4 spacetime: $f(R) = g^{-1}(R) = 1 + R^2$ $A(R) = \phi(R) = 0$. We are interested in solutions that asymptote to this background.

We can rewrite our ansatz and equations of motion in Fefferman-Graham coordinates (defined such that $g_{zz} = 1/z^2$ and $g_{zb} = 0$, where z is the radial distance with boundary at $z = 0$, and $x^b = \{t, \theta, \psi\}$ are the boundary coordinates) [148, 149, 23]. In general an asymptotically AdS_4 spacetime has the following Taylor expansion of the metric around the holographic boundary $z = 0$ [27, 29] (and 1.2.3):

$$
\begin{aligned}
&ds^2 = \frac{1}{z^2}\left[\mathrm{d}z^2 + g_{ab}(z,x)\mathrm{d}x^a\mathrm{d}x^b\right] , \\
&g_{ab}\big|_{z\to 0} = g^{(0)}_{ab}(x) + \cdots + z^3 g^{(3)}_{ab}(x) + \cdots , \quad \text{with} \quad \langle T_{ab}\rangle \equiv \frac{3}{16\pi G_4}\, g^{(3)}_{ab}
\end{aligned}
\tag{5.2.1}
$$

and where $g^{(0)}(x)$ and $g^{(3)}(x)$ are the two integration "constants" of the expansion[1]; the first dots include only even powers of z (smaller than 3) and depend only on $g^{(0)}$ (thus being the same for solutions that asymptote to global AdS_4) while the second dots depend on the two independent terms $g^{(0)}, g^{(3)}$. Within the AdS/CFT duality we are (typically) interested in Dirichlet boundary conditions (BCs) that do not deform the conformal metric $g^{(0)}$: the dual holographic CFT is formulated on this fixed background (see Chapter 1). This is the static Einstein Universe $\mathbb{R}_t \times S^2$, $ds^2_\partial = -dT^2 + d\Omega^2_{(2)}$. Given this Dirichlet BC our task is to solve the equations of motion in the bulk, subject to regular BCs at the horizon or radial origin, to read $g^{(3)}$. Using the holographic renormalization formalism, this gives us the expectation value of the holographic stress tensor $\langle T_{ab}(x)\rangle$ which specifies and describes the boundary CFT [29, 26, 27]. This Dirichlet BC also ensures that there is no dissipation of energy at the asymptotic boundary (see Appendix A of [30]). For this reason these Dirichlet BCs can be denoted as 'reflecting boundary conditions' [2].

[1] Our solutions are static and spherically symmetric so there is no x dependence.

[2] We can however have other reflecting BCs that preserve the charges but not the static Einstein Universe

We still need to discuss the asymptotic BCs for the Maxwell and massless scalar fields. A Taylor expansion of the equations of motion at the conformal boundary yields,

$$\begin{aligned} A_t(R) &\simeq \mu + \frac{\rho}{R} + \cdots \\ \phi(R) &\simeq \frac{\sigma}{R^{\Delta_-}} + \cdots + \frac{\varepsilon}{R^{\Delta_+}} + \cdots , \quad \text{with} \quad \Delta_\pm = \frac{3}{2} \pm \frac{3}{2} , \end{aligned} \tag{5.2.2}$$

where μ and ρ are the chemical potential and charge density, respectively, and ε and σ are the two arbitrary integration constants describing the decay of the massless scalar field. Since we are considering massless scalar fields, normalisability implies that $\sigma = 0$, see (4.2.2) and the discussion below.

To summarize, at the asymptotic boundary ($R \to \infty$) we will impose Dirichlet BCs such that our solutions at large R behave as

$$\begin{aligned} f(R) &= 1 + R^2 + \frac{m_0}{R} + \mathcal{O}(1/R^2), \\ A(R) &= \mu + \frac{\rho}{R} + \mathcal{O}(1/R), \\ \phi(R) &= \frac{\varepsilon}{R^3} + \mathcal{O}(1/R^5) \end{aligned} \tag{5.2.3}$$

with the dots representing terms that are a function of $m_0, \mu, \rho, \varepsilon$.

Consider now the inner boundary of our solution. This is a *fictitious* boundary since it is a coordinate singularity at the edge of our integration domain, but it is at a finite proper distance from other points [50]. In the present study, this can be the origin of the radial coordinate, $R = 0$, if we look into a soliton (boson star). Or, it can be a horizon at $R = R_+$ if the solution is a black hole, a condition that is imposed by demanding that $f(R_+) = 0$. In both cases to find the physical BCs we can Euclideanise the metric with a Wick rotation and require regularity of the metric and matter fields in Cartesian coordinates, as explained in detail in the review [50] [3].

For a soliton, a Taylor expansion of the equations of motion at the origin yields,

$$\begin{aligned} f(R) &= f_0 + \mathcal{O}\left(R^2\right), \\ A(R) &= a_0 + \mathcal{O}\left(R^2\right), \\ \phi(R) &= \phi_0 + \mathcal{O}\left(R^2\right), \end{aligned} \tag{5.2.4}$$

where $\{f_0, a_0, \phi_0\}$ are arbitrary integration constants and all higher order terms in (5.2.4) are even powers of R with coefficients fixed in terms of $\{f_0, a_0, \phi_0\}$. Here we have already imposed smoothness of the fields at the origin by imposing a *defining* BC (in the nomen-

conformal boundary.

[3] For the gauge field, this refers to the gauge invariant field strength tensor $F = \mathrm{d}A$, rather than the gauge potential A

clature of [50]). Namely, we set to zero three integration constants (one for each field f, g, and ϕ) which are associated to terms that diverge as $R \to 0$. Following the nomenclature of [50], if we wish, we can now use this defining BC together with the equations of motion to impose a *derived* BC to find the soliton. For example, it follows from (5.2.4) that a good derived BC is a Neumann BC for the three fields at $R = 0$ since the derivative of all of them vanishes.

On the other hand, if the solution is a black hole, a Taylor expansion around its horizon − defined as the locus $f(R_+) = 0$ − yields

$$\begin{aligned} f(R) &= f_0(R - R_+) + \mathcal{O}\left((R - R_+)^2\right), \\ A(R) &= a_0(R - R_+) + \mathcal{O}\left((R - R_+)^2\right), \\ \phi(R) &= \phi_0 + \mathcal{O}\left((R - R_+)^2\right), \end{aligned} \tag{5.2.5}$$

after imposing defining BCs that set three integration constants to zero (one for each function) to have smoothness as $R \to R_+$. We are left with the remaining three arbitrary integration constants $\{f_0, a_0, \phi_0\}$, and all higher order terms in (5.2.5) are fixed as a function of $\{f_0, a_0, \phi_0\}$.

At this stage we can ask how many parameters we need to describe the soliton and hairy black hole that we want to construct. The theory is fixed once we choose the mass and charge of the scalar field. At the UV asymptotic boundary we have a total of five free parameters $\{c_0, m_0, \mu, \rho, \varepsilon\}$ to which we need to add the cosmological radius L and the horizon radius R_+ (if present). As explained previously, we can use the two scaling symmetries (3.0.3) and (3.0.4) to fix L and c_0. We are left with four UV free parameters $\{m_0, \mu, \rho, \varepsilon\}$ and the horizon radius R_+. On the other hand, in the IR we have a total of three free parameters $\{f_0, a_0, \phi_0\}$ (both in the soliton and black hole case). Therefore, any black hole of the theory is described by $4_{UV} + 1_H - 3_{IR} = 2$ parameters. The AdS_4 −Reissner-Nördstrom black hole is indeed a 2-parameter family of black holes. More importantly, we also find that the hairy black holes we want to construct are described by two parameters. These are the mass and the electric charge of the black hole. Alternatively (but equivalently) we can take these to be the horizon radius R_+ and the amplitude of the scalar condensate ε. On the other hand, any soliton of the theory is described by $4_{UV} - 3_{IR} = 1$ parameter. This can be the mass of the soliton (which fixes its charge) or, alternatively, the amplitude of the scalar condensate ε.

5.3 Conserved and thermodynamic quantities

Once we have solved for the fields $\{f, g, A, \phi\}$ we can read the gauge invariant thermodynamic quantities that describe hairy black holes or solitons.

To find the energy we use holographic renormalization [29, 26, 27]. Applying the prescription to our ansatz with expansion at the boundary given by (5.2.3) the energy is defined as

$$\frac{M}{L} = -\frac{m_0}{2}. \tag{5.3.1}$$

To define the conserved electric charge, we use Gauss' law. Consider a 2-sphere S^2 at constant time t and R in the limit $R \to \infty$. The electrical charge is

$$Q = \lim_{R\to\infty} \frac{1}{16\pi} \int_{S^2} \star F, \tag{5.3.2}$$

where $\star F$ is the Hodge dual of the field strength. As a function of the asymptotic expansion parameters defined in (5.2.3) this gives,

$$\frac{Q}{L} = -\frac{\rho}{2}. \tag{5.3.3}$$

The value of the temperature for a soliton is undefined, and its entropy is zero as it does not have a horizon. Our black holes have a Killing horizon at $R = R_+$ generated by the Killing vector field $K = \partial_t$. Their temperature is thus given by its surface gravity over 2π which yields,

$$T_H L = \frac{1}{4\pi} \frac{f'(R)}{\sqrt{f(R)g(R)}}\Big|_{R_+}. \tag{5.3.4}$$

The entropy of the black hole is a quarter of horizon area. In terms of the expansion parameters introduced in (5.2.5), the temperature and entropy are

$$\begin{aligned} T_H\, L &= \frac{f_0\left(3R_+^2+1\right)}{2\sqrt{2}\pi\sqrt{R_+\left(3R_+^2+1\right)\left(a_0^2 R_+ + 2f_0\right)}}, \\ \frac{S}{L^2} &= \pi R_+^2. \end{aligned} \tag{5.3.5}$$

The chemical potential μ is defined in (5.2.3). It is the difference between the value of the electromagnetic field at infinity and at the horizon[4].

[4]Recall that we work in the gauge where $A\big|_{r_+} = 0$. With a gauge transformation, we can instead work in the gauge $A\big|_{\infty} = 0$ and the scalar field acquires a harmonic time dependence.

Stable solutions must satisfy the first law of thermodynamics:

$$\mathrm{d}M = T_H \mathrm{d}S + \mu \mathrm{d}Q, \quad \text{for black holes,} \tag{5.3.6}$$

$$\mathrm{d}M = \mu \mathrm{d}Q, \quad \text{for solitons.} \tag{5.3.7}$$

5.4 Small solitons (boson stars)

In section 4.2.1 we revisited the normal mode frequency spectrum of global AdS_4. These frequencies are quantized according to (4.2.5). A far-reaching property of this spectrum is that the imaginary part of the frequency vanishes: the associated eingenmodes are not dissipative. Moving beyond linear order in perturbation theory in the amplitude of the scalar field, we might then consider the back-reaction of these scalar normal modes on the gravitational and electromagnetic field. Since the leading order is not radiative we might suspect that the normal mode can be back-reacted to all orders and yield a boson star, i.e. a horizonless solution with static electromagnetic and gravitational fields and a complex scalar field with time dependence $e^{-i\omega t}$. We should further expect that the frequency ω is given at leading order by (4.2.5) but gets corrected as we climb the expansion ladder. We can further explore the U(1) gauge transformation freedom to rewrite this solution in a gauge where the frequency vanishes and the scalar field is real. This static solution is equivalent to the boson star but usually called a soliton. As explained in section 5.2, this soliton is a 1-parameter family of solutions that we can take to be the asymptotic amplitude ε of the scalar field as described in (5.2.3).

In this section we construct the ground state soliton − i.e. the soliton with lowest energy which at leading order is described by the lowest normal mode (4.2.6) − up to fourth order in ε. At leading order we have $A = \frac{3}{e}\, dT$. To obtain the soliton, we solve perturbatively the three second order ODEs for $\{f, A, \phi\}$ (3.0.6), subject to the boundary conditions (5.2.3) and (5.2.4) at the asymptotic boundary and at the origin, respectively. The pair of integration constants associated to each ODE is fixed by the boundary conditions. We build up the perturbative solution in a power series expansion of the fields in ε around global AdS_4,

$$\begin{aligned} f(R) &= 1 + R^2 + \sum_{n\geq 1} \varepsilon^{2n} f_{2n}(R), \\ A(R) &= \frac{3}{e} + \sum_{n\geq 1} \varepsilon^{2n} A_{2n}(R), \\ \phi(R) &= \frac{\varepsilon}{(1+R^2)^{3/2}} + \sum_{n\geq 1} \varepsilon^{2n+1} \phi_{2n+1}(R). \end{aligned} \tag{5.4.1}$$

When $\varepsilon = 0$ we recover global AdS_4 as expected. The $\mathcal{O}(\varepsilon)$ scalar field and its derivatives

source the first non-trivial contribution to the electromagnetic and gravitational fields at order $\mathcal{O}(\varepsilon^2)$. The structure of the equations of motion is then such that the odd (even) powers of ε never contribute to the electro-gravitational (scalar) fields.

The equations of motion can be solved analytically order by order for arbitrary order but the expressions for the solutions quickly become quite long. One can find the final (i.e. after imposing the boundary conditions and thus fixing all integration constants) coefficient functions $f_{2n}(R), A_{2n}(R)$ and $\phi_{2n+1}(R)$ up to order $n = 2$ in Appendix B of [1]. This order is enough to extract the relevant physical conclusions of our study.

Using these field expansions we can compute the gauge invariant thermodynamic quantities discussed in section 5.3. Namely, the mass M_{sol}, charge Q_{sol} and chemical potential μ_{sol} of the ground state soliton up to order $\mathcal{O}(\varepsilon^6)$ are:

$$\begin{aligned} M_{sol}/L =& \frac{9\pi}{32}\,\varepsilon^2 - \frac{3\pi\left(-301e^2+60\pi^2\left(e^2-9\right)+2898\right)}{10240}\,\varepsilon^4+\mathcal{O}(\varepsilon^6),\\ Q_{sol}/L =& \frac{3}{32}\pi e\,\varepsilon^2 - \frac{\pi e\left(-196e^2+60\pi^2\left(e^2-9\right)+2583\right)}{10240}\,\varepsilon^4+\mathcal{O}(\varepsilon^6),\\ \mu_{sol} =& \frac{3}{e}+\frac{21\left(e^2-3\right)}{32e}\,\varepsilon^2+\frac{\varepsilon^4}{204800\,e}\big[-339814e^4+3159903e^2\\ &+300\pi^2(92e^4-834e^2+2079)-7714818\big]+\mathcal{O}(\varepsilon^6). \end{aligned} \tag{5.4.2}$$

As a non-trivial check of our computation, one can check that these quantities satisfy the first law of thermodynamics for solitons (5.3.7) up to the required order $\mathcal{O}(\varepsilon^6)$.

We postpone the physical discussion of our soliton results (5.4.2) to section 5.6.

5.5 Small hairy black holes

In this section we construct perturbatively the hairy black holes whose leading order thermodynamics was discussed in section 4.4.

5.5.1 Setting up the perturbation problem

As explained in section 5.2, the hairy black holes of our theory are a two-parameter family of solutions that we can take to be the asymptotic scalar amplitude ε and the horizon radius R_+. Thus, their perturbative construction requires that we do a double expansion of the fields in powers of ε and R_+. In order to be able to solve analytically the equations of motion (3.0.6)-(3.0.7) we must resort to a matched asymptotic expansion, similar to those done in a similar context in [51, 125, 53, 126, 97] and also in 4.2.3 before. We divide the

outer domain of communications of our black hole into two regions; a near-region where $r_+ \leq r \ll L$ and a far-region where $r \gg r_+$. Restricting the analysis to small black holes that have $r_+/L \ll 1$, the two regions have an overlapping zone, $r_+ \ll r \ll L$. In this overlapping region, we can match the set of independent parameters that are generated by solving the perturbative equations of motion in each of the two regions.

The chemical potential of the solution should itself have a double expansion in powers of ε and R_+,

$$\mu = \sum_{n\geq 0} \varepsilon^{2n} \sum_{k\geq 0} R^k \mu_{2n,k}. \tag{5.5.1}$$

Indeed, recall that the soliton is the back-reaction of a normal mode of AdS to higher orders. At leading oder the chemical potential of the soliton is related, via a gauge transformation, to an AdS normal mode frequency. We saw that this is corrected at higher orders. Thus, we must allow for similar corrections when the horizon is present. We shall construct the hairy black hole family whose zero-radius limit is the *ground state* soliton of section 5.4 (so with lowest energy for a given charge).[5]

In the far region, $R \gg R_+$, the hairy black hole can be seen as a small perturbation in R_+ and ε around global AdS. We use the superscript ^{out} when referring to far region fields which have the double expansion:

$$\begin{aligned} f^{out}(R) &= \sum_{n\geq 0} \varepsilon^{2n} \sum_{k\geq 0} R_+^k \, f^{out}_{2n,k}(R), \qquad A^{out}(R) = \sum_{n\geq 0} \varepsilon^{2n} \sum_{k\geq 0} R_+^k \, A^{out}_{2n,k}(R), \\ \phi^{out}(R) &= \sum_{n\geq 0} \varepsilon^{2n+1} \sum_{k\geq 0} R_+^k \, \phi^{out}_{2n+1,k}(R). \end{aligned} \tag{5.5.2}$$

This expansion already anticipates that odd (even) powers of the scalar condensate do not correct the fields f, A (ϕ).

At each order $\{n, k\}$ the perturbed equations of motion can be solved analytically (with the help of *Mathematica*) to find the far fields up to a total of 6 integration constants (recall that the equations of motion are a system of 3 second order ODEs). In addition, the system also depends on the chemical potential corrections $\mu_{2n,k}$. The requirement that the far-region fields obey the asymptotic boundary conditions (5.2.3) typically fixes 4 of the integration constants (those associated to $\phi^{out}_{2n+1,k}$, one associated to $f^{out}_{2n,k}$ and another to $A^{out}_{2n,k}$). We are left with two integration constants and $\mu_{2n,k}$ that will be determined by the requirement that the far fields match the near-region fields in the overlapping region. To prepare the system for the matching we need to take the small radius R expansion of $f^{(out)}, A^{(out)}, \phi^{out}$ (with the expansion coefficients available at the order under consideration). We find that these are singular as $R \to 0$, diverging with a power of $\frac{R_+}{R}$. This indicates that the far-region analysis breaks down at $R \sim R_+$. This justifies why the far-region analysis is valid

[5] A similar construction could be done for excited hairy black holes.

only for $R \gg R_+$. Also, it follows that in the far-region we can safely do a Taylor expansion in $R \ll 1$ and $\varepsilon \ll 1$ since the large hierarchy of scales between the solution parameters and the distance guarantees that they do not compete.

Consider now the near-region, $R_+ \leq R \ll 1$. This time the Taylor expansions in $R \ll 1$ and $\varepsilon \ll 1$ should proceed with some caution since the small parameters can now be of similar order as the radius R_+. This is closely connected with the fact that the far-region solution breaks down when $R/R_+ \sim \mathcal{O}(1)$. This suggests that to proceed with the near-region analysis we should define new radial, y, and time, τ, coordinates as

$$y = \frac{R}{R_+}, \qquad \tau = \frac{T}{R_+}. \tag{5.5.3}$$

The near region now corresponds to $1 \leq y \ll R_+^{-1}$. If we further require that $R_+ \ll 1$ one sees that the near region corresponds to $y \geq 1 \gg R_+$ (and $y \gg \varepsilon$). In particular, we can now safely do Taylor expansions in $R_+ \ll 1$ and $\varepsilon \ll 1$ since the radial coordinate y and the black hole parameters have a large hierarchy of scales [6]. To have further physical insight it is also instructive to rewrite the RN-AdS$_4$ solution (4.2.7) in the new coordinate system (5.5.3):

$$\begin{aligned}
&\mathrm{d}s^2 = R_+^2 \left(-f(y)\mathrm{d}\tau^2 + \frac{\mathrm{d}y^2}{f(y)} + y^2 \mathrm{d}\Omega_2^2 \right), \\
&f(y) = 1 - \frac{1}{y} - \frac{1}{y}\left(\frac{1}{2}\mu^2 \left(1 - \frac{1}{y} \right) + R_+^2 \left(1 - y^3 \right) \right), \\
&A_\tau(y) = R_+ \, A_T(y) = R_+ \, \mu \left(1 - \frac{1}{y} \right), \\
&\phi(y) = 0.
\end{aligned} \tag{5.5.4}$$

The explicit factor of $R_+ \ll 1$ in $A_\tau(y)$ indicates that in the near region the electric field is weak and the system can be seen as a small perturbation around the neutral solution. The same should hold when we add a small scalar condensate to the system. The near fields of the hairy black hole thus have the double expansion,

$$\begin{aligned}
&f^{in}(y) = \sum_{n\geq 0} \varepsilon^{2n} \sum_{k\geq 0} R_+^k \, f^{in}_{2n,k}(y), \qquad A^{in}(y) = \sum_{n\geq 0} \varepsilon^{2n} \sum_{k\geq 0} R_+^k \, A^{in}_{2n,k}(y), \\
&\phi^{in}(y) = \sum_{n\geq 0} \varepsilon^{2n+1} \sum_{k\geq 0} R_+^k \, \phi^{in}_{2n+1,k}(y).
\end{aligned} \tag{5.5.5}$$

At each order $\{n, k\}$, we can solve the perturbed equations of motion analytically to find the near fields up to a total of 6 near region integration constants. Imposing the horizon boundary conditions (5.2.5) typically fixes 3 of the integration constants (one associated to

[6] At the heart of the matching expansion procedure, note that a factor of R_+ (one of the expansion parameters) is absorbed in the new coordinates.

$\phi^{in}_{2n+1,k}$, one to $f^{in}_{2n,k}$ and another to $A^{in}_{2n,k}$). The 3 leftover near field integration constants are left undetermined until we match the far and near region fields in the overlapping region. For the matching, we first need to restore the original coordinates $\{T, R\}$ and take the large radius limit of $f^{in}(R)$, $A^{in}(R)$, $\phi^{in}(R)$ (with the expansion coefficients available at the given order). We find that these diverge as a power of R, which shows that the near region analysis breaks down at $R \sim 1$. This explains why the near region analysis is valid only for $R \ll 1$.

In section 4.2.3 we presented an example of how the mathced asymptotic expansion works. Hence we do not discuss the details of the procedure but rather present the final thermodynamic results obtained from it. In the publication [1] that this research produced one can find a detailed computation as well as the final results for the metric, gauge and scalar fields. These functions are in Appendices $C.1$ and $C.2$ of [1].

5.5.2 Thermodynamic quantities

In the presentation of our results, we take $\epsilon \ll 1$ and $R_+ \ll 1$ and we assume that $\mathcal{O}(\epsilon^2) \sim \mathcal{O}(R_+)$. The latter assumption implies that terms with the same $(n+k)$ contribute equally to the perturbative expansion, i.e. $\mathcal{O}\left(\epsilon^0, R_+^2\right) \sim \mathcal{O}\left(\epsilon^2, R_+\right) \sim \mathcal{O}\left(\epsilon^4, R_+^0\right)$. We did the consistent perturbative expansion analysis up to $(n+k) = 2$, which is sufficient for our purposes. Extending the perturbative analysis to higher orders is possible, but increasingly cumbersome.

The fields computed in section 5.5 allow to compute the relevant physical properties of hairy black holes. The dimensionless mass M, electric charge Q, chemical potential μ, entropy S, and temperature T are:

$$
\begin{aligned}
M/L =& \Big[\Big(\frac{9}{4e^2}+\frac{1}{2}\Big)R_+ + \frac{6(2e^2-9)}{\pi e^4}\,R_+^2 + \mathcal{O}(R_+^3)\Big] + \varepsilon^2\Big[\frac{9\pi}{32} + \frac{9(27\pi^2-2(e^2+9))}{128e^2}\,R_+ \\
&+ \mathcal{O}(R_+^2)\Big] + \varepsilon^4\Big[-\frac{3\pi(-301e^2+60\pi^2(e^2-9)+2898)}{10240} + \mathcal{O}(R_+^1)\Big] + \mathcal{O}(\varepsilon^6), \\
Q/L =& \Big[\frac{3}{2e}\,R_+ + \frac{2(2e^2-9)}{\pi e^3}\,R_+^2 + \mathcal{O}(R_+^3)\Big] + \varepsilon^2\Big[\frac{3\pi e}{32} + \frac{(-38e^2+81\pi^2+90)}{128e}\,R_+ \\
&+ \mathcal{O}(R_+^2)\Big] + \varepsilon^4\Big[-\frac{\pi e(-196e^2+60\pi^2(e^2-9)+2583)}{10240} + \mathcal{O}(R_+^1)\Big] + \mathcal{O}(\varepsilon^6), \\
\mu =& \Big[\frac{3}{e} + \frac{4(2e^2-9)}{\pi e^3}\,R_+ + \frac{(2e^2-9)[-256e^2+9\pi^2(10e^2-9)+2688]}{32\pi^2e^5}\,R_+^2 \\
&+ \mathcal{O}(R_+^3)\Big] + \varepsilon^2\Big[\frac{21(e^2-3)}{32e} + \frac{1}{9600\pi e^3}\big[75\pi^2(236e^4-1809e^2+4212) \\
&- 8(25330e^4-264861e^2+685503)R_+\big] + \mathcal{O}(R_+^2)\Big] + \varepsilon^4\Big[\frac{1}{204800e}\big[-339814e^4 \\
&+ 3159903e^2 + 300\pi^2(92e^4-834e^2+2079) - 7714818\big] + \mathcal{O}(R_+^1)\Big] + \mathcal{O}(\varepsilon^6),
\end{aligned}
$$

$$
\begin{aligned}
S/L^2 =&\pi R_+^2, \qquad (5.5.6)\\
TL =&\frac{1}{4\pi R_+}\Bigg\{\Big[\frac{2e^2-9}{2e^2}-\frac{12\left(2e^2-9\right)}{\pi e^4}\,R_+ + \frac{1}{32\pi^2 e^6}\big(96\pi^2e^6-540\pi^2e^4+512e^4\\
&+2916\pi^2e^2-13824e^2-2187\pi^2+51840\big)R_+^2+\mathcal{O}(R_+^3)\Big]+\varepsilon^2\Big[-\frac{3\left(5e^2+9\right)}{32e^2}\\
&-\frac{3R_+}{6400\pi e^4}(7300\pi^2e^4-89760e^4-87750\pi^2e^2+982992e^2+289575\pi^2-2640816)\\
&+\mathcal{O}(R_+^2)\Big]+\varepsilon^4\Big[\frac{1}{204800e^2}(-66600\pi^2e^4+716782e^4+653400\pi^2e^2-6564933e^2\\
&-1761750\pi^2+16179426)+\mathcal{O}(R_+^1)\Big]+\mathcal{O}(\varepsilon^6)\Bigg\}.
\end{aligned}
$$

In the next section we discuss physical checks to these quantities and withdraw physical conclusions.

5.6 Discussion of physical properties

5.6.1 Checking the hairy solutions and their interpretation

The thermodynamic quantities (5.5.6) for the hairy black hole must pass a few checks that already give valuable information about their physical interpretation.

Firstly, when we set the horizon radius to zero, $R_+ \to 0$, we get the thermodynamical quantities (5.4.2) of the soliton. Recall that the latter was obtained without any matching asymptotic expansion. This also confirms that the soliton is the zero horizon radius limit of the hairy black hole. We have assumed this was the case in our construction and the fact that the computation can be done is consistent with it.

Secondly, when we set the scalar condensate amplitude to zero, $\varepsilon \to 0$, we get the thermodynamical quantities (4.2.10) of the RN-AdS_4 black hole, with a very specific chemical potential namely,

$$\mu = \frac{3}{e}+\frac{4(2e^2-9)}{\pi e^3}\,R_+ + \frac{(2e^2-9)[-256e^2+9\pi^2(10e^2-9)+2688]}{32\pi^2e^5}\,R_+^2+\mathcal{O}(R_+^3). \quad (5.6.1)$$

That is, although the RN-AdS_4 black hole is a 2-parameter family of solutions, the $\varepsilon \to 0$ limit of the hairy black hole gives a particular 1-parameter sub-family of RN-AdS_4 parametrized by R_+ and chemical potential fixed by (5.6.1). This is precisely the RN-AdS_4 1-parameter family at the onset of the superradiant instability studied in section 4.2.3. To see this is indeed the case start by recalling that in section 4.2.3 we studied scalar field perturbations with Fourier time dependence $\phi(T,R) \sim e^{-i\omega T}\phi(R)$ and found

that the frequency is quantized as described in (4.2.14) and (4.2.21). In particular, the frequency has a positive imaginary part for $\omega > e\mu$ signalling the superradiant instability. The onset of the superradiant instability occurs when the imaginary part of the frequency vanishes and we can work in the $U(1)$ gauge where the real part of the frequency vanishes. If we impose these superradiant onset conditions on (4.2.21) and solve with respect to the chemical potential in a series expansion in R_+ up to order $\mathcal{O}\left(R_+^2\right)$ we precisely get (5.6.1). This is an important check to our computations and, together with the information from the last paragraph, confirms that hairy black holes are indeed a 2-parameter family of solutions that spans an area in a phase diagram that has the onset curve of the RN-AdS$_4$ superradiance and the soliton curve as boundaries. At leading order, these are the boundaries (4.4.5) predicted by the simple thermodynamical model of section 4.4 and that will be very clear in the left panel of Fig. 5.6.1 (red and black curves).

The first law of thermodynamics provides the third check. Indeed, we can explicitly verify that the thermodynamic quantities (5.5.6) do obey the first law (5.3.6) up to order $(n+k) = 2$. We emphasize this is a fundamental and non-trivial check of our results.

To summarize, we have constructed analytically the hairy black hole within perturbation theory up to order $(n + k) = 2$ (and we could extend this construction to higher order). This was done solving directly the perturbed equations of motion (3.0.6)-(3.0.7) of the theory as a boundary value problem.

We can confirm that the simple non-interacting thermodynamic model of section 4.4 − which does *not* use the equations of motion − yields the correct leading order thermodynamics, i.e. the leading terms of (5.5.6). First note that at leading order it follows from (5.5.6) that $\mu = \frac{3}{e}$. Assuming, as justified above, that $\mathcal{O}(\epsilon^2) \sim \mathcal{O}(R_+)$, the leading order contributions of the expansion (5.5.6) allow to express analytically R_+ and ε in terms of M and Q,

$$\begin{aligned} R_+ &= \frac{4e(eM-3Q)}{2e^2-9} + \mathcal{O}\left(M^2, Q^2, MQ\right), \\ \varepsilon &= \sqrt{\frac{32\left(\left(2e^2+9\right)Q-6eM\right)}{3\pi e\left(2e^2-9\right)}} + \mathcal{O}\left(M^2, Q^2, MQ\right), \end{aligned} \tag{5.6.2}$$

which we insert in the expressions for the other thermodynamic quantities to find that at leading order in M and Q one has:

$$\begin{aligned} \mu &= \frac{3}{e} + \mathcal{O}\left(M, Q\right), \\ S &= \frac{16\pi e^2(Me-3Q)^2}{\left(9-2e^2\right)^2} + \mathcal{O}\left(M^2, Q^2, MQ\right), \\ T &= \frac{\left(9-2e^2\right)^2}{32\pi e^3(Me-3Q)} + \mathcal{O}\left(M^2, Q^2, MQ\right). \end{aligned} \tag{5.6.3}$$

These quantities do match the result of the non-interacting model (4.4.4). This confirms that the non-interacting thermodynamic model, in spite of its crude simplicity, is quite robust and does indeed capture the fundamental leading order properties of the hairy black hole system at very low cost. This explicit confirmation adds to those done in similar hairy black hole systems in [51, 125, 53, 126, 30, 98].

A more detailed discussion of the regime of validity of our perturbation theory is also in order. By construction, it should be valid only for $\varepsilon \ll 1$ and $R_+ \ll 1$. On the other hand, the scalar charge of the hair must obey $e \gtrsim \frac{3}{\sqrt{2}} \sim 2.12$ to have superradiant hairy black holes. However, since the black holes are a small expansion around AdS$_4$, e should not be too large to avoid large back-reactions. This suggests that it is appropriate to require at most $\epsilon \lesssim 0.1$, $R_+ \lesssim 0.1$ and $\frac{3}{\sqrt{2}} \lesssim e \lesssim 3$, say. Inserting these bounds into the thermodynamic formulas (4.2.10), (5.4.2), and (5.5.6) we get approximate upper bounds for the physical charges. For example, for $e = 2.5$ we should look into masses and charges that, in AdS units, are themselves below 10^{-1}. However the reader interested on making a direct comparison between our perturbative results and exact numerical constructions that emerge from a nonlinear code or from the endpoint of the superradiant time evolution might require more precise statements. We will have the opportunity to give precise criteria in the following discussion: see footnote 8.

We have found that the gravitational Higgs model with action (3.0.1) admits several solutions: global AdS$_4$, RN-AdS$_4$ BH, the ground state soliton, the ground state hairy black hole and an infinite tower of excited solitons and hairy black holes[7]. For a given electric charge, the latter excited solutions always have larger energy than the ground state partners so we do not discuss them further.

Naturally, these thermal phases of the theory compete with each other. This competition can be framed in one of the three possible ensembles: the microcanonical, canonical or grand-canonical ensembles. Hairy black holes are the dominant solution in the microcanonical ensemble as discussed in the next subsection. However, they are never the dominant solution in the canonical and grand-canonical ensemble, thus we will not discuss those ensembles here. The discussion of the canonical and grand-canonical phase diagrams can be found in the publication produced from this research [1] sections VII.C and VII.D.

Recall that the thermodynamic quantities of the RN-AdS$_4$ black hole, (ground state) soliton and hairy black hole are given in (4.2.10), (5.4.2), and (5.5.6), respectively [150, 151].

Our results are better illustrated with some plots. Recall that the gravitational Higgs theory with action (3.0.1) is only fully defined once the particular value for the scalar field

[7] Recall that the ground state solutions have their perturbative root in the lowest normal mode frequency of global AdS$_4$, and the excited states emerge from the remaining infinite tower of normal mode frequencies.

charge $q = e/L$ is specified. For definiteness we will choose the particular value $e = 2.5$ in our plots.

5.6.2 Phase diagram in the microcanonical ensemble

In the microcanonical ensemble the energy M and electric charge Q of the system are fixed and the the entropy S is the relevant thermodynamic potential to discuss the competition between the several thermal phases: the phase with higher entropy is the favoured one (global AdS_4 and the soliton have vanishing entropy).

In Fig. 5.6.1 we display the phase diagram M vs Q of the microcanonical ensemble for $e = 2.5$ (our perturbative expressions are valid for small M, Q). To make the diagram more clear, in the vertical axis we actually plot the difference between the mass of the solution and the mass of the extremal RN-AdS_4 with the same electric charge, $\Delta M \equiv M - M_{ext}$. So RN-$AdS_4$ black holes exist in regions I and II where $\Delta M \geq 0$. The black line with negative slope describes the soliton. Hairy black holes exist in regions II and III: they fill the area limited by the soliton curve (where $R_+ \to 0$) all the way up to the magenta line with positive slope (with $\varepsilon = 0$). The latter also describes RN-AdS_4 black holes at the onset of superradiance. So RN-AdS_4 black holes below (above) the magenta line are unstable (stable) to superradiance.

In region II there is no uniqueness since RN-AdS_4 and hairy black holes coexist with the same M and Q. To find the preferred phase in the microcanonical ensemble we must compare their entropy S. We find that for a given electric charge Q the hairy black hole always has higher entropy and is thus the favoured solution, whenever they coexist. This is illustrated with a particular example in the right panel of Fig. 5.6.1 where we fix the electric charge to be $Q/L = 0.01$ and plot S vs M (again for $e = 2.5$). The blue line describes the RN-AdS_4 black hole and extends from arbitrarily large M and S all the way down to the extremal configuration A. It is stable along this path until it reaches point B that signals the onset of the superradiant instability (so BA describes unstable RN-AdS_4). At this point B there is a *second order phase transition*[8] to the hairy black hole branch that extends all the way down to the zero-horizon radius ($S = 0$) where it meets the soliton (point C). This dominance of the hairy black hole in the microcanonical ensemble extends to all values of the electric and scalar charges (again, in the regime where our perturbative results hold).

[8] This provides a further check of our computations. Indeed, note that the first law requires that at a second order phase transition the slope dS/dM is the same for the two branches since T is the same at the bifurcation point (and $dQ = 0$ in the right panel of Fig. 5.6.1). This is clearly the case in our plot. However, if we start departing from the regime of validity of our perturbation analysis we increasingly find that the merger is not perfect and the slopes of the two branches no longer match. This is the best criterion to identify the regime of validity of (5.5.6).

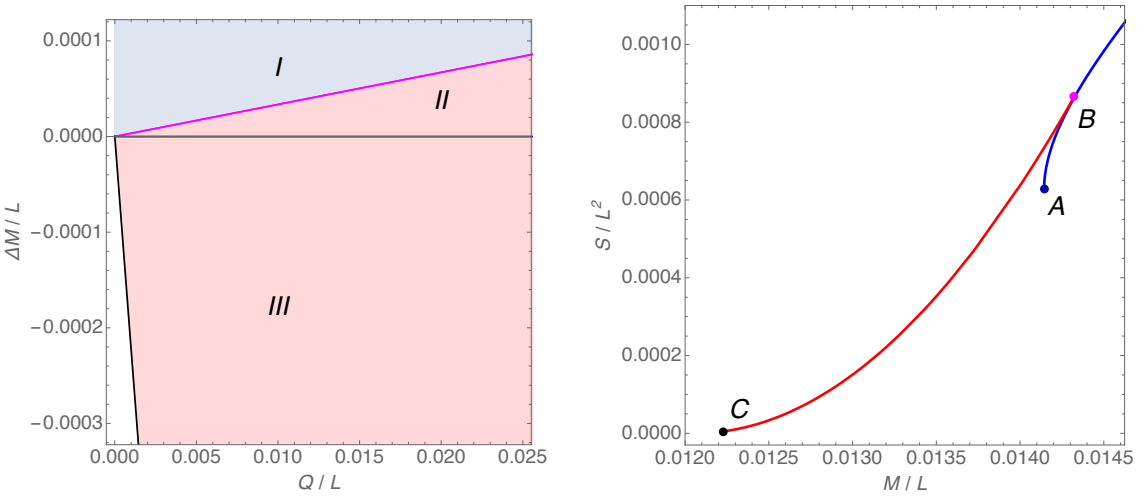

Figure 5.6.1: **Left Panel:** Microcanonical ensemble phase diagram $\Delta M = M - M_{ext}$ vs Q for $e = 2.5$. RN-AdS$_4$ black hole exist in regions I and II, with the magenta line with positive slope describing the onset curve of superradiant instability. The black line with negative slope describes the soliton. Hairy black holes exist in between the two above lines, i.e. in regions II and III (red shaded). **Right Panel:** Entropy as a function of the mass at constant value of the charge $Q/L = 0.01$ and $e = 2.5$. The unbounded blue line starting at A (extremality) is the RN-AdS$_4$ black hole and the red line BC is the hairy back hole branch that ends on the soliton C. The merger point B is the superradiant zero-mode.

Our findings also permit robust conclusions about the endpoint of the superradiant instability of RN-AdS$_4$ BHs. Typically, numerical simulations are done at fixed energy and charge. Consider starting with a RN-AdS$_4$ that is within the curve AB and thus unstable to superradiance. By the second law of thermodynamics, the entropy of the system can only increase. Assuming that there is no other black hole solution in the spectrum of the theory besides the ones discussed so far, the system must evolve towards the hairy black hole that has the same M and Q but higher entropy. The latter can be pinpointed in (5.5.6) or in Fig. 5.6.1. By construction, this hairy black hole is stable to superradiance and we have no arguments suggesting that it is unstable to any other mechanism. Of course, our findings say nothing about how the system actually evolves in time but the endpoint of the numerical simulation that gives this information can be tested against (5.5.6).[9]

[9] Also recall that for $\sqrt{3/2} < e < 3/\sqrt{2}$ there are hairy black holes that emerge from the near-horizon scalar condensation instability that are not captured by our "superradiant" solutions (5.5.6). But they can be found as the endpoint of a time evolution simulation or by solving numerically the elliptic system of equations (3.0.6)-(3.0.7).

CHAPTER 6

Evading no-hair theorems: hairy black holes in a Minkowski box

In this Chapter we solve the system of equations of the Einstein-Maxwell theory with a charged scalar field enclosed in a cavity. Our main goal is to find the regular and asymptotically flat charged hairy black hole of the theory that describes the endpoint of the instabilities presented in Chapter 4. We further analyse the thermodynamic properties in the microcanonical ensemble of the known solutions and conclude that hairy black holes are the dominant phase in their region of existence.

6.1 Summary of results

This Chapter is devoted to the study of the phase diagram of static asymptotically flat (regular) solutions of the Einstein-Maxwell theory with a complex scalar field confined inside a box. In particular, this can be the phase diagram in the microcanonical ensemble, where we plot the entropy of the solutions as a function of their mass and electric charge. We use dimensionless quantities measured in units of the box radius L. A familiar member of this phase diagram is the Reissner-Nordström black hole (RN BH) placed inside the cavity. The interior solution of this caged RN BH was already discussed in the seminal works [152, 153, 154] and, more recently, in [155, 114]. This solution has vanishing scalar field but is linearly unstable to a scalar field perturbation. At the onset of the instability, the scalar field perturbation is regular *both* at the past and future event horizons of the

black hole. Consequently, we might expect that the back-reaction of this linear scalar perturbation to higher orders in perturbation theory results in a black hole solution that is regular everywhere and asymptotes to Minkowski spacetime. By continuity, this hairy black hole solution should extend away from the onset curve. That is to say, in the phase diagram, the instability onset curve of caged RN BH should also signal a bifurcation to a new branch of solutions of asymptotically flat hairy black holes. This new family should exist for a wide range of mass and electric charge. In particular, this should lead to non-uniqueness of solutions since hairy and caged RN BH should exist with the same mass and charge.

In the region of mass and charge where they co-exist, hairy black holes have higher (dimensionless) entropy than caged RN BH. Thus, an unstable caged RN BH naturally evolves in time into the hairy black hole with the same mass and charge while preserving the second law of thermodynamics. These hairy black holes describe the endpoint of the time evolution simulations done in [107, 117, 118].

Additionally, hairy black holes that we have been describing have a zero horizon radius limit where they reduce to a hairy soliton solution. This is a horizonless asymptotically flat solution with a scalar field confined inside the Minkowski cavity. Again, gravitational collapse is balanced by the electric repulsion. Under a $U(1)$ gauge transformation this hairy soliton has a dual boson star description in which the scalar field with frequency ω has time dependence $e^{i\omega t}$. Such a solution exists since it is the back-reaction of a normal mode that fits inside a Minkowski cavity (however the gravitoelectric fields have no time dependence since they are sourced by the norm of a complex scalar field).

To construct these hairy solutions we solve the equations of Einstein-Maxwell theory with a complex scalar field that is forced to be confined inside the box. Ref. [114] already discussed some thermodynamic properties of the hairy solutions in the grand-canonical ensemble. However, [114] constructed these solutions numerically and focused their attention on the description of the solutions only in the interior of the box. We will complement and extend their analysis in distinct directions. First, we find the hairy solutions analytically within perturbation theory which will allow to unveil physical aspects of the solution. More importantly, we will extend the solutions beyond the cavity and construct the full solution also in the exterior region. This is fundamental to find the energy-momentum of the box, *i.e.* the Lanczos-Darmois-Israel surface stress tensor that the cavity must have to yield a solution that obeys the Israel junction conditions and is thus continuous across the surface layer [142, 143, 144, 145]. To our best knowledge, this is the first instance where the Israel surface tensor is discussed in black hole bomb systems.

The discussion of black hole bombs is incomplete and even misleading without analysing this Israel surface stress tensor. For general cavities, the associated Israel tensor does not

obey the energy conditions, in particular the weak energy condition. To have a hairy black hole-mirror system that obeys the energy conditions we have to start with a box in a Minkowski background that already has a specific energy-momentum content (hence non-vanishing energy density and pressure) even before we place a soliton or horizon inside it. We parametrize these quantities with a parameter η that has a non-vanishing value to yield a physical hairy black hole-mirror system. In view of our findings, it will be interesting to revisit the time evolutions of [107, 117, 118] to discuss also the surface stress tensor of the system.

Refs. [113, 115, 116] also discussed hairy black holes and solitons in the context of black hole bomb setups. However, their hairy solutions do not confine the scalar field inside the box. Thus this scalar field can leak from the box and extend to the asymptotic region where it sources logarithmic divergences in the gravitoelectric fields. Consequently, they are not asymptotically flat. Our solutions are fundamentally distinct since they are asymptotically flat (and regular everywhere) hairy solutions that evade the no-hair theorems of [46, 132, 47, 133]. The presence of the box and its boundary conditions/surface stress tensor allow one to find that the RN BH solution is not the only family of asymptotically flat, spherically symmetric and static (regular) black hole solutions of Einstein-Maxwell theory.

An interesting byproduct of our analysis is that we will conclude that the thermodynamics and physics of black hole bomb systems is most appropriately discussed in terms of the Brown-York quasilocal thermodynamic quantities of the system [146]. Recall that the Israel surface stress tensor can be obtained integrating a Gauss-Codazzi equation along the normal direction to the surface layer [142, 143, 144, 145, 156]. Equivalently, it can be obtained by taking the difference of the Brown-York quasilocal energy-momentum tensor outside and inside the surface layer [146]. These observations are the starting point to conclude that black hole bombs (and other systems with Israel boundary shells) must obey a quasilocal version of the first law of thermodynamics. This important property seems to have been missed in previous discussions of systems with Israel junction conditions. In particular, we propose that these gauge invariant quantities are relevant quantities to monitor in time evolution studies of black hole bomb systems.

The plan of the Chapter is as follows. In section 6.2 we discuss the boundary conditions that supplement the equations of motion in (3.0.6). Special attention is given to the discussion of the Israel junction conditions and Brown-York quasilocal charges. Hairy solitons are constructed within perturbation theory in section 6.4. The properties of RN BH confined in a box are discussed in section 6.5. Perturbation theory and a matched asymptotic expansion are used to construct the hairy black holes in section 6.6. The physical properties of the solutions are then discussed in detail in section 6.7. We describe the thermodynamic properties of the solutions, the Israel surface stress tensor of the system and analyse the necessary conditions to obey the energy conditions.

6.2 Boundary conditions

We consider the theory described by (3.0.1) with cosmological constant $\Lambda = 0$, and solutions to the theory of the form (3.0.2). The set of equations of motion of the theory are given in (3.0.6). In this Chapter we are restricting to massless scalar fields.

The most notable solution of (3.0.1) is Minkowski spacetime: $f(R) = g^{-1}(R) = 1$ $A(R) = \phi(R) = 0$. We are interested in solutions that asymptote to this background.

In order to have a well-posed boundary value problem we must specify the boundary conditions in the inner and asymptotic boundaries of our spacetime. Additionally, we need to impose junction conditions at the timelike hypersurface Σ at $R = 1$ where the box is located. We are interested in asymptotically flat solutions with vanishing scalar field at and outside this box, $\phi(R \geq 1) = 0$.

The inner boundary can be the origin $R = 0$ of our coordinate system (for horizonless solitonic solutions) or a Killing horizon with radius $R = R_+$ defined as the locus $f(R_+) = 0$, when we have a black hole solution. The system is described by three second order ODE's which means that there are six arbitrary integration constants when we do a Taylor expansion around the inner boundary. However, as a Dirichlet boundary condition we need to set three of these to zero in order to eliminate terms that would diverge at this boundary [50]. We are thus left with only three constants f_0, A_0, ϕ_0 (say) such that the regular fields have the Taylor expansion:

$$f(0) = f_0 + \mathcal{O}(R), \qquad A(0) = A_0 + \mathcal{O}(R), \qquad \phi(0) = \phi_0 + \mathcal{O}(R), \tag{6.2.1}$$

at the origin of the soliton, or

$$\begin{aligned} &f(R_+) = f_0(R - R_+) + \mathcal{O}((R - R_+)^2), \\ &A(R_+) = A_0(R - R_+) + \mathcal{O}((R - R_+)^2), \qquad \phi(R_+) = \phi_0 + \mathcal{O}((R - R_+)^2), \end{aligned} \tag{6.2.2}$$

at the horizon radius of a black hole solution. Here we made the choice of working in the gauge where $A(R_+) = 0$.

Consider now the outer boundary of our spacetime, namely the asymptotic infinity. Outside the box $\phi = 0$ and the equations of motion are solved by the solution: $f^{out}(R) = c_f - \frac{M_0}{R} + \frac{\rho^2}{2R^2}$, $A^{out}(R) = c_A + \frac{\rho}{R}$ and $g^{out}(R) = c_f / f^{out}(R)$ (onwards we use the superscript ^{out} to represent fields outside the box). Here, c_f, M_0, c_A and ρ are arbitrary integration constants. These are not constrained, *i.e.* for any value of these constants we have an asymptotically flat solution. As argued in (3.0.4) we set $c_f = 1$.

The solution to the equations of motion outside the box is

$$f(R)\big|_{R\geq 1} = 1 - \frac{M_0}{R} + \frac{\rho^2}{2R^2}\,, \qquad A(R)\big|_{R\geq 1} = c_A + \frac{\rho}{R}\,, \qquad \phi(R)\big|_{R\geq 1} = 0\,, \tag{6.2.3}$$

Birkhoff's theorem for the Einstein-Maxwell theory states that the only static spherically symmetric asymptotically flat solution is described by the RN BH solution (6.2.3). Note however that (6.2.3) leaves three free integration constants, M_0, c_A, ρ, which will be determined once we have the solution inside the box.

Our solutions are asymptotically flat. Therefore, some of the parameters in (6.2.3) are related to the ADM conserved charges [157]. The adimensional ADM mass and electric charge of the system are given by (in units $G_N \equiv 1$):

$$\begin{aligned} M/L &= \lim_{R\to\infty} \frac{R^2 f'(R)}{2\sqrt{f(R)g(R)}} = \frac{M_0}{2}, \\ Q/L &= \lim_{R\to\infty} \frac{R^2 A'(R)}{2f(R)g(R)} = -\frac{\rho}{2}. \end{aligned} \tag{6.2.4}$$

These ADM conserved charges measured at the asymptotic boundary include the contribution from the energy-momentum content of the box that confines the scalar hair. In the next subsection we discuss the effect of this box in more detail.

6.2.1 Junction conditions at the box surface layer and associated Israel surface tensor

Our discussion of the boundary conditions at the inner and outer boundaries of our integration domain is complete. However, the requirement that the scalar field vanishes at the box Σ located at $R = 1$ (*and* outside it) comes with a cost. We will construct our hairy solutions perturbatively in the amplitude ε of the scalar field. In our perturbation scheme, we define unambiguously the expansion parameter ε to be such that $\phi^{out}(R \geq 1) = 0$ and, in the interior of the box, the first derivative of the scalar field is ε at *all* orders of the expansion,[1]

$$\phi^{in}\big|_{R=1} = \phi^{out}\big|_{R=1} = 0, \qquad \phi^{out}(R) = 0, \qquad \phi'^{\,in}\big|_{R=1} \equiv \varepsilon, \tag{6.2.5}$$

for $R \leq 1$ the scalar field will be forced to have a Taylor expansion of the form $\phi\big|_{R=1} = \varepsilon(R-1) + \mathcal{O}(\varepsilon(R-1)^2) + \mathcal{O}(\varepsilon^3(R-1)^2)$. We are forcing a jump in the derivative of the scalar field normal to the cavity hypersurface. The surface layer Σ must have a scalar

[1] Another natural choice to fix the perturbation scheme would have been to fix the expansion parameter to be the value of the scalar field at the horizon (black hole case) or at the origin (soliton case) at all orders. However, with this choice it would not be so straightforward to show that the zero horizon radius limit of the hairy black hole is the hairy soliton.

charge density $4\pi\rho_\phi = -\partial_R\Phi\big|_{R=1}$ that sources this jump. The difference between the scalar field charge contained on a sphere just outside (where it vanishes) and just inside the surface layer is then

$$[Q_\phi] \equiv Q_\phi\big|^{out}_{R=1} - Q_\phi\big|^{in}_{R=1} = -\varepsilon \tag{6.2.6}$$

which defines unambiguously ε.

Naturally, this forced condition on the scalar field has a further cost: we need to impose junction conditions at the timelike hypersurface Σ – defined by $\mathfrak{f}(R) = R-1 = 0$ and with outward unit normal $n_\mu = \partial_\mu\mathfrak{f}/|\partial\mathfrak{f}|$ ($n_\mu n^\mu = 1$) – on the other fields of the system. Ideally, we would like to have a smooth crossing, *i.e.* that the gravitational and gauge fields and their normal derivatives are continuous at Σ. But we are not guaranteed that this can be done. To discuss this issue further it is good to set some notation. From the perspective of an observer in the interior region, the cavity surface Σ is parametrically described by $R = 1$ and $T = T^{in}(\tau) = \tau$ such that the induced line element and induced gauge 1-form of the shell read

$$\begin{aligned} \mathrm{d}s^2|_{\Sigma^{in}} &= h^{in}_{ab}\,\mathrm{d}\xi^a\mathrm{d}\xi^b = -f^{in}|_{R=1}\mathrm{d}\tau^2 + \mathrm{d}\Omega_2^2\,, \\ A|_{\Sigma^{in}} &= a^{in}_a\mathrm{d}\xi^a = A^{in}|_{R=1}\mathrm{d}\tau\,, \end{aligned} \tag{6.2.7}$$

where ξ^a describe coordinates in Σ, h^{in}_{ab} is the induced metric in Σ and a^{in}_a is the induced gauge potential in Σ. On the other hand, as seen from outside the cavity shell, Σ is parametrically described by $R = 1$ and $T = T^{out}(\tau) = N\tau$ so that the induced line element and the induced gauge 1-form are

$$\begin{aligned} \mathrm{d}s^2|_{\Sigma^{out}} &= h^{out}_{ab}\,\mathrm{d}\xi^a\mathrm{d}\xi^b = -N^2 f^{out}|_{R=1}\mathrm{d}\tau^2 + \mathrm{d}\Omega_2^2\,, \\ A|_{\Sigma^{out}} &= a^{out}_a\mathrm{d}\xi^a = NA^{out}|_{R=1}\mathrm{d}\tau\,, \end{aligned} \tag{6.2.8}$$

The reparametrization freedom parameter N will be chosen as follows. We use the scaling symmetry (3.0.4) in each region to set

$$f^{in}\big|_{R=1} = 1\,, \qquad f^{out}\big|_{R\to\infty} = 1\,, \tag{6.2.9}$$

at all orders in ε; note that the second condition repeats the statement just before (6.2.3). An appropriate choice of the reparametrization freedom parameter N will allow (6.2.9) to be obeyed.[2]

The junction conditions required to join smoothly two spacetimes at a timelike hypersurface Σ were studied by Israel [142, 143, 144, 145] built on previous work of Lanczos and Darmois. Next, we review these conditions. A solution is smooth at Σ if and only if: 1) the induced

[2]Note that, in an alternative but equivalent scheme, we could choose to parametrize Σ by $R = 1$ and $T = T^{out}(\tau) = \tau$ and then transfer the reparametrization freedom encoded by N into f^{out}_0 and A^{out}_0. In this case one would have $f^{out}\big|_{R\to\infty} \neq 1$ instead of (6.2.3), (6.4.3) or (6.6.4).

metric h_{ab} and induced gauge potential a_a are continuous ($i.e. \mathrm{d}s^2|_{\Sigma^{in}} = \mathrm{d}s^2|_{\Sigma^{out}}$ and $A|_{\Sigma^{in}} = A|_{\Sigma^{out}}$), and 2) the extrinsic curvature K_{ab} (essentially the normal derivative of the induced metric) and the normal derivative of the induced gauge field, f_{aR}, are continuous. If we denote the solution inside (outside) Σ by the superscript ^{in} (^{out}), the Israel junction conditions can be written as

$$a_a^{in}\big|_{R=1} = a_a^{out}\big|_{R=1}\,, \tag{6.2.10a}$$

$$h_{ab}^{in}\big|_{R=1} = h_{ab}^{out}\big|_{R=1}\,; \tag{6.2.10b}$$

$$f_{aR}^{in}\big|_{R=1} = f_{aR}^{out}\big|_{R=1}\,, \tag{6.2.10c}$$

$$K_{ab}^{in}\big|_{R=1} = K_{ab}^{out}\big|_{R=1}; \tag{6.2.10d}$$

where $h_{ab} = g_{ab} - n_a n_b$ is the induced metric at Σ and $K_{ab} = h_a{}^c \nabla_c n_b$ is the extrinsic curvature.

If, as it is our case, the exterior curvature condition (6.2.10d) is not satisfied then the solution is singular at Σ. This is interpreted as due to the presence of a Lanczos-Darmois-Israel surface stress tensor $\mathcal{S}_{ab}$ at the hypersurface layer proportional to the difference of the extrinsic curvature on both sides of the hypersurface. More concretely, the Lanczos-Darmois-Israel surface stress tensor induced in Σ is [142, 143, 144, 145]

$$\mathcal{S}_{ab} = -\frac{1}{8\pi}\Big([K_{ab}] - [K]h_{ab}\Big), \tag{6.2.11}$$

where K is the trace of the extrinsic curvature and $[K_{ab}] \equiv K_{ab}^{out}\big|_{R=1} - K_{ab}^{in}\big|_{R=1}$. This surface tensor is the pull-back of the energy-momentum tensor integrated over a small region around the hypersurface Σ. It is obtained by integrating the appropriate Gauss-Codazzi equation [142, 143, 144, 145, 156]. Essentially, (6.2.11) describes the energy-momentum tensor of the cavity (the "internal structure" of the mirror) that we have to build to confine the scalar field inside. With our explicit construction of the hairy solutions of the system we will be able to compute this Lanczos-Darmois-Israel stress tensor. To our best knowledge, this gives the first explicit description of the box matter content of a black hole bomb.

Lanczos-Darmois-Israel surface stress tensor obeys the conservation law [142, 143, 144, 145],

$$\mathcal{D}^b \mathcal{S}_{ab} = -T_{\mu\nu} h^\mu{}_a n^\nu \tag{6.2.12}$$

where $\mathcal{D}_a$ is the covariant derivative w.r.t. the 3-dimensional induced metric h_{ab} on Σ, $h^\mu{}_a$ is the 4-dimensional tensor that projects quantities onto the hypersurface Σ, and $T_{\mu\nu}$ the energy-momentum tensor of (3.0.1).[3] This follows from the definition (6.2.11) and from the ADM Hamiltonian constraint (from the contracted Gauss-Codazzi equation along the

[3] For our hairy system, $n^\mu T_{\mu\nu} h^\nu{}_b = 0$. Thus (6.2.12) boils down to $\mathcal{D}^b \mathcal{S}_{ab} = 0$.

normal to Σ). On the other hand, the ADM momentum constraint, the normal-normal contracted Gauss-Codazzi equation yields the relation [142, 143, 144, 145]

$$\frac{1}{2}\left(K^{out}_{ab}+K^{in}_{ab}\right)\mathcal{S}^{ab}=[T_{\mu\nu}n^{\mu}n^{\nu}] \tag{6.2.13}$$

where the square brackets again represent the difference between the quantity just outside and just inside Σ.

In our case the Lanczos-Darmois-Israel surface stress tensor (6.2.11) ensures that the scalar hair is confined to the interior of the box with radius $R=1$. The outward normal to Σ is $n=\sqrt{g}\,dr$, the 3-dimensional induced metric on Σ is $h_{ab}=g_{ab}$ (for $a,b=\{t,\theta,\phi\}$) and the non-vanishing extrinsic curvature components are

$$K^{t}_{\ t}=-\frac{f'(R)}{2f(R)\sqrt{g(R)}}\,,\qquad K^{i}_{\ j}=\frac{1}{R\sqrt{g}}\,\delta^{i}_{\ j}\,, \tag{6.2.14}$$

with $\delta^{i}_{\ j}$ being the Kronecker symbol ($i,j=\theta,\phi$). One of the main results of our study will be that we *cannot* make the extrinsic curvature (6.2.14) continuous across Σ if we require that the scalar field vanishes at and outside the box − see (6.2.5) − as is required for the black hole bomb system.

6.3 Brown-York quasilocal formalism and the Israel surface stress tensor

The Lanczos-Darmois-Israel surface stress tensor (6.2.11) was originally derived by integrating the Gauss-Codazzi equations along the direction orthogonal to the thin surface layer [143, 142, 156]. However, it can be equivalently derived using the quasilocal Brown-York formalism [146]. This derivation further enlightens the physical interpretation of the tensor [146]. Therefore, here we will highlight some of the key properties of the Brown-York energy-momentum tensor and its relation with the Lanczos-Darmois-Israel tensor.

The Brown-York surface energy-momentum stress tensor of a $R=const$ timelike hypersurface Σ (with unit normal n, induced metric h_{ab} and extrinsic curvature K_{ab}) − *e.g.* our cavity wall − is given by [146]

$$\mathcal{T}_{ab}=-\frac{1}{8\pi}\Big(K_{ab}-Kh_{ab}\Big). \tag{6.3.1}$$

It follows from the Einstein equation, $G_{\mu\nu}=8\pi T_{\mu\nu}$, that the surface energy-momentum tensor $\mathcal{T}_{ab}$ obeys the conservation law $\mathcal{D}^{a}\mathcal{T}_{ab}=n^{\mu}T_{\mu\nu}h^{\nu}_{\ b}$, which in our case reduces simply

to $\mathcal{D}^a\mathcal{T}_{ab} = 0$ since $n^\mu T_{\mu\nu} h^\nu{}_b = 0$.[4]

The Brown-York energy, momentum and spatial stress surface densities on Σ are computed introducing a $T = const$ spacelike hypersurface Σ_T with unit normal u ($u^2 = -1$; in our case $u = \sqrt{f}dT$) that intersects orthogonally the timelike hypersurface Σ at a 2-dimensional surface B (in our case a 2-sphere of radius R, $B \equiv S^2$). The statement that Σ_T is orthogonal to Σ means that $u \cdot n|_\Sigma = 0$. Then the unit normal n in spacetime to the three-boundary Σ is also the unit normal in Σ_T to the two-boundary B. In these conditions, let $\sigma^{ab} = g^{ab} - n^a n^b + u^a u^b$ be the induced metric on B, σ be the associated determinant, and let i, j run over the coordinates of the 2-sphere such that $\sigma^a{}_i$ is the 3-dimensional tensor that projects quantities onto B. Then the Brown-York surface energy density $\tilde{\rho}$, surface momentum density $\tilde{j}_i$ and spatial stress surface densities $\tilde{p}_{ij}$ are

$$\tilde{\rho} \equiv u_a u_b \mathcal{T}^{ab} = -\mathcal{T}^T{}_T, \tag{6.3.2a}$$

$$\tilde{j}_i \equiv -\sigma_{ia} u_b \mathcal{T}^{ab}, \tag{6.3.2b}$$

$$\tilde{p}_{ij} \equiv \sigma_{ia}\sigma_{jb}\mathcal{T}^{ab}. \tag{6.3.2c}$$

To these expressions, we must still apply the appropriate reference background (denoted by the subscript $_0$) subtraction procedure detailed in [146]. For example, the physical energy surface density is $\rho = \tilde{\rho} - \tilde{\rho}_0$ and similarly for the other quantities. In our case the reference background for this subtraction procedure is Minkowski spacetime. Once this is done we find that, for our system, the Brown-York surface charge densities on a 2-sphere with radius R are:

$$\rho L = \frac{1}{4\pi}\frac{1}{R}\left(1 - \frac{1}{\sqrt{g}}\right), \tag{6.3.3a}$$

$$j_i = 0, \tag{6.3.3b}$$

$$p^i{}_j/L = \frac{R^2}{8\pi}\left(\frac{f'}{2f\sqrt{g}} + \frac{1}{R\sqrt{g}} - \frac{1}{R}\right)\sigma^i{}_j\,. \tag{6.3.3c}$$

The Brown-York quasilocal mass contained inside a 2-sphere with radius $R = 1$ is then ($G_N \equiv 1$)

$$\begin{aligned} \mathcal{M}/L &= \int_B d^2x\sqrt{\sigma}\rho \\ &= R\left(1 - \frac{1}{\sqrt{g}}\right)\Big|_{R=1}. \end{aligned} \tag{6.3.4}$$

Note that, as required for a good definition of quasilocal mass, when we send the S^2 radius to infinity, $R \to \infty$, the Bown-York mass (6.3.4) reduces to the ADM mass (6.2.4). This

[4] The quantities $\mathcal{D}_a$ and $h^\nu{}_b$ were already defined below (6.2.13). After (6.3.5) it will be clear that (6.2.11) follows from (6.3.1).

is explicitly checked using (3.0.7) and (6.2.3).

As highlighted in [146], by construction, the Lanczos-Darmois-Israel surface energy tensor $\mathcal{S}_{ab}$ (6.2.11) of the thin shell Σ (with $R = 1$ in our case) is given by the difference between the Brown-York surface tensor just outside and inside the surface layer

$$\mathcal{S}_{ab} \equiv [\mathcal{T}_{ab}] = \mathcal{T}_{ab}\big|^{out}_{R=1} - \mathcal{T}_{ab}\big|^{in}_{R=1}\,, \tag{6.3.5}$$

The Brown-York quasilocal charge inside a 2-sphere with radius $R = 1$ follows from Gauss's law evaluated at the spherical boundary,

$$\begin{aligned} \mathcal{Q}/L|_{R\to 1} &= \frac{1}{8\pi}\int_{\Sigma} \star F \\ &= \sqrt{g(R)}\frac{R^2 A'(R)}{2g(R)f(R)}\Big|_{R=1}. \end{aligned} \tag{6.3.6}$$

To complete the thermodynamic description of our solutions we still need to define the chemical potential, temperature and entropy. The chemical potential is defined as the difference between the gauge potential at the box and at the horizon,

$$\mu = A(1) - A(R_+). \tag{6.3.7}$$

Finally the temperature and the entropy are defined from the surface gravity at the horizon and from the horizon area:

$$T_H L = \lim_{R\to R_+} \frac{f'(R)}{4\pi\sqrt{f(R)g(R)}}, \qquad S/L^2 = \pi R_+^2. \tag{6.3.8}$$

The quasilocal mass and electric charge must satisfy a quasilocal form of the first law of thermodynamics:

$$\mathrm{d}\mathcal{M} = T_H\,\mathrm{d}S + \mu\,\mathrm{d}\mathcal{Q}, \quad \text{for black holes,} \tag{6.3.9}$$

$$\mathrm{d}\mathcal{M} = \mu\,\mathrm{d}\mathcal{Q}, \quad \text{for solitons.} \tag{6.3.10}$$

We will use these relations as a non-trivial check of our solutions.

6.4 Small solitons (boson stars) confined in a box

Consider a box Σ placed at $r = L$ (*i.e.*$R = 1$) in a Minkowski background with a constant gauge field $A = A_0\,\mathrm{d}T$. We can now consider adding a scalar field $\phi(R)$ to get an asymptotically flat hairy soliton that is regular at the origin and vanishes at and outside the box, $\phi(R \geq 1) = 0$. Here, we will construct this solution perturbatively in the amplitude ε of the scalar field. In our pertubation scheme, we choose unambiguously our expansion parameter to be $\varepsilon \equiv \phi'(R = 1)$ at *all* expansion orders in ε (there are no corrections to $\phi'(R = 1)$ at order ε^2 or higher). Also, we find the energy-momentum content that the thin shell Σ must have to yield a physical setup that obeys the energy conditions.

Not all perturbations fit inside the box. Those that do so are the normal modes of the system and have their dimensionless frequency $\Omega_p \equiv \omega_p L$ quantized as

$$\Omega_{\ell,p} = \sqrt{j^2_{\ell+\frac{1}{2},p} + M^2} - A_0 e \tag{6.4.1}$$

as described in Chapter 4. Here, M and e are the dimensionless mass and charge of the scalar field, respectively, and ℓ and p are the angular and radial quantum numbers that give the number of nodes of the normal mode along the polar and radial directions, respectively. Finally, $j_{\ell+\frac{1}{2},p}$ is the location of the zeros of the Bessel function $J_\nu(z)$, for $\nu = \ell + \frac{1}{2} \in \mathbb{R}$. We work in a gauge where the scalar field is static: its quantized frequency vanishes at the expense of fixing an appropriate chemical potential A_0 for the background field. In these conditions, the ground state solution (with lowest energy, $p = 1$) for a spherically symmetric ($\ell = 0$) massless scalar field is described by $\Omega_{0,1} = j_{\frac{1}{2},1} - A_0 e = \pi - A_0 e$. In the static gauge, the background gauge field is given by $A_0 = \frac{\pi}{e}$. This is the case we will describe in detail. Solutions with different parameters ℓ, p, M can be constructed in a similar way.

We can now ask whether we can back-react this normal mode solution to higher orders in perturbation theory (*i.e.* to higher orders in the amplitude ε) and eventually at full non-linear order. This question has a positive answer if we can keep the solution with the desired asymptotics regular at the origin at all orders. If so, the theory admits a soliton solution. Naturally, as the order of the expansion grows beyond linear order, the non-linearities of the field equations imply that the scalar field sources corrections on the gravitational and electric field. Therefore, not only ϕ but also f and A have an expansion in the amplitude ε. Furthermore, note that although the scalar field vanishes outside the box at all perturbation orders, the gravitational and electric fields outside the box will be corrected at each order as a consequence of requiring the induced fields to be continuous at the box. In addition, these Israel junction conditions will determine the energy-momentum tensor that the box at $R = 1$ must have to be able to accommodate such a solution. The purpose of this section is to construct perturbatively this soliton.

In the conditions just described, the fields of the soliton solution have the expansion

$$\begin{aligned} f^{(\mathfrak{R})}(R) &= \sum_{n\geq 0} \varepsilon^{2n} f^{(\mathfrak{R})}_{2n}(R), \\ A^{(\mathfrak{R})}(R) &= \sum_{n\geq 0} \varepsilon^{2n} A^{(\mathfrak{R})}_{2n}(R), \\ \phi^{(\mathfrak{R})}(R) &= \sum_{n\geq 0} \varepsilon^{2n+1} \phi^{(\mathfrak{R})}_{2n+1}(R), \end{aligned} \tag{6.4.2}$$

where the superscript $^{(\mathfrak{R})}$ indicates whether we are considering the region inside ($^{(\mathfrak{R})=in}$) or outside ($^{(\mathfrak{R})=out}$) the box located at $R=1$. We use the scaling symmetry (3.0.4) in each region to impose (6.2.9) at all orders in ε, *i.e.*

$$f^{in}\big|_{R=1} = 1\,, \qquad f^{out}\big|_{R\to\infty} = 1\,. \tag{6.4.3}$$

In the interior region, as described in (6.2.7), the cavity surface Σ is parametrically described by $R=1$ and $T = T^{in}(\tau) = \tau$ such that the induced line element of the shell reads $\mathrm{d}s^2|_{\Sigma^{in}} = -f^{in}|_{(R=1)}\mathrm{d}\tau^2 + \mathrm{d}\Omega_2^2$ and the induced gauge 1-form is $A|_{\Sigma^{in}} = A^{in}|_{(R=1)}\mathrm{d}\tau$. At leading order ($n=0$) we have a scalar field perturbation around the Minkowski background ($f_0^{in}=1$) with a constant gauge potential $A_0^{in} = a_0$. The most general solution of the associated Klein-Gordon equation is $\phi(R) = R^{-1}\left(\beta_1 e^{-iea_0R} + \beta_2 e^{iea_0R}\right)$. To avoid a divergence $1/R$ at the origin we must choose $\beta_2 = -\beta_1$. At the box, the condition $\phi(R=1)=0$ – see (6.2.5) – requires $A_0^{in} = a_0 = p\frac{\pi}{e}$ for $p = 1, 2, 3, \cdots$ and we focus on the $p=1$ case. This will give the ground state soliton with lowest energy, i.e. the soliton that corresponds to the back-reaction of the spherically symmetric ($\ell = 0$) normal mode of Minkowski in a box with the lowest frequency. Finally, (6.2.5) implies that $\beta_1 = -i/(2\pi)$. In these conditions, the regular fields inside the box read

$$f_0^{in} = 1, \qquad A_0^{in} = \frac{\pi}{e}, \qquad \phi_1^{in}(R) = -\frac{\sin(\pi R)}{\pi R}\,. \tag{6.4.4}$$

As discussed in (6.2.8), when seen from outside, the cavity shell Σ is parametrically described by $R=1$ and $T = T^{out}(\tau) = N\tau$ so that the induced line element is $\mathrm{d}s^2|_{\Sigma^{out}} = -N^2 f^{out}|_{(R=1)}\mathrm{d}\tau^2 + \mathrm{d}\Omega_2^2$ and the induced gauge 1-form is $A|_{\Sigma^{out}} = NA^{out}|_{(R=1)}\mathrm{d}\tau$. Solving the equations of motion outside the box at leading order yields:

$$f_0^{out}(R) = C_2^{f_0} - \frac{\eta}{R} + \frac{(C_1^{A_0})^2}{2R^2}, \qquad A_0^{out}(R) = \frac{C_1^{A_0}}{R} + C_2^{A_0}. \tag{6.4.5}$$

The boundary conditions (6.2.3), *i.e.*(6.4.3), imply that $C_2^{f_0} = 1$. On the other hand the

junction conditions (6.2.10a)-(6.2.10c) at the box,

$$\begin{aligned} &f_0^{in}(1)\,\mathrm{d}\tau^2 = N^2 f_0^{out}(1)\,\mathrm{d}\tau^2 \qquad \Leftrightarrow \quad 1 = N^2\left(1-\eta+\frac{(C_1^{A_0})^2}{2}\right), \\ &A_0^{in}(1)\,\mathrm{d}\tau = N A_0^{out}(1)\,\mathrm{d}\tau \qquad \Leftrightarrow \quad \frac{\pi}{e} = N\left(C_2^{A_0}-C_1^{A_0}\right), \\ &A_0^{in\,\prime}(1)\,\mathrm{d}\tau\mathrm{d}R = N A_0^{out\,\prime}(1)\,\mathrm{d}\tau\mathrm{d}R \quad \Leftrightarrow \quad 0 = C_1^{A_0} N\,. \end{aligned} \tag{6.4.6}$$

fix three other integration constants (including the reparametrization factor):

$$C_1^{A_0} = 0, \qquad C_2^{A_0} = \frac{\pi}{e}\frac{1}{N}, \qquad N = \frac{1}{\sqrt{1-\eta}}\,. \tag{6.4.7}$$

The integration constant η is undetermined. It characterizes the energy-momentum content of the box as discussed below. Altogether the solution at leading order ($n=0$) is

$$\begin{aligned} &f_0^{in}(R) = 1\,, && A_0^{in}(R) = \frac{\pi}{e}\,, && \phi_1^{in}(R) = -\frac{\sin(\pi R)}{\pi R}\,; \\ &f_0^{out}(R) = 1-\frac{\eta}{R}\,, && A_0^{out}(R) = \frac{\pi}{e}\sqrt{1-\eta}\,, && \phi_1^{out}(R) = 0\,; \\ &N = \frac{1}{\sqrt{1-\eta}}\,. \end{aligned} \tag{6.4.8}$$

In these conditions, the leading order $n=0$ Lanczos-Darmois-Israel surface stress tensor (6.2.11) has the non-vanishing components

$$\mathcal{S}^t{}_t = -\frac{1}{4\pi}\left(1-\sqrt{1-\eta}\right)+\mathcal{O}(\varepsilon^2)\,, \qquad \mathcal{S}^i{}_i = \left(\frac{1-\frac{1}{2}\eta}{8\pi\sqrt{1-\eta}}-1\right)+\mathcal{O}(\varepsilon^2)\,, \tag{6.4.9}$$

where $i=2,3$ runs over the S^2 coordinates, and $\mathcal{O}(\varepsilon^2)$ reminds us that this tensor will receive corrections at order $n=1$. The reader will observe that we have not imposed the final Israel junction condition (6.2.10d). We *could* do it and thus fix the leftover integration constant η to vanish to have a continuous extrinsic curvature across Σ and thus a vanishing Lanczos-Darmois-Israel tensor (6.4.9) at zeroth order in the expansion. Had we chosen to do so, at leading order the surface layer Σ would have no energy density neither pressure. Thus, it would just split the spacetime into interior and exterior regions that are both described by the Minkowski solution (with a constant gauge field) with the interior region also containing a linear scalar field that, at order $n=0$, has not yet back-reacted on the gravitoelectric fields neither on the box surface stress tensor. However, we will *not* fix η: we will not require the extrinsic curvature to be continuous at leading order $n=0$. The reason being that at order $n=1$ we will find that the Lanczos-Darmois-Israel surface stress tensor gets negative contributions proportional to ε^2 that would violate all the energy conditions! (Indeed see the final result (6.4.12).) So to have a *physical* box that confines the scalar field inside it in the conditions (6.2.5), we must choose a box

that at leading order $n = 0$ has a non-vanishing Lanczos-Darmois-Israel surface tensor (6.4.9). The associated positive energy density and pressure will be able to accommodate the higher order negative contributions and allow the energy conditions to be obeyed. In these conditions, if $0 < \eta \leq 1$ the ADM mass is non-vanishing: the surface layer has energy-momentum surface tensor described by (6.4.9) (η) which has an associated mass that can be read asymptotically. Therefore, the interior solution is Minkowski spacetime with a linear scalar field and the exterior solution is described by the Schwarzschild geometry with ADM mass proportional to η.[5] The hairy solitons are thus a 2-parameter family of solutions described by the expansion parameter ε and by the energy density of the cavity (that also fixes uniquely its pressure). Note that we are choosing the simplest physical box that can confine the scalar field: it has no surface electric charge density. If we wish, this cavity can also have an electric charge density in which case the exterior solution would be described by the RN BH geometry (the hairy solitons would be a 3-parameter family of solutions).

This completes the analysis up to $\mathcal{O}(\varepsilon^1)$. A similar procedure can be used to extend the construction of the soliton to higher orders ($n > 0$) in ε. In principle, we should be able to choose the integration constants at each order such that the solution is regular (6.2.1) and asymptotically flat (6.2.3) as well as satisfying the Israel junction conditions (6.2.10a)-(6.2.10c). To present the results (6.4.10) below we have completed this exercise and determined the fields f, A, ϕ up to order $\mathcal{O}(\varepsilon^5)$ but we do not present the auxiliary computations because they are not further enlightening. One can find the explicit computations at order $n = 1$ in the publication [3].

Once we have obtained the fields f, A, ϕ up to order $\mathcal{O}(\varepsilon^5)$ we can compute the (gauge invariant) Brown-York quasilocal thermodynamic quantities at Σ_{in} (defined in subsection 6.3) for the soliton up to $\mathcal{O}(\varepsilon^6)$[6]. As the soliton has no horizon, the entropy is zero and the temperature is undefined. On the other hand, the Brown-York quasilocal mass (6.3.4), quasilocal charge (6.3.6) and chemical potential $\mu \equiv A^{in}\big|_{R=1}$ are given by

$$\begin{aligned}
\mathcal{M}/L &= \varepsilon^2 \frac{1}{2} + \varepsilon^4 \frac{15\pi^2 - 6e^2 - 16\pi\left[2\,\mathrm{Si}(2\pi) - \mathrm{Si}(4\pi)\right]}{24\pi^2} + \mathcal{O}(\varepsilon^6), \\
\mathcal{Q}/L &= \varepsilon^2 \frac{e}{2\pi} + \varepsilon^4 \frac{e}{8\pi^4}\Big[-\left(8\pi^2 - e^2\right)\left[2\,\mathrm{Si}(2\pi) - \mathrm{Si}(4\pi)\right] + 4\pi\left(e^2 - 2\pi^2\right)\Big] + \mathcal{O}(\varepsilon^6), \\
\mu &= \frac{\pi}{e} + \varepsilon^2 \frac{\left(8\pi^2 - 3e^2\right)\left[2\,\mathrm{Si}(2\pi) - \mathrm{Si}(4\pi)\right] + 3\pi\left(2e^2 - 3\pi^2\right)}{6\pi^2 e} + \mathcal{O}(\varepsilon^4).
\end{aligned} \tag{6.4.10}$$

As a non-trivial check of our computations, these thermodynamic quantities satisfy the quasilocal version of the first law of thermodynamics (6.3.10), $\mathrm{d}\mathcal{M} = \mu\,\mathrm{d}\mathcal{Q}$. At leading

[5] Actually, apart from the presence of scalar field that motivates here the need for an Israel surface layer, this setup is the textbook example of a Lanczos-Darmois-Israel static thin shell separating Minkowski spacetime in the interior from the Schwarzschild geometry in the exterior: see *e.g.* section 3.10 of Poisson's textbook (with rotation $a = 0$) [158].

[6] Note that f, A, ϕ up to order $\mathcal{O}(\varepsilon^6)$ determines the chemical potential up to order $\mathcal{O}(\varepsilon^4)$.

order, $\mu = \pi/e \equiv \tilde{\Omega}/e$, which corresponds to the lowest normal mode frequency $\tilde{\Omega} = \tilde{\omega}L = \pi$ that can fit inside the spherical box Σ [2].

The ADM mass and the charge measured by an asymptotic observer include the contribution associated to the energy-momentum tensor of the box Σ and thus they depend on the constant η that characterizes the matter content of the box; see discussion associated to (6.4.9). They are given by

$$\begin{aligned} M/L &= \frac{\eta}{2} + \varepsilon^4 \frac{(1-\eta)e^2}{4\pi^2} + \mathcal{O}(\varepsilon^6), \\ Q/L &= \varepsilon^2 \frac{e\sqrt{1-\eta}}{2\pi} + \varepsilon^4 \frac{e\sqrt{1-\eta}}{8\pi^4}\Big(10\pi^3 - 4\pi e^2 - \left(8\pi^2 - e^2\right)\left[2\,\mathrm{Si}(2\pi) - \mathrm{Si}(4\pi)\right]\Big) + \mathcal{O}(\varepsilon^6)\,. \end{aligned} \tag{6.4.11}$$

The Lanczos-Darmois-Israel surface energy-momentum tensor (6.2.11) at Σ has non-vanishing components given by:

$$\begin{aligned} S^t{}_t &= \frac{1}{8\pi}\left[2\left(-1+\sqrt{1-\eta}\right) + \varepsilon^2 + \varepsilon^4\left(\frac{5}{4} - \frac{e^2}{2\pi^2} - \frac{4\left[2\,\mathrm{Si}(2\pi) - \mathrm{Si}(4\pi)\right]}{3\pi}\right) + \mathcal{O}\left(\varepsilon^6\right)\right], \\ S^x{}_x &= S^\phi{}_\phi = \frac{1}{8\pi}\left[\left(\frac{1-\frac{1}{2}\eta}{\sqrt{1-\eta}} - 1\right) - \frac{\varepsilon^2}{2} + \frac{\varepsilon^4}{8}\left(1 + \frac{2e^2}{\pi^2}\left(1-\sqrt{1-\eta}\right)\right) + \mathcal{O}\left(\varepsilon^6\right)\right]. \end{aligned} \tag{6.4.12}$$

In section 6.7.1 we further discuss the physical interpretation of this energy-momentum tensor.

Finally note that under a gauge transformation we can move to a frame where the scalar field is complex, $\phi = |\phi|e^{-i\omega t}$, and it oscillates in time with a frequency ω. In this case the solitonic solution is often called a boson star.

6.5 Reissner-Nordström black hole confined in a box

In section 6.6 we shall construct perturbatively an asymptotically flat hairy black hole solution whose scalar field is confined inside a cavity. In the absence of a horizon radius and scalar field, this cavity has no charge density but it has an energy density and pressure described by the Israel surface tensor (6.4.9), parametrized by the constant η. In the limit where the horizon radius vanishes, our hairy solution reduces to the hairy soliton found in section 6.4. On the other hand, when the scalar field is absent, the hairy black hole of section 6.6 reduces to a solution that describes a RN BH with horizon inside the Israel cavity. In this section we describe the gravitational and electric field of this solution. The interior solution and aspects of the thermodynamic properties of this solution (mainly in

the grand-canonical ensemble) were already discussed in the seminal works [152, 153, 154] and, more recently, in [155, 114]. Here, for completeness, we also describe the fields in the region exterior to the box. For small energy and charge, the hairy black hole of section 6.6 can be seen as the solution that emerges from placing the small caged RN black hole of this section on top of the caged hairy soliton of section 6.4.

Consider first the region $R \leq 1$ inside the cavity located at $R = 1$. The general solution to the equations of motion (3.0.6) with the scalar field set to zero is given by:

$$f^{in}(R) = B_2^f - \frac{B_1^f}{R} + \frac{(B_1^A)^2}{2R^2}\,, \qquad A^{in}(R) = B_2^A - \frac{B_1^A}{R}. \tag{6.5.1}$$

Boundary conditions at the horizon (6.2.2) fix two integration constants, $B_1^A = B_2^A R_+$ and $B_1^f = R_+\left(\frac{1}{2}(B_2^f)^2 + B_2^f\right)$. At the box location, we use the scaling symmetry (3.0.4) to require $f^{in}(1) = 1$. We also introduce the chemical potential (6.3.7) as it appears in the quasilocal first law (6.3.9): $\mu = A^{in}(1) - A^{in}(R_+)$. These two conditions fix the two remaining constants as $B_2^A = \frac{\mu}{1-R_+}$ and $B_2^f = \frac{2-R_+(2-\mu^2)}{2(1-R_+)^2}$. Altogether, the fields of a RN BH whose horizon is confined inside a box located at $R = 1$ are:

$$\begin{aligned} f^{in}(R) &= \frac{2-R_+(2-\mu^2)}{2(1-R_+)^2} - \frac{R_+\left[\mu^2(1+R_+)+2(1-R_+)\right]}{2R(1-R_+)^2} + \frac{\mu^2 R_+^2}{2R^2(1-R_+)^2}, \\ A^{in}(R) &= \frac{\mu}{1-R_+}\left(1-\frac{R_+}{R}\right), \qquad g^{in}(R) = \frac{2-R_+(2-\mu^2)}{2(1-R_+)^2}\frac{1}{f^{in}(R)}\,. \end{aligned} \tag{6.5.2}$$

Consider now the solution outside the box, $R \geq 1$. The most general solution reads

$$f^{out}(R) = C_2^f - \frac{C_1^f}{R} + \frac{(C_1^A)^2}{2R^2}\,, \qquad A^{out}(R) = C_2^A - \frac{C_1^A}{R}. \tag{6.5.3}$$

We use the scaling symmetry (3.0.4) to set $f^{out}|_{R\to\infty} = 1$ which fixes $C_2^f = 1$. To fix the remaining integration constants we apply the Israel junction conditions (6.2.10a)-(6.2.10c) across the timelike hypersurface Σ. Moreover, we use the parametrizations (6.2.7)-(6.2.8) for the surface layer Σ.

We want to confine the horizon radius of the RN BH inside the 'same cavity' that cages the hairy soliton of the previous section. By this statement we mean that the Israel surface tensor of the caged RN (and of our hairy solutions) reduces to the Israel surface tensor (6.4.9) when $R_+ \to 0$ (and/or $\varepsilon \to 0$). This requires that we use exactly the same reparametrization factor $N = (1-\eta)^{-1/2}$ that was found in (6.4.8) and which describes the Israel surface tensor (6.4.9) of our box. This fixes $C_1^f = \frac{\eta\left[2(1-R_+)^2-\mu^2R_+^2\right]+\mu^2R_+^2}{2(1-R_+)^2}$, $C_1^A =$

$\mu R_+ \frac{\sqrt{1-\eta}}{1-R_+}$, and $C_2^A = \mu \frac{\sqrt{1-\eta}}{1-R_+}$. The final solution outside the surface layer reads

$$\begin{aligned} f^{out}(R) &= 1 - \frac{1}{R}\frac{\eta\left[2(1-R_+)^2 - \mu^2 R_+^2\right] + \mu^2 R_+^2}{2(1-R_+)^2} + \frac{1}{R^2}\frac{(1-\eta)\mu^2 R_+^2}{2(1-R_+)^2}\,, \\ A^{out}(R) &= \frac{\mu\sqrt{1-\eta}}{1-R_+}\left(1 - \frac{R_+}{R}\right), \qquad\qquad g^{out}(R) = \frac{1}{f^{out}(R)}\,. \end{aligned} \tag{6.5.4}$$

where η is the parameter that describes the Israel surface tensor (6.4.9) of our box (even before we place a scalar field or horizon inside it). In particular, if we set $R_+ = 0$, (6.5.2) and (6.5.4) reduce to (6.4.8) with $\phi = 0$. That is to say, the zero horizon radius limit of the caged RN BH solution (6.5.2) and (6.5.4) describes the same solution as the zero scalar field limit of the soliton (6.4.8). This common solution simply describes a surface layer cavity, placed in Minkowski space, with Israel surface tensor (6.4.9).[7] In these conditions, the cavity is the same and it will be consistent to place the small caged RN black hole of this section at the center of the caged hairy soliton of the previous section, as we do in section 6.6.

With the interior solution (6.5.2), we can use the quasilocal formalism presented in section 6.3 to compute the quasilocal thermodynamic quantities of a caged RN black hole as a function of the horizon radius and the chemical potential:

$$\begin{aligned} T_H L &= \frac{2-\mu^2}{4\pi R_+\sqrt{2}\sqrt{2-(2-\mu^2)\,R_+}}, \qquad S/L^2 = \pi R_+^2. \\ \mathcal{M}/L &= 1 - \frac{(1-R_+)\sqrt{2}}{\sqrt{2-(2-\mu^2)\,R_+}}, \qquad \mathcal{Q}/L = \frac{\mu R_+}{\sqrt{2}\sqrt{2-(2-\mu^2)\,R_+}}. \end{aligned} \tag{6.5.5}$$

Notice that extremal black holes have chemical potential $\mu = \sqrt{2}$, hence RN BH inside a box exist in the region of parameters $\mu \in [0, \sqrt{2}]$ and $R_+ \in]0, 1[$. These quasilocal thermodynamic quantities obey the quasilocal first law (6.3.9). We will further discuss the quasilocal thermodynamic properties of the caged RN BH in section 6.7.2.

As an aside note, observe that a small horizon radius expansion of the RN quasilocal thermodynamics (6.5.5) yields, at leading order,

$$\begin{aligned} T_H L &= \frac{1}{8\pi R_+}(2-\mu^2) + \mathcal{O}(R_+), \qquad S_H/L^2 = \pi R_+^2\,, \\ \mathcal{M}/L &= \frac{R_+(2+\mu^2)}{4} + \mathcal{O}(R_+^2), \qquad \mathcal{Q}/L = \frac{\mu R_+}{2} + \mathcal{O}(R_+^2). \end{aligned} \tag{6.5.6}$$

[7] That is, when we set $R_+ = 0$ one gets $f^{in}(R) = 1$, $A_t^{in}(R) = \mu$ and $f^{out}(R) = 1 - \eta/R$, $A_t^{out}(R) = \mu\sqrt{1-\eta}$. Note that the time reparametrization factor $N = (1-\eta)^{-1/2}$ guarantees that $f^{out}|_{R\to\infty} = 1$. This setup (with $\mu = 0$) is the textbook example of a Lanczos-Darmois-Israel static thin shell separating Minkowski spacetime in the interior from the Schwarzschild geometry in the exterior with η being proportional to the mass of the shell as measured by an asymptotic observer: see *e.g.* section 3.10 of [158] (with rotation $a = 0$).

These leading order quantities coincide with the familiar ADM thermodynamic quantities of a RN black hole in the *absence* of a cavity. This is to be expected since taking the limit $R_+ \equiv \frac{r_+}{L} \to 0$ implies $r_+ \ll L$ which is the same as taking the limit $L \to \infty$ where the box is transported to the asymptotic region. In this limit we should indeed recover the ADM quantities of a RN black hole. Making contact with section 4.4 , note that the non-interacting thermodynamic model (which only captures the leading order thermodynamics of the system) makes use of this property.

For completeness, from (6.2.4) and the asymptotic behaviour of (6.5.4), we can also read the ADM mass and charge of the caged RN black hole system,

$$M/L = \frac{\eta}{2} + R_+^2 \frac{\mu^2(1-\eta)}{4(1-R_+)^2}\,, \qquad Q/L = \frac{\mu R_+ \sqrt{(1-\eta)}}{2(1-R_+)}\,. \tag{6.5.7}$$

6.6 Small hairy black holes confined in a box

In section 6.4 we found that our theory (3.0.1) has hairy soliton solutions in addition to the caged RN BH solutions of section 6.5. In these conditions, as argued in section 4.4, the theory should admit a third solution − a hairy black hole − that in the small energy/charge limit can be thought of as placing a small caged RN BH on top of a hairy soliton. Following this intuition, the leading order thermodynamics of these hairy black holes has been computed (without solving the equations of motion) in section 4.4 using a simple thermodynamic model that assumes that the hairy black hole is a non-interacting mixture of two constituents: the soliton and the caged RN black hole. The two solutions can indeed be 'merged' to yield a hairy black hole as long as the two components are in thermodynamic equilibrium and have the same chemical potential (4.4.3).

On the other hand, there is yet another argument in favour of the existence of hairy black hole solutions. It is well established that RN black holes are unstable to the superradiant and near-horizon scalar condensation instabilities [108, 109, 110, 111, 112, 113, 107, 114, 115, 117, 118, 119, 120, 2]. It is then natural to expect that if we take such an unstable RN black hole as initial data, the system should time evolve towards a new solution that has scalar hair floating above the horizon, with the electric repulsion balancing the gravitational collapse. If so, this hairy black hole should have higher entropy (for a given mass and charge) than the initial system. These hairy black holes should then be the endpoint of the superradiant instability of a RN black hole in a box. A time evolution study done recently confirmed that a RN BH perturbed with a scalar field indeed evolves towards a hairy black hole [108, 110, 107, 117, 118].

In this section, we solve the equations of motion of (3.0.6) perturbatively to construct

these static hairy black holes. We will confirm that, at least for small mass and charge, the intuition of the previous paragraphs is correct. Our hairy black holes should therefore be the endpoint of the superradiant instability of a RN BH in a box.

6.6.1 Setting up the perturbation problem

Asymptotically flat hairy black holes of the Einstein-Maxwell theory confined inside a box must solve the equations of motion (3.0.6), subject to boundary conditions (6.2.2), (6.2.3) and Israel junction conditions (6.2.10a)-(6.2.10c). We construct them perturbatively and find analytical expressions for the fields. The hairy black holes of our theory are a two-parameter family of solutions that we can take to be the asymptotic scalar amplitude ε defined as the derivative of the scalar field at the $R = 1$ box $-$ see (6.2.5) $-$ and the horizon radius R_+. Therefore, the perturbative construction requires a double expansion of the fields in powers of ε and R_+ [8]. To be able to solve analytically the equations of motion, we do a matched asymptotic expansion, similar to those done in a similar context in AdS backgrounds in [51, 125, 128, 53, 126, 97] and used in Chapters 4 and 5. An explicit example of implementation of the method is done in 4.2.3. However, here we also need to impose the junction conditions at the mirror located at $r = L$ ($R = 1$). As for the soliton case, the box location divides the spacetime into the *inside* (^{in}; $r \leq L$) and *outside* (^{out}, $r \geq L$) regions and we use the Israel junction conditions to match the fields of these two regions at the box hypersurface $r = L$ ($R = 1$). But, this time, we further divide the inside region (^{in}; $r \leq L$) into two sub-domains: the *near* region $r_+ \leq r \ll L$ ($^{in-near}$) and the *far* region where $r_+ \ll r < L$ ($^{in-far}$). Considering small black holes that have $r_+/L \ll 1$, the near and far regions inside the box have an overlapping zone, $r_+ \ll r \ll L$. In this overlapping region, we can match the set of independent parameters that are generated by solving the perturbative equations of motion in each of the near and far regions.

We can start our perturbative construction. First note that the chemical potential of the hairy black hole should itself have a double expansion in powers of ε and R_+,

$$\mu = \sum_{n\geq 0} \varepsilon^{2n} \sum_{k\geq 0} R_+^k \mu_{2n,k}. \tag{6.6.1}$$

We also justified this in 5.5.1. We shall construct the hairy black hole family whose zero-radius limit is the *ground state* soliton of section 6.4 (so with lowest energy for a given charge).[9] In our analysis we take $\varepsilon \ll 1$ and $R_+ \ll 1$ and we assume that $\mathcal{O}(\varepsilon^2) \sim \mathcal{O}(R_+)$. It follows that terms with same $(n + k)$ contribute equally to the perturbative expansion, e.g. $\mathcal{O}\left(\varepsilon^0, R_+^2\right) \sim \mathcal{O}\left(\varepsilon^2, R_+\right) \sim \mathcal{O}\left(\varepsilon^4, R_+^0\right)$.

[8] If one wanted to go beyond the perturbative expansion, one should solve numerically the set of equations (3.0.6).

[9] A similar construction can be done for the excited hairy black holes.

Outside the box, $R \geq 1$, the black hole can be considered to be a small perturbation in ε and R_+ of Minkowski spacetime and the scalar field is required to vanish. In addition to (6.6.1), the fields in this region (we use the superscript ^{out} to refer to this zone) have the double expansion

$$\begin{aligned} f^{out}(R) &= \sum_{n\geq 0} \varepsilon^{2n} \sum_{k\geq 0} R_+^k \, f^{out}_{2n,k}(R), \qquad A^{out}(R) = \sum_{n\geq 0} \varepsilon^{2n} \sum_{k\geq 0} R_+^k \, A^{out}_{2n,k}(R), \\ \phi^{out}(R) &= 0\,, \end{aligned} \tag{6.6.2}$$

where we took into account that odd powers of ε do not give corrections of the fields $f,\ A$.

In the far region inside the box, $R_+ \ll R < 1$, the fields of the hairy black hole still have a similar double expansion but this time the scalar field is also present (we use the superscript $^{in-far}$ to refer to this domain):

$$\begin{aligned} f^{in-far}(R) &= \sum_{n\geq 0} \varepsilon^{2n} \sum_{k\geq 0} R_+^k \, f^{in-far}_{2n,k}(R), \qquad A^{in-far}(R) = \sum_{n\geq 0} \varepsilon^{2n} \sum_{k\geq 0} R_+^k \, A^{in-far}_{2n,k}(R), \\ \phi^{in-far}(R) &= \sum_{n\geq 0} \varepsilon^{2n+1} \sum_{k\geq 0} R_+^k \, \phi^{in-far}_{2n+1,k}(R). \end{aligned} \tag{6.6.3}$$

By construction, our hairy black hole solution has a smooth $R_+ \to 0$ limit where it reduces to the hairy soliton constructed in the previous section. To make this limit straightforward, we use the scaling symmetry (3.0.4) in each region to require that

$$f^{in-far}\big|_{R=1} = 1\,, \qquad f^{out}\big|_{R\to\infty} = 1\,, \tag{6.6.4}$$

which is equivalent to (6.4.3).

The outside fields (denoted collectively by Q^{out}) must obey the boundary conditions (6.2.3) and these outside fields further have to be matched with the inside-far region fields Q^{in-far} at the timelike hypersurface Σ using the parametrizations (6.2.7)-(6.2.8) and the Israel junction conditions (6.2.10a)-(6.2.10c). In particular, we are constructing our hairy black hole by placing the caged RN BH of section 6.5 on top of the soliton of section 6.4. Both of these constituents are confined inside the same cavity. This means that we use exactly the same reparametrization factor $N = (1-\eta)^{-1/2}$ that was found in (6.4.8) and that describes the Israel surface tensor (6.4.9) of our box.[10]

More concretely, we solve the equations at each order $\{n, k\}$ analytically (with the help of

[10]Recall that η essentially describes the energy-momentum tensor of the box we choose to start with, even before it receives corrections proportional to the scalar field amplitude ε and horizon radius R_+. We cannot set it to zero or else the energy conditions are not obeyed, as discussed below (6.4.9) and in (6.4.12). Our caged RN BHs and hairy solutions have a Israel surface stress tensor that reduces to (6.4.9) when $R_+ \to 0$ and/or $\varepsilon \to 0$

Mathematica) and find the *out* (*in-far*) fields up to a total of 4 (6) integration constants. The boundary conditions (6.2.3) for the metric fix some constant(s). The Israel junction conditions at the box (6.2.10a)-(6.2.10c) fix extra integration constants. We are left with a few integration constants and a chemical potential coefficient of (6.6.1), to be fixed by the matching with the inside-near region, as described next.

We take the small radius R limit of the inside-far fields, $Q^{in-far}(R)\big|_{R\ll 1}$ in order to prepare these fields to be matched with the inside-near region fields (collectively denoted by $Q^{in-near}$) to be discussed below. The fields Q^{in-far} turn out to be divergent when $R\to 0$ as $\frac{R_+}{R}$. This gives an indication that the solutions do not hold for $R\sim R_+$, which is reasonable as we can no longer consider the black hole to be a small perturbation of the Minkowski spacetime at this scale. This justifies why the far-region analysis inside the box is valid only for $R\gg R_+$. Also, it follows that in the far-region we can safely do a Taylor expansion in $R_+\ll 1$ and $\varepsilon\ll 1$ since the large hierarchy of scales between the solution parameters R_+,ε and R guarantees that they do not compete.

Consider finally the inside-near region, $R_+\leq R\ll 1$. Here, Taylor expansions in $R_+\ll 1$ and $\varepsilon\ll 1$ should be done with some caution since these small parameters can now be of similar order as R. This is closely connected with the fact that the inside-far region solution above breaks down when $R/R_+\sim\mathcal{O}(1)$. This suggests that to proceed with the inside-near region analysis we should first introduce new radial, y, and time, τ, coordinates as

$$y=\frac{R}{R_+},\qquad \tau=\frac{T}{R_+}. \tag{6.6.5}$$

In this new frame, the inside-near region corresponds to $1\leq y\ll R_+^{-1}$. If we further require that $R_+\ll 1$ (as is necessarily the case in our perturbative expansion) one concludes that the inside-near region corresponds to $R_+\ll 1\leq y$ (and $y\gg\varepsilon$). In particular, Taylor expansions in $R_+\ll 1$ and $\varepsilon\ll 1$ can now be safely done since the radial coordinate y and the black hole parameters R_+,ε have a large hierarchy of scales[11]. Further physical insight is gained if we rewrite the caged RN solution (6.5.2) in the new coordinate system (6.6.5):

$$\begin{aligned} \mathrm{d}s^2 &= R_+^2\Big(-f(y)\mathrm{d}\tau^2+g(y)\mathrm{d}y^2+y^2\mathrm{d}\Omega_2^2\Big), \\ f(y) &= \left(1-\frac{1}{y}\right)\frac{2-\left(2-\mu^2\right)R_+-\frac{\mu^2}{y}}{2(1-R_+)^2}, \\ A_\tau(y) &= R_+\,A_T(y)=R_+\,\frac{\mu}{1-R_+}\left(1-\frac{1}{y}\right). \end{aligned} \tag{6.6.6}$$

The explicit factor of $R_+\ll 1$ in $A_\tau(y)$ shows that in the inside-near region the electric field is weak. Thus, at leading order, the gauge field is suppressed in the equations of

[11] A key step for the success of the matching expansion procedure is that a factor of R_+ (one of the expansion parameters) is absorbed in the new coordinates (6.6.5).

motion and the system is to be seen as a small perturbation around the neutral solution. The same holds when we add a small scalar condensate to the system. The near fields of the hairy black hole thus have the double expansion (we use the superscript $^{in-near}$ to refer to this region):

$$f^{in-near}(y) = \sum_{n\geq 0} \varepsilon^{2n} \sum_{k\geq 0} R_+^k \, f_{2n,k}^{in-near}(y), \qquad A^{in-near}(y) = \sum_{n\geq 0} \varepsilon^{2n} \sum_{k\geq 0} R_+^k \, A_{2n,k}^{in-near}(y),$$
$$\phi^{in-near}(y) = \sum_{n\geq 0} \varepsilon^{2n+1} \sum_{k\geq 0} R_+^k \, \phi_{2n+1,k}^{in-near}(y). \tag{6.6.7}$$

In these conditions we can now solve analytically the equations of motion (3.0.6)-(3.0.7) for $Q^{in-near}(y)$. One has to consider these equations with the change of variables (6.6.5) at each order in $\{n, k\}$. As the set of equations is a system of 3 ODEs for f, A and ϕ at each order we have a total of 6 integration constants to be fixed. Three are determined by the boundary conditions at the horizon (6.2.1) (one for each field) and the other three constants are fixed by the matching with the inside-far region solution in the overlapping region $R_+ \ll R \ll 1$. For this matching, we restore the coordinates $\{T,\ R\}$ and consider the large radius expansion of the inside-near fields, $Q^{in-near}(R)\big|_{R\gg 1}$ (with the expansion coefficients available at the given order). We find that these diverge as a power of R, which shows that the near region analysis breaks down at $R \sim 1$. This explains why the near region analysis is valid only for $R \ll 1$. We can then match the two regions in powers of ε, R_+ and R to fix the three integrations constants that were not yet determined.

In the end of the day, after imposing boundary, junction and matching conditions at each order, we are left only with a free parameter that characterizes the energy-momentum content of the box.

Examples of the matching asymptotic expansion procedure can be found in the literature [51, 125, 128, 53, 126, 97, 50, 1] as well as in section 4.2.3. Specific examples for this particular setup can be found in the publication [3].

6.6.2 Thermodynamic quantities

With the perturbation expansion presented in the previous subsection and using the matched asymptotic expansion we have found the scalar, gauge and gravitational fields perturbatively. We can now insert these fields into the expressions for the quasilocal thermodynamics of subsection 6.3 to compute the thermodynamic quantities of the hairy BH. In the perturbation expansion we have assumed that $\mathcal{O}(\varepsilon^2) \sim \mathcal{O}(R_+)$. This assumption implies that terms with the same $(n+k)$ contribute equally to the perturbative expansion, *e.g.* $\mathcal{O}\left(\varepsilon^0, R_+^2\right) \sim \mathcal{O}\left(\varepsilon^2, R_+\right) \sim \mathcal{O}\left(\varepsilon^4, R_+^0\right)$. We did this consistent perturbative expansion

up to the order necessary to get the thermodynamic quantities that verify the first law of thermodynamics up to order $(n+k)=2$. This is enough to get our main result best summarized later in Fig. 6.7.1.

Using (6.2.4), the dimensionless quasilocal energy $\mathcal{M}$, quasilocal charge $\mathcal{Q}$, chemical potential μ, temperature T and entropy of the small hairy black holes are given by:

$$
\begin{aligned}
\mathcal{M}/L =& \left[\frac{R_+}{4}\left(\frac{\pi^2}{e^2}+2\right)+\frac{R_+^2}{32e^4}\left(\pi^4\Big(8[\mathrm{Ci}(2\pi)-\gamma-\ln(2\pi)]+5\Big)+4\left(e^2+\pi^2\right)e^2\right)\right.\\
&\left.+\mathcal{O}(R_+^3)\right]+\varepsilon^2\left[\frac{1}{2}+\frac{R_+}{12\pi e^2}\left(9\pi^3\Big[\gamma-\mathrm{Ci}(2\pi)-2+\ln(2\pi)\Big]+\left(8\pi^2-3e^2\right)\right.\right.\\
&\left.\left.\Big[2\mathrm{Si}(2\pi)-\mathrm{Si}(4\pi)\Big]\right)+\mathcal{O}(R_+^2)\right]+\varepsilon^4\left[\frac{15\pi^2-6e^2+16\pi\big[\mathrm{Si}(4\pi)-2\mathrm{Si}(2\pi)\big]}{24\pi^2}\right.\\
&\left.+\mathcal{O}(R_+)\right]+\mathcal{O}(\varepsilon^6)\\
\mathcal{Q}/L =& \left[\frac{\pi R_+}{2e}+\frac{R_+^2}{8e^3}\left(\pi^3\Big(2[\mathrm{Ci}(2\pi)-\gamma-\ln(2\pi)]+1\Big)+2\pi e^2\right)+\mathcal{O}(R_+^3)\right]+\varepsilon^2\left[\frac{e}{2\pi}\right.\\
&\left.+\frac{R_+}{12\pi^2 e}\left(12\pi^3\Big(\gamma-\mathrm{Ci}(2\pi)+\ln(2\pi)-\frac{7}{4}\Big)+\left(8\pi^2-3e^2\right)\big[2\mathrm{Si}(2\pi)-\mathrm{Si}(4\pi)\big]\right)\right.\\
&\left.+\mathcal{O}(R_+^2)\right]-\left[\varepsilon^4\frac{e\left(\left(8\pi^2-e^2\right)(2\mathrm{Si}(2\pi)-\mathrm{Si}(4\pi))+4\pi e^2-8\pi^3\right)}{8\pi^4}+\mathcal{O}(R_+)\right]\\
&+\mathcal{O}(\varepsilon^6), \qquad (6.6.8)\\
\mu =& \left[\frac{\pi}{e}-R_+\frac{\pi^3}{2e^3}\Big(\gamma-\mathrm{Ci}(2\pi)-1+\ln(2\pi)\Big)+\mathcal{O}(R_+^2)\right]\\
&+\varepsilon^2\left[\frac{8\pi^2-3e^2}{6\pi^2 e}\Big(2\mathrm{Si}(2\pi)-\mathrm{Si}(4\pi)\Big)+\frac{e}{\pi}-\frac{3\pi}{2e}+\mathcal{O}(R_+)\right]+\mathcal{O}(\varepsilon^4),\\
TL =& \frac{1}{4\pi R_+}\left\{\left[1-\frac{\pi^2}{2e^2}+\frac{R_+}{8e^4}\left(4\pi^4\Big(\gamma-\mathrm{Ci}(2\pi)+\ln(2\pi)-\frac{3}{4}\Big)+4\left(e^2-\pi^2\right)e^2\right)\right.\right.\\
&\left.\left.+\mathcal{O}(R_+^2)\right]+\varepsilon^2\left[\frac{3e^2-8\pi^2}{6\pi e^2}\Big(2\mathrm{Si}(2\pi)-\mathrm{Si}(4\pi)\Big)-\frac{\pi^2}{2e^2}\Big(\gamma-\mathrm{Ci}(2\pi)-4\right.\right.\\
&\left.\left.+\ln(2\pi)\Big)-1+\mathcal{O}(R_+)\right]+\mathcal{O}(\varepsilon^4)\right\},\\
S/L^2 =& \pi R_+^2.
\end{aligned}
$$

Recall that $\mathrm{Ci}(x)=-\int_x^\infty \frac{\cos z}{z}\mathrm{d}z$ and $\mathrm{Si}(x)=\int_0^x \frac{\sin z}{z}\mathrm{d}z$ are the cosine and sine integral functions, respectively, and $\gamma\sim 0.577216$ is Euler's constant.

As an important check of the computations, notice that these thermodynamic quantities satisfy the quasilocal form of the first law of thermodynamics (6.3.9). Moreover, when $R_+ = 0$, (6.6.8) reduces to the soliton thermodynamics (6.4.10) and, when $\varepsilon = 0$, (6.6.8) yields the caged RN black hole thermodynamics (6.5.5) (once we insert μ in (6.6.8) into (6.5.5) and take a series expansion up to $\mathcal{O}(R_+^2)$).

From these thermodynamic quantities (6.6.8), we can confirm that the simple non-interacting thermodynamic model presented in section 4.4 − which does *not* use the equations of motion − captures the correct *leading* order thermodynamics. First note that, at leading order, it follows from (6.6.8) that $\mu = \frac{\pi}{e}$. Assuming, as justified above, that $\mathcal{O}(\varepsilon^2) \sim \mathcal{O}(R_+)$, the leading order contributions of the expansion (6.6.8) allow to express analytically R_+ and ε in terms of $\mathcal{M}$ and $\mathcal{Q}$,

$$\begin{aligned} R_+ &= \frac{4e(e\mathcal{M} - \pi\mathcal{Q})}{2e^2 - \pi^2} + \mathcal{O}\left(\mathcal{M}^2, \mathcal{Q}^2, \mathcal{M}\mathcal{Q}\right), \\ \varepsilon^2 &= \frac{2\pi\left(2e^2\mathcal{Q} - 2\pi e\mathcal{M} + \pi^2\mathcal{Q}\right)}{2e^3 - \pi^2 e} + \mathcal{O}\left(\mathcal{M}^2, \mathcal{Q}^2, \mathcal{M}\mathcal{Q}\right), \end{aligned} \tag{6.6.9}$$

which we insert in the expressions for the other thermodynamic quantities to find that at leading order in $\mathcal{M}$ and $\mathcal{Q}$ one has:

$$\begin{aligned} \mu &= \frac{\pi}{e} + \mathcal{O}\left(\mathcal{M}, \mathcal{Q}\right), \\ S/L^2 &= \frac{16\pi e^2(e\mathcal{M} - \pi\mathcal{Q})^2}{\left(\pi^2 - 2e^2\right)^2} + \mathcal{O}\left(\mathcal{M}^2, \mathcal{Q}^2, \mathcal{M}\mathcal{Q}\right), \\ TL &= \frac{\left(\pi^2 - 2e^2\right)^2}{32\pi e^3(e\mathcal{M} - \pi\mathcal{Q})} + \mathcal{O}\left(\mathcal{M}^2, \mathcal{Q}^2, \mathcal{M}\mathcal{Q}\right). \end{aligned} \tag{6.6.10}$$

These quantities (6.6.10) match the result of the non-interacting model presented in equation (4.4.4). Thus the non-interacting thermodynamic model does indeed capture the leading order properties of this hairy black hole system at very low cost. This explicit confirmation adds to those done in similar hairy black hole systems in [51, 125, 128, 53, 126, 30, 98] and 5.5.2 and realize in simple terms the idea that we can place a small black hole, without hair, of the theory at the core of its hairy soliton to get the hairy black hole of the theory.

For completeness, note that an asymptotic observer measures the ADM mass and ADM

charge of the hairy black hole to be:[12]

$$
\begin{aligned}
M/L =& \left[\frac{\eta}{2}+R_+^2\frac{\pi^2(1-\eta)}{4e^2}+\mathcal{O}(R_+^3)\right]+\varepsilon^2\left(R_+\frac{1-\eta}{2}+\mathcal{O}(R_+^2)\right)\\
&+\varepsilon^4\left(\frac{e^2(1-\eta)}{4\pi^2}+\mathcal{O}(R_+)\right)+\mathcal{O}(\varepsilon^6), \qquad (6.6.11)\\
Q/L =& \left[R_+\sqrt{1-\eta}\frac{\pi}{2e}+R_+^2\frac{\pi\sqrt{1-\eta}}{4e^3}\Big(2e^2+\pi^2\big[1-\gamma+\mathrm{Ci}(2\pi)-\ln(2\pi)\big]\Big)+\mathcal{O}(R_+^3)\right]\\
&+\varepsilon^2\left[\frac{e\sqrt{1-\eta}}{2\pi}+R_+\left(\frac{\sqrt{1-\eta}}{24\pi^2 e}\Big(6\pi e^2+3\pi^3\big[8\gamma-10\mathrm{Ci}(2\pi)-11+8\ln(2\pi)\big]\right.\right.\\
&\left.+(16\pi^2-6e^2)\big[2\mathrm{Si}(2\pi)-\mathrm{Si}(4\pi)\big]\Big)+\frac{\sqrt{1-\eta}}{e}\mathcal{C}_1\right)+\mathcal{O}(R_+^2)\left.\right]+\varepsilon^4\left[\frac{e\sqrt{1-\eta}}{8\pi^4}\right.\\
&\left.\Big(\big(e^2-8\pi^2\big)\big[2\mathrm{Si}(2\pi)-\mathrm{Si}(4\pi)\big]-4\pi e^2+10\pi^3\Big)+\mathcal{O}(R_+)\right]+\mathcal{O}(\varepsilon^6).
\end{aligned}
$$

Finally, the Lanczos-Darmois-Israel surface energy-momentum tensor (6.2.11) at the surface layer Σ has non-vanishing components given by:

$$
\begin{aligned}
S^t{}_t =& \frac{1}{8\pi}\left\{\left[-2\left(1-\sqrt{1-\eta}\right)+R_+\left(1+\frac{\pi^2}{2e^2}\right)+R_+^2\left(\frac{e^2+\pi^2}{4e^2}+\frac{\pi^4}{16e^4}\Big(5-8\big[\gamma-\right.\right.\right.\\
&\left.\left.\left.\mathrm{Ci}(2\pi)+\ln(2\pi)\big]\Big)\right)+\mathcal{O}(R_+^3)\right]+\varepsilon^2\left[1+R_+\left(\frac{8\pi^2-3e^2}{6\pi e^2}\big[2\mathrm{Si}(2\pi)-\mathrm{Si}(4\pi)\big]+\right.\right.\\
&\left.\left.\frac{3\pi^2}{2e^2}\Big(\gamma-\mathrm{Ci}(2\pi)+\ln(2\pi)-2\Big)\right)+\mathcal{O}(R_+^2)\right]+\varepsilon^4\left[\frac{5}{4}-\frac{e^2}{2\pi^2}-\frac{4\big[2\mathrm{Si}(2\pi)-\mathrm{Si}(4\pi)\big]}{3\pi}\right]+\\
&\mathcal{O}\left(\varepsilon^6\right)\Bigg\}, \qquad (6.6.12)\\
S^x{}_x = S^\phi{}_\phi =& \frac{1}{8\pi}\left\{\left[\frac{2\left(1-\sqrt{1-\eta}\right)-\eta}{2\sqrt{1-\eta}}-R_+^2\left(\frac{\left(\pi^2-2e^2\right)^2}{32e^4}+\frac{\pi^2}{8e^2}\sqrt{1-\eta}\right)+\mathcal{O}(R_+^3)\right]+\right.\\
&\left.\frac{\varepsilon^2}{2}\left[-1+R_+\Big(1-\sqrt{1-\eta}\Big)+\mathcal{O}(R_+^2)\right]+\frac{\varepsilon^4}{8}\left[1+\frac{2e^2}{\pi^2}\left(1-\sqrt{1-\eta}\right)\right]+\mathcal{O}\left(\varepsilon^6\right)\right\}.
\end{aligned}
$$

When $R_+=0$ this reduces to (6.4.12), as it should.

[12] The constant $\mathcal{C}_1$ in the expression for Q is given by:

$$
\begin{aligned}
\mathcal{C}_1 =& \frac{1}{8}\pi\left[2i\pi\left(G^{3,1}_{2,3}\left(-2i\pi\,\middle|\,\begin{matrix}-1,1\\-1,0,0\end{matrix}\right)-G^{3,1}_{2,3}\left(2i\pi\,\middle|\,\begin{matrix}-1,1\\-1,0,0\end{matrix}\right)\right)-G^{3,1}_{2,3}\left(-2i\pi\,\middle|\,\begin{matrix}0,2\\0,0,1\end{matrix}\right)\right.\\
&\left.-G^{3,1}_{2,3}\left(2i\pi\,\middle|\,\begin{matrix}0,2\\0,0,1\end{matrix}\right)\right]\simeq -0.0177191, \quad \text{where } G^{m\,n}_{p\,q}\left(x\,\middle|\,\begin{matrix}a_1,\ldots,a_p\\b_1,\ldots,b_q\end{matrix}\right) \text{ is the MeijerG function.}
\end{aligned}
$$

These ADM quantities should obey a first law of thermodynamics that includes a term that accounts for the thermodynamic contribution of the Israel surface layer.

6.7 Discussion of physical properties

6.7.1 Israel surface stress tensor and energy conditions

Scalar fields confined inside a box were already studied in the literature: 1) at the linear level [108, 109, 110, 111, 112, 119, 120, 121, 122, 123, 124], 2) as a nonlinear elliptic problem (although without having flat asymptotics [113, 115, 116] or without discussing the exterior solution [114]), and 3) as an initial-value problem [107, 117, 118]. However, to the best of our knowledge, the properties of the "internal structure" of the cavity that is necessary to confine the scalar field were never analysed. It was never discussed whether the energy-momentum content of the mirror necessary to confine the scalar field is physically acceptable and, if so, what are its properties. Now that we have the regular and asymptotically flat hairy solitons and hairy black holes of the theory we can analyse the Lanczos-Darmois-Israel surface stress tensor (6.2.11) and address these questions. At the frontline, we have to ask whether it does obey or not the energy conditions.

As pointed out before, in our construction we have imposed the Israel junction conditions on the gravitoelectric fields at the surface layer Σ. We decided to impose that the component of the electric field orthogonal to Σ is continuous across σ hence the surface has no electric charge density, which motivated our choice. With these conditions on Σ the system is left with a free parameter. Essentially we have a 1-parameter family of solutions, that is labeled by the parameter η, that differ on the energy-momentum content of the surface layer Σ or, equivalently, on the total mass of the solution. η determines the mass of the shell and thus of the hairy solution (as can be checked inspecting the mass formulas in (6.4.11) and (6.6.11)). Different choices of η dictate a distinct extrinsic curvature jump at Σ and consequently a different Lanczos-Darmois-Israel surface stress tensor.

In (6.4.12) and (6.6.12) we have computed the three non-vanishing components of the tensor $S^a{}_b$ for the soliton and hairy black hole, respectively. As a consequence of the conservation law for the Brown-York stress tensor (see subsection 6.3), the Lanczos-Darmois-Israel surface tensor is also conserved, $\mathcal{D}_a S^{ab} = 0$, as we can explicitly check. Further note that the zero horizon radius limit of the hairy black hole is the soliton and thus that (6.6.12) reduces to (6.4.12) when we set $R_+ \to 0$.

The Lanczos-Darmois-Israel surface tensor can be written in the perfect fluid form, $\mathcal{S}_{(a)(b)} = \mathcal{E} u_{(a)} u_{(b)} + \mathcal{P}(h_{(a)(b)} + u_{(a)} u_{(b)})$, with $u = f^{-1/2}\partial_t$ and local energy density $\mathcal{E} = [\rho]$ and

pressure $\mathcal{P} = [p]$ given by[13]

$$\mathcal{E} = -S^t{}_t\,, \qquad \mathcal{P} = S^x{}_x = S^\phi{}_\phi, \tag{6.7.1}$$

with $S^t{}_t, S^x{}_x, S^\phi{}_\phi$ defined in (6.4.12) and (6.6.12) for the soliton and hairy black hole respectively.

Physical surface layers must have a stress tensor (an energy density and pressure) that obeys the energy conditions. Different versions of these energy conditions read ($i = 1, 2$) [159]:

$$\text{Weak energy condition:} \qquad \mathcal{E} \geq 0 \quad \wedge \quad \mathcal{E} + \mathcal{P}_i \geq 0\,; \tag{6.7.2}$$

$$\text{Strong energy condition:} \qquad \mathcal{E} + \mathcal{P}_i \geq 0 \quad \wedge \quad \mathcal{E} + \sum_{i=1}^{2} \mathcal{P}_i \geq 0\,; \tag{6.7.3}$$

$$\text{Null energy condition:} \qquad \mathcal{E} + \mathcal{P}_i \geq 0\,; \tag{6.7.4}$$

$$\text{Dominant energy condition:} \qquad \mathcal{E} + |\mathcal{P}_i| \geq 0\,, \tag{6.7.5}$$

Set $R_+ = 0$ and $\varepsilon = 0$ in (6.6.12) and (6.7.1). A physical surface layer with $0 < \eta \leq 1$ has an energy density and pressure and associated jump in the extrinsic curvature. Solutions with these parameters split the spacetime into an interior region that is Minkowski spacetime and an exterior region which is described by the Schwarzschild geometry with ADM mass proportional to η, $M = \eta L/2$. If we choose $\eta = 0$, the surface layer is absent.

Now, consider the hairy solitons whose surface layer Σ has stress tensor (6.4.12), *i.e.* let $\varepsilon \neq 0$ but $R_+ = 0$ in (6.6.12) and (6.7.1). An inspection of these quantities quickly concludes that for $\eta = 0$, none of the energy conditions (6.7.2) is obeyed. As discussed already below (6.4.9), we must have $\eta \neq 0$ to guarantee that they (or a relevant subset of them) are obeyed. Actually, we can find the minimum shell parameter η, as a power expansion in ε, above which (with $\eta < 1$) the energy conditions (or a select subset of them) are obeyed. Consider now the hairy black hole with $\varepsilon \neq 0$ and $R_+ \neq 0$ in (6.6.12) and (6.7.1). There is still a minimum shell parameter η, which we can express as a double power expansion in ε and R_+, above which (with $\eta < 1$) the energy conditions (or a select subset of them) are obeyed. To conclude this discussion on the energy conditions, as an important byproduct of our study, we have found the energy-momentum content that a

[13] These densities can also be computed following a different, but equivalent, route (see *e.g.* [159]). Introduce the orthogonal tetrad on Σ, $e_{(0)} = f^{-1/2}\partial_t$, $e_{(k)} = r^{-1}\hat{e}_{(k)}$, $(k = 1, 2)$, such that $h_{uv}e_{(a)}{}^u e_{(b)}{}^v = \eta_{(a)(b)}$ with $\eta_{(a)(b)} = \mathrm{diag}\{-1, 1, 1\}$ being the 3-dimensional Minkowski metric and $\hat{e}_{(k)\,i}\hat{e}^{(k)}{}_j = \sigma_{ij}$. The components of the Lanczos-Darmois-Israel energy-momentum tensor (6.2.11) (at Σ) in the tetrad frame are then $\mathcal{S}_{(a)(b)} = e_{(a)}{}^u e_{(b)}{}^v \mathcal{S}_{uv}$ and one has $\mathcal{S}_{(a)(b)}e^{(b)} = \lambda\, e_{(a)}$ which is an eigenvalue equation. That is, $\lambda = \{-\mathcal{E}, \mathcal{P}_i\}$ are the eigenvalues (with $\mathcal{E}$ the energy density and $\mathcal{P}_i$ the two principal pressures) and $e_{(a)}$ are the associated unit eigenvectors (principal directions). In particular, $e_{(0)}$ is the 3-velocity of a box observer in her local rest frame.

mirror must have to confine a hairy soliton or hairy black hole inside of it.

6.7.2 Phase diagram of asymptotically flat solutions in a box

Einstein-Maxwell theory with a complex scalar field (with a given scalar field mass and electric charge) is described by action (3.0.1). The only asymptotically flat solutions of this theory are Minkowski spacetime and the Reissner-Nordström black hole family of solutions, which have a vanishing scalar field. However, if we introduce a reflecting box that confines the scalar field, we have found that the theory admits several regular asymptotically flat solutions. These are the caged RN BH (section 6.5), the ground state soliton (section 6.4), the ground state hairy black hole (section 6.6) and an infinite tower of excited solitons and hairy black holes[14]. For a given scalar field electric charge, the latter excited solutions always have larger energy than the ground state solutions so we do not discuss them further.

It is natural to expect that the thermal phases of the theory compete with each other. It is thus important to display the several solutions of the theory in a phase diagram of (regular) asymptotically flat boxed solutions. For example, it is important to display the region of existence of each of these solutions in a mass-charge phase diagram as well as to present a microcanonical phase diagram in which we plot the entropy of the solutions as a function of their mass and electric charge.[15]

We find appropriate to work with the Brown-York quasilocal mass $\mathcal{M}$ and charge $\mathcal{Q}$. Essentially, this is because these quasilocal quantities are independent of the parameter η that describes the energy-momentum content of the shell that confines the scalar field.[16] The quasilocal thermodynamics of the (ground state) soliton, caged RN black hole, and hairy black hole are given in (6.4.10), (6.5.5) and (6.6.8), respectively (for vanishing scalar field mass $m = 0$).

The left panel of Fig. 6.7.1 shows the region of existence of caged RN black holes, (ground state) solitons and (ground state) hairy BHs for a scalar field charge $e \equiv qL = 3.5$[17]. The diagram is qualitatively similar for other values of e that are above the superradiant bound

[14] Recall that the ground state solutions have their perturbative root in the lowest normal mode frequency of Minkowski spacetime, and the excited states emerge from the remaining infinite tower of normal mode frequencies.

[15] RN black holes caged inside a box were discussed in the grand-canonical ensemble in [154]. Moreover, [114] constructed numerically the hairy solutions of the system and discussed them in the grand-canonical ensemble. At least for small charges where our perturbative analysis is valid, hairy black holes can be the dominant thermal phase only in the microcanonical ensemble so we restrict our discussion to this ensemble.

[16] Essentially, these different solutions differ from each other in the interior region and the energy-momentum content of this region is best captured by the quasilocal thermodynamics. Further recall that these quasilocal quantities obey the quasilocal first law of thermodynamics (6.3.9) and (6.3.10), which we used to check our final results.

[17] In Chapter 4 we have also picked the value $qL = 3.5$ to display the quasinormal modes of RN in a box and characterize the regions of instability. For consistency we have kept the same value in this discussion.

i.e. $e > \frac{\pi}{\sqrt{2}}$. The horizontal axis scans the dimensionless quasilocal charge $\mathcal{Q}/L$ while the vertical axis plots the difference $\Delta\mathcal{M} \equiv \mathcal{M} - \mathcal{M}_{ext}$ between the dimensionless quasilocal mass $\mathcal{M}/L$ of a given solution and the mass $\mathcal{M}_{ext}$ of the extremal caged RN BH that has the same electric charge. So, the extremal caged RN BH family is represented by the horizontal blue line with $\Delta\mathcal{M} = 0$. RN BHs exist above the blue line, in regions I and II. In region II, RN BHs are unstable, with the magenta line separating regions I and II describing the onset of superradiance. The black line (with negative slope) describes the hairy soliton branch. Hairy black holes exist in regions II and III. That is, they merge with the RN BH family at the onset of superradiance − described by (6.6.8) with $\varepsilon = 0$ − and extend all the way down to the soliton line − described by (6.6.8) with $R_+ = 0$. In region II we have non-uniqueness of solutions for a given quasilocal mass and charge.

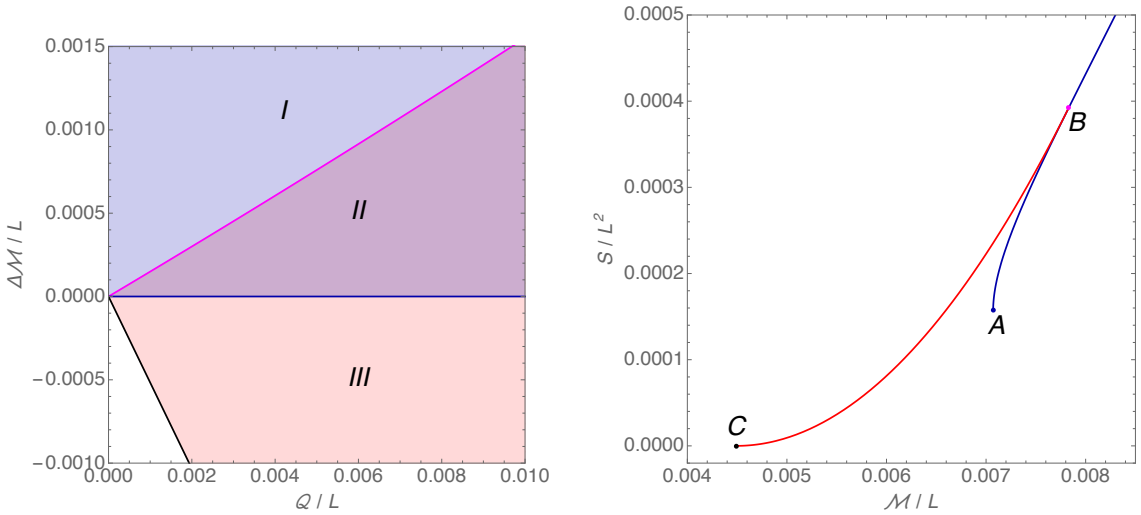

Figure 6.7.1: **Left Panel:** Region of existence of solutions. We plot the quasilocal mass difference $\Delta\mathcal{M} = \mathcal{M} - \mathcal{M}_{ext}$ (between a given solution and the extremal caged RN BH with the same charge $\mathcal{Q}$) as a function of the quasilocal electric $\mathcal{Q}$ for $e = qL = 3.5$. Caged RN black holes exist in regions I and II. The magenta line with positive slope splitting these two regions describes the onset curve of the superradiant instability (RN BHs are unstable in region II). The black line with negative slope describes the soliton family. Hairy black holes exist in between these two lines, *i.e.* in regions II and III (red shaded area). **Right Panel:** Phase diagram in the microcanonical ensemble *i.e.* adimensional entropy S/L^2 as a function of the adimensional quasilocal mass $\mathcal{M}/L$ at constant value of the quasilocal charge $\mathcal{Q}/L = 0.005$ and $e = 3.5$. The blue line starting at A (extremality) is the RN black hole and the red line BC is the hairy back hole branch that ends at the soliton C. The merger point B (superradiant instability onset) signals a second order phase transition.

In the right panel of Fig. 6.7.1 we plot the dimensionless entropy S/L^2 as a function of the quasilocal mass $\mathcal{M}/L$ for a fixed quasilocal charge $\mathcal{Q}/L = 0.005$, again for $qL = 3.5$. This phase diagram is qualitatively similar for other (small values) $\mathcal{Q}/L$ and qL. The caged RN BH branch (blue curve) exists for large mass and charge and extends all the way down to point A. This point A represents the extremal RN configuration with $T = 0$ but finite entropy (it corresponds to the point with $\mathcal{Q}/L = 0.005$ in the blue horizontal line of the left

panel). Point B signals the onset of superradiance: caged RN BHs between point B and A are unstable. The onset of superradiance (point B) signals a second order phase transition to the branch of hairy black holes (which is stable to superradiance) and extends from point B towards point C (that has vanishing entropy). The latter, is the limit $R_+ \to 0$ of the hairy BH family and describes the hairy soliton with $\mathcal{Q}/L = 0.005$. The former (point B) describes the hairy BH branch in the limit $\varepsilon \to 0$ where it merges with the RN family.

In the microcanonical ensemble the energy $\mathcal{M}$ and the charge $\mathcal{Q}$ are held fixed and the relevant thermodynamic potential is the entropy S. The thermal phase that has the highest entropy for a given mass and charge is the dominant phase in this ensemble (recall that the soliton and Minkowski spacetime in a box have vanishing entropy as they do not have a horizon). Therefore, from the right panel of Fig. 6.7.1 we conclude that hairy BHs are the favoured thermal phase in the microcanonical ensemble. In particular, this is true in the region of phase space where they coexist with caged RN black holes. This dominance extends to all other values of the electric charge $\mathcal{Q}/L$ (where our perturbative analysis holds) and $e = qL$. Thus hairy black holes are the dominant phase in the microcanonical ensemble in their region of existence (regions II and III in the left panel of Fig. 6.7.1). These hairy black holes are stable to superradiance and we do not have any arguments suggesting they are unstable to any other mechanism within the theory described by the action (3.0.1).

The regime of validity of our perturbative computations can be inferred from the right panel plot of Fig. 6.7.1. Indeed, recall that the (quasilocal) first law of thermodynamics requires that at a second order phase transition the slope $\mathrm{d}S/\mathrm{d}\mathcal{M}$ is the same for the two branches of solutions that merge (since T is the same at the bifurcation point and $\mathrm{d}\mathcal{Q} = 0$ in the right panel of Fig. 6.7.1). This is clearly the case in our plot. However, if we start departing from the regime of validity of our perturbative analysis we increasingly find that the merger is not perfect and the slopes of the two branches no longer match. We find that this is the best criteria to identify the regime of validity of our thermodynamic results (6.6.8). With this criteria we can quantify the regime of validity. Typically, by construction, our perturbative results are valid for $\varepsilon \ll 1$ and $R_+ \ll 1$. Moreover, the scalar field charge cannot be too large to avoid large back reactions. Altogether, we restrict ourselves to $\varepsilon \lesssim 0.1$, $R_+ \lesssim 0.1$ and $\frac{\pi}{\sqrt{2}} \leq e \lesssim 4$, where $\frac{\pi}{\sqrt{2}}$ is the superradiant bound 4.3.10. With these bounds into consideration we find that for a scalar field charge $e = 3.5$ the mass and the charge must be below $\lesssim 0.07$ and $\lesssim 0.05$, respectively.

Our findings allow for a solid expectation about the endpoint of the superradiant instability of RN BHs caged in a box in asymptotically flat backgrounds. Consider the time evolution of a caged RN BH in the segment AB which is perturbed by a charged scalar field. As caged RN BHs in this region are unstable to superradiance, they should evolve to another black hole solution that is stable to this mechanism. The second law of thermodynamics

implies that the entropy can only increase. Then we should expect the unstable RN BH to evolve to the hairy black hole solution we have constructed.

CHAPTER 7

Discussion

This Part has been focused in the study of charged systems in asymptotically AdS_4 and asymptotically flat with a box spacetimes. Firstly, in Chapter 4, we have identified the regions in parameter space that render RN BHs unstable. We have used analytical as well as numerical results. Analytically we have been able to find, in a perturbative expansion about the horizon radius, frequencies and, in particular for the AdS case, we have obtained the leading order imaginary part that signals the onset of the instability.

For both cases we have identified the onset of instabilities for large black holes using the heuristic methods first used to find the near horizon condensation instability. Of particular interest, this instability is present in the asymptotically flat boxed case which had not been identified in previous literature. It follows that the near-horizon scalar condensation instability should co-exist with the superradiant instability also in the original Kerr black hole bomb system of Press and Teukolsky [57]. The onset of the frequencies is a zero-mode and thus opens the possibility of finding a new stable solution that branches off RN BHs at the onset.

The linear mode analytical study has been completed with a numerical analysis. The AdS system has been studied in more depth before, hence we have simply identified the onsets of the instabilities in section 4.2.5. The curves signalling the onsets are valuable to identify initial Cauchy data for the numerical evolution systems.

We have performed a more thorough numerical analysis for the boxed case since the most unstable mode $\ell = 0$ had only been studied in the time domain. We have characterised in detail not only the onset curves but also the frequencies, identifying the regions that are most unstable. In figure 4.3.2 we have identified the onset charge as a function of the radius for different chemical potentials and showed the approach to the analytical values obtained in sections 4.3.2 and 4.3.3. We emphasize that the bound deduced from the near-horizon condensation instability is sharp and had not been identified before for this system.

We pointed out that, in a phase diagram of static solutions of the theory, the onset curve also signals the bifurcation point to a new family of solutions that describe charged hairy black holes with scalar hair floating above the horizon. Hence any nonlinear construction of such hairy solutions can also be tested using the linear onset results: the onset curve must be a boundary for the two dimensional surface where hairy black holes exist. Without using the equations of motion, we can predict the leading order thermodynamics of these charged hairy black holes. For that, we used a non-interacting thermodynamic model that assumes that, at leading order in perturbation theory, the hairy black hole can be seen as a small RN BH placed at the core of the soliton of the theory, whose linear term is the normal modes, as long as these two constituents are in thermodynamic equilibrium (if they have the same chemical potential).

After analysing the linear problem of scalar perturbations in RN backgrounds, and identifying the unstable regions in parameter space, we have constructed the hairy black holes that are the endpoint of the instabilities in Chapters 5 and 6 . This involves solving a set of three coupled nonlinear ODE's. Thus we have used a perturbative expansion in the horizon radius and the amplitude of the scalar field to linearise the equations and solve them order by order in perturbation theory. In addition we have used a matched asymptotic expansion method to solve the equations. We have done this procedure consistently in order to identify the thermodynamic quantities (equations (5.5.6) and (6.6.8) for AdS_4 and asymptotically flat with a box cases respectively) until satisfying the first law at third order in perturbation theory: $\mathcal{O}(\epsilon^4)$, $\mathcal{O}(\epsilon^2 R_+)$, $\mathcal{O}(R_+^2)$, each included. The asymptotically AdS case adds to similar studies done previously [51, 126] in five dimensions.

These systems also admit regular horizonless solutions known as solitons. They can be found perturbatively from the backreaction of the normal modes. Using the $U(1)$ gauge freedom of the systems these solitons can be turned into periodic solutions known as boson stars.

From the thermodynamic quantities we have been able to analyse the microcanonical ensemble and confirm that hairy black holes have more entropy for a given mass and charge than any other solution in the theory and thus can be the endpoint of the instabilities. The microcanonical phase diagrams for the boxed (figure 6.7.1) and AdS (figure 5.6.1)

cases are very similar. Notice, though, that in order to analyse the phase diagram in the boxed case we have used the Brown-York quasilocal formalism. This approach has allowed us to identify the black hole quasilocal thermodynamic quantities without any explicit dependence on the box matter content.

Finally, to completely solve the boxed case, we have obtained the Israel energy-momentum tensor of the box. From its result and from the energy conditions one can determine the content that the box must initially have in order to sustain the pressure exerted by the system. The fact that a black hole bomb system in the presence of a box requires an Israel stress tensor and the associated properties are matters that were not considered in the previous studies of black hole bomb systems.

Part III

Multi-oscillators

In this Part we study nonlinear horizonless pseudo-periodic solutions to Einstein's equations with a scalar field. These solutions are coined multi-oscillators. A particular case of multi-oscillator is the boson star which was studied in the previous Part and which can be see as a single-oscillator within the family of multi-oscillators. These solutions have been studied in AdS [87] in the context of the non-linear instability (see 2.3). In particular, the study of these multi-oscillators can be used to map the islands of stability in AdS that were discussed in the Introduction.

As a byproduct of the study we will find a new family of solutions in asymptotically flat spacetimes. Indeed, as in AdS, there also exist asymptotically flat boson stars [91, 92]. In Chapter 10 we will use the same construction used to find multi-oscillators in AdS to backreact the perturbations of the boson star and thus find asymptotically flat multi-oscillators.

Since the methods used throughout this Part are very similar, we will first present the general setup which is common throughout this Part in Chapter 8.

This part is mostly contained in the publication [4] co-authored with Matthew Choptuik and Benson Way and in a forecoming paper co-authored with Benson Way.

CHAPTER 8

General setup

In this part we consider 4-dimensional Einstein gravity minimally coupled to a complex scalar field φ . The associated action is

$$S = \frac{1}{16\pi G_4}\int \mathrm{d}^4x\sqrt{-g}\left[R - 2\Lambda - 2\partial_\mu\varphi(\partial^\mu\varphi)^\dagger + 2V(|\varphi|)\right], \tag{8.0.1}$$

where R is the Ricci scalar, Λ is the cosmological constant and the potential $V(|\varphi|) = m^2\varphi\varphi^*$, with m the mass of the scalar field. We fix Newton's constant as $G_4 = 1$. In the asymptotically AdS cases we take $\Lambda = \frac{(d-1)(d-2)}{L^2}$ while in the asymptotically flat cases $\Lambda = 0$.

We will consider spherically symmetric solutions to the equations of motion derived from the action (8.0.1). However, depending on the problem we solve, we will use a different gauge to write the metric and thus we will explicitly show it in each case.

Technically, the construction of multi-oscillators is made simpler if we write the associate scalar field in a particular form: A complex scalar field can always be written in the form

$$\varphi(t,r) = e^{i\omega_1 t}\left(\varphi_r + i\varphi_i\right), \tag{8.0.2}$$

where both φ_r and φ_i are real functions of the radial coordinate r and the time coordinate t.

Multi-oscillators are characterised by the number of non-commensurate frequencies in which the solutions oscillate. Thus a single-oscillator is characterised by one frequency ω_1, a double oscillator by two frequencies ω_1, ω_2 and in general a multi-oscillator by k frequencies ω_k. A quasiperiodic function f on k frequencies has a spectral expansion

$$f(t,r) = \sum_{n_1,\ldots,n_k} A_{n_1,\ldots,n_k}(r) e^{in_1\omega_1 t + \ldots + in_k\omega_k t} \,, \tag{8.0.3}$$

which contains the same spectral information as

$$f(t_1,\ldots,t_k,r) = \sum_{n_1,\ldots,n_k} A_{n_1,\ldots,n_k}(r) e^{in_1\omega_1 t_1 + \ldots + in_k\omega_k t_k} \,, \tag{8.0.4}$$

and whose derivatives are equivalent if $\partial_t \to \partial_{t_1} + \ldots + \partial_{t_k}$. But note that the functions themselves are not equivalent under $t \to t_1 + \ldots + t_k$, so to have an equivalence between the two descriptions, the equations of motion must be independent of t, except for appearances of the derivative ∂_t and the functions f. This is the case of the equations we will encounter in this Part.

Multi-oscillators can therefore be found by setting $\partial_t \to \partial_{t_1} + \ldots + \partial_{t_k}$ in the equations of motion, promoting the functions $f_i(t,r) \to f_i(t_1,\ldots,t_k,r)$, and demanding each coordinate t_i to be periodic on frequency ω_i. In general, the result of this process defines a boundary value problem on $k+1$ coordinates which can be solved numerically.

We have somewhat simplified this process in our ansatz by placing one of the frequencies ω_1 into an overall phase - see (8.0.2) - thus removing the time dependence on t_1. Single-oscillators can therefore be found setting $\varphi_i = 0$ and removing any time dependence in the functions, leading to a set of ODEs in r. Double oscillators can be found by allowing the $\varphi_{r,i}$ to be independent of t_1 and periodic on the coordinate t_2 with frequency ω_2, leading to a a PDE in t_2 and r.

The method just explained allows to find double-oscillators as a boundary value problem in two coordinates: t_2 which has period ω_2 and r. We use this method for our construction in Chapter 9 and Chapter 10.

CHAPTER 9

New islands of stability with double-trace deformations

This Chapter is focused in the study of the nonlinear instability of AdS. We will study the impact of changing the boundary conditions of the scalar field in asymptotically AdS backgrounds by introducing a double-trace deformation. As a motivation for the Chapter we will first present an analytic perturbative computation, similar to the ones done in [64], that hints at the existence of the nonlinear instability.

9.1 Summary

The first evidence suggesting that global AdS spacetime with reflecting boundary conditions may allow arbitrarily small energy excitations to form black holes was presented in [63]. The first phenomenological evidence was presented in [64] where it was shown through a numerical evolution that initial data consisting of a Gaussian distributed scalar field would always form a black hole regardless of the inital energy. In addition this publication also presented a perturbative analysis motivating the collapse on the commensurability of the frequency spectrum and establishing a relation between the time of collapse and the break down of perturbation theory. It was also shown that one-mode initial data does not have a break down in the perturbative construction, but one can rather solve perturbatively the equations leading to the formation of a horizonless periodic solution.

Soon after, it was realised that small deviations of one-mode initial data do not collapse either, leading to non-collapsing initial data forming a set called *islands of stability* [78]. There does not exist an exhaustive proof clearly establishing which initial data may lead to instability and which not, thus the study of existence and width of these islands of stability remains an open problem with important implications for the nonlinear instability of AdS and its interpretation within the field theory dual provided by the AdS/CFT correspondence [11, 13, 12].

In this Chapter we study islands of stability in asymptotically AdS spacetime in four dimensions when a scalar field perturbation with a double-trace deformation is introduced [33]. For concreteness, the massive scalar field will have a mass $m^2L^2 = -2$, which lies between the BF bound $m^2_{BF}L^2 = -9/4$ and the unitary bound $m^2_*L^2 = -5/4$ (see section 1.2.2). We will introdue a double-trace deformation and asymptotic Robin boundary conditions for the scalar field parametrised by κ. We use κ to quantify the deviation of the asymptotic boundary condition from the Dirichlet boundary condition, which is resonant. More concretely, let t be the time measured by an observer at the boundary of AdS and x a radial coordinate with support in $[0, \pi/2]$; the asymptotic behaviour of the scalar field is

$$\varphi(t,x)|_{x\to\frac{\pi}{2}} = \varphi_1(t) + \varphi_2(t)\left(x - \frac{\pi}{2}\right) + \mathcal{O}\left(x - \frac{\pi}{2}\right)^2. \tag{9.1.1}$$

We will consider for the scalar field, double-trace boundary conditions of the form

$$\sin\left(\frac{\pi}{2}\kappa\right)\varphi_1(t) - \cos\left(\frac{\pi}{2}\kappa\right)\varphi_2(t) = 0, \tag{9.1.2}$$

with $0 \leq \kappa \leq 1$. Thus $\kappa = 1$ corresponds to Dirichlet boundary conditions and $\kappa = 0$ to Neumann boundary conditions.

There is by now, substantial evidence that two-mode-equal-amplitude [1] initial data always leads to collapse, and thus lies outside the islands of stability [78, 160, 80, 79, 85, 83, 82, 81, 84, 86, 87].

Taking the two previous considerations into account, we will consider two-mode-equal-amplitude initial data with double-trace deformation. A linear study of the system allows to find the trascendental equation (9.3.4) that normal mode frequencies obey as a function of κ. In particular, we recover the commensurate cases of Dirichlet ($\kappa = 1$) and Neumann ($\kappa = 0$) boundary conditions.

We follow [87] to determine the regions of non-collapsing initial data. We construct solutions to the full nonlinear equations that do not collapse on any timescale. That is, we will find double-oscillator solutions which are periodic in two frequencies and that at the perturbative level are the backreactions of two normal modes. These double-oscillators do

[1] In the following sections we will give a precise meaning of this two-mode-equal-amplitude concept.

not exist for Dirichlet boundary conditions as was shown in [87]. However, since for $\kappa < 1$ the spectrum of frequencies is non-commensurable, one can resum perturbation theory and thus these solutions exist, at least for small enough energies. Our first objective is to find the region of existence of double-oscillators as a function of the non-commensurability of the spectum.

However,in the Neumann bounday condition case we will encounter that the results are not as expected, as we find double-oscillator solutions that appear to exist for arbitrarily small energy even though the spectrum of energies is commensurable. Thus the second part of our study is to confirm the existence of such solutions in a time evolution simulation. We give as initial data the double-oscillator solutions and we allow the system to evolve for a long period of time (an order of magnitude larger than expected time for collapse). We will confirm that, indeed, in the Neumann case, equal-amplitude multi-oscillators exist. This will also show that the structure of solutions and of the instability of asymptotically AdS spacetime may be less universal than expected.

9.2 Setup

In Part II we showed that we can use scaling symmetries in order to express all dimensionful quantities in units of L. This effectively sets $L = 1$ and this is the approach we follow in this Chapter. Our ansatz is given by

$$\mathrm{d}s^2 = \frac{1}{\cos^2 x}\left(-f\delta^2\mathrm{d}t^2 + \frac{dx^2}{f} + \sin^2 x\,\mathrm{d}\Omega_2\right)\,, \tag{9.2.1}$$

$$\varphi(t,x) = e^{i\omega_1 t}\cos x\,(\varphi_r + \varphi_i)\,. \tag{9.2.2}$$

We recall that we set the mass of the scalar field to be $m^2 = -2$. We require all fields to be regular in the spacetime. In addition to the double-trace boundary conditions for the scalar field considered in equation (9.1.2), we require the metric fields to asymptote to AdS, and in particular we choose the gauge where

$$\delta\left(t,\frac{\pi}{2}\right) = 1, \quad f\left(t,\frac{\pi}{2}\right) = 1. \tag{9.2.3}$$

To solve numerically the equations of motion we introduce the new functions $f_i,\ i \in$

$\{1,2,3,4\}$:

$$\begin{aligned}
\delta &= 1-\cos^2 x\, f_1,\\
f &= 1+\sin^2 x\cos^2 x\left(\cos x f_2(t,x)+\varphi_i^2+\varphi_r^2\right),\\
\varphi_r &= f_3,\\
\varphi_i &= f_4.
\end{aligned} \tag{9.2.4}$$

With these considerations the Hamiltonian constraint equation defines a conserved quantity $\mathcal{E}$

$$\mathcal{E}=\bar{f}_2\left(t,\frac{\pi}{2}\right)+\tan\left(\frac{\pi}{2}\kappa\right)\left(\bar{f}_3\left(t,\frac{\pi}{2}\right)+\bar{f}_4\left(t,\frac{\pi}{2}\right)\right). \tag{9.2.5}$$

In the boundary value problem we obtain solutions over a full period. Thus the bar specifies that we take the mean to compute $\mathcal{E}$ and use its standard deviation as a numerical check. In the time evolution setup, we compute the energy at each time, thus the mean is no longer needed.

The equations of motion in our setup consist of two of Einstein's equations and two real Klein Gordon equations (one for each field φ_r and φ_i). In addition, Einstein's equations also include the constraint equation that we use in our numerical setups as a further consistency check.

9.3 Perturbative analysis

Before solving the equations of motion numerically we analyse perturbatively the equations. The Klein Gordon equation in an AdS background is a Sturm-Liouville problem with operator L:

$$\partial_{t,t}\varphi+L\varphi=0,\quad L=\frac{-1}{\tan^2 x}\partial_x\left(\tan^2 x\partial_x\right). \tag{9.3.1}$$

The operator thus defines a scalar product in $\left(0,\frac{\pi}{2}\right)$:

$$(f,g):=\int_0^{\frac{\pi}{2}} f\,g\tan^2 x\mathrm{d}x. \tag{9.3.2}$$

The Klein Gordon equation admits the following *regular* solutions:

$$\hat{e}_n(t,x)=C_n\,e^{i\omega_n t}\frac{\mathrm{sinc}\left(\omega_n x\right)}{\mathrm{sinc}\left(x\right)}, \tag{9.3.3}$$

where the constants are chosen so that $(\hat{e}_n, \hat{e}_m) = \delta_{n,m}$ and with $\mathrm{sinc}(x) = \frac{\sin x}{x}$ for $x \neq 0$ and $\mathrm{sinc}(0) = 1$. The eigenfunctions $\{\hat{e}_n\}_n$ form a basis in the Hilbert space. Imposing the boundary conditions (9.1.2) to the scalar field (9.3.3), the frequencies are quantized. The frequencies ω_n are the solutions to the equation:

$$\sin\left(\frac{\pi}{2}\kappa\right)\sin\left(\frac{\pi}{2}\omega_n\right) - \omega_n \cos\left(\frac{\pi}{2}\kappa\right)\cos\left(\frac{\pi}{2}\omega_n\right) = 0. \tag{9.3.4}$$

Notice that a Dirichlet boundary condition corresponds to $\kappa = 1$ and the frequencies are given by $\omega_n = 2, 4, 6 \ldots$ $\kappa = 0$ corresponds to Neumann boundary conditions and the frequencies are given by $\omega_n = 1, 3, 5 \ldots$ Hence both cases have a spectrum of frequencies that is commensurate.

Interestingly, one can check that starting with the Dirichlet boundary condition corresponding to $\omega_n = 2\,n$ one can continuously decrease κ and connect to the frequency at the Neumann bound with $\omega_n = 2\,n + 1$. Thus the frequency at the Neumann bound $\omega_0 = 1$ is not connected to the Dirichlet case but rather a new frequency appears when $\kappa \leq \frac{2}{\pi}\tan^{-1}\left(\frac{2}{\pi}\right)$.

To proceed to the next order in a perturbative expansion we focus on the Dirichlet case for which the basis and frequency spectrum is

$$\hat{e}_n(x) = \frac{4n\,\mathrm{sinc}(2nx)}{\sqrt{\pi}\,\mathrm{sinc}(x)}, \quad \omega_n = 2n; \quad n \in \mathbb{N}. \tag{9.3.5}$$

We use as initial data what is known as two-mode-equal-ampliude initial data first used in [64] as the simplest nonlinearly unstable model[2]. The general solution to the equation (9.3.1) is given by

$$\varphi(t,x) = \sum_{n\geq 0} a_n \cos(\omega_n t + \beta_n)\hat{e}_n(x), \tag{9.3.6}$$

with a_n and β_n determined by the initial conditions.

We are ready to define the problem we will solve perturbatively and in particular define the expansion parameter ε. We will solve the time evolution system with initial data of the form

$$\varphi^r(t,x) = \varepsilon\left(\hat{e}_1(x) + \cos\left((\omega_2 - \omega_1)t\right)\hat{e}_2(x)\right), \quad \varphi^i(t,x) = \varepsilon\left(\sin\left((\omega_2 - \omega_1)t\right)\hat{e}_2(x)\right). \tag{9.3.7}$$

Notice that this initial condition can also be written in the simpler form

$$\varphi = \varepsilon\cos(x)\left(e^{i\omega_1 t}\hat{e}_1(x) + e^{i\omega_2 t}\hat{e}_2(x)\right). \tag{9.3.8}$$

[2]We will show, while performing this perturbative computation, why the one-mode initial data is stable.

We have chosen the form (9.3.7) for consistency with the numerical computation as explained in the previous Chapter 8. Two-mode-equal-amplitude has now a precise meaning since both Fourier and normal modes are orthonormalised. Thus one mode is formed of a Fourier mode and a normal mode. The initial data (9.3.8) has two such modes and their amplitude is essentially given by ε.

Now we proceed to solve the Einstein-Klein Gordon system of equations perturbatively in ε. We will use an expansion of the fields as

$$\begin{aligned} f(t,x) = 1 + \sum_{i\geq 1} \varepsilon^{2i} f_{2i}(t,x), \qquad \delta(t,x) = 1 + \sum_{i\geq 1} \varepsilon^{2i} \delta_{2i}(t,x), \\ \varphi(t,x) = \sum_{i\geq 0} \varepsilon^{2i+1} \varphi_{2i+1}(t,x), \end{aligned} \tag{9.3.9}$$

where φ_1 is given by (9.3.8). The resulting solutions should be parameterised by the parameter ε. Since our initial data is parametrised by the frequency, backreaction will also introduce corrections to the frequencies and thus they also have an expansion described by:

$$\omega_1 = 2 + \sum_{i\geq 1} \varepsilon^{2i} \omega_{1,2i}, \qquad \omega_2 = 4 + \sum_{i\geq 1} \varepsilon^{2i} \omega_{2,2i}. \tag{9.3.10}$$

The coefficients at second order can be solved exactly yielding

$$\begin{aligned} \delta_2(t,x) &= \frac{8(-10x + 2\sin(2x) + \sin(6x))\cos^2(x)\cot(x)}{\pi} - \frac{128\cos(2t)\sin^2(x)\cos^4(x)}{\pi}, \\ f_2(r) &= -\frac{64\cos(2t)\cos(2x)\cos^4(x)}{\pi} - \frac{16(4\cos(2x) + 6\cos(4x) + 13)\cos^4(x)}{3\pi}. \end{aligned} \tag{9.3.11}$$

At third order the Klein-Gordon equation takes the form

$$\partial_{t,t}\varphi^r - 2\omega_1 \varphi_3^i - L_\varphi \varphi_3^r = S_r(t,x), \tag{9.3.12}$$

with $S_r(t,x)$ a source that depends on the fields φ_1, f_2 and δ_2 and their derivatives. The field φ_3^i obeys a similar equation with the changes $\varphi_3^i \leftrightarrow \varphi_3^r$, $S_r(t,x) \to S_i(t,x)$ and $\omega_1 \to -\omega_1$.

We solve these equations by projecting onto the Fourier sine and cosine basis. Due to possible ressonances, we choose an ansatz for the scalar fields at third order of the form:

$$\varphi_3^r(t,x) = \sum_{n=0,2,4,6} \left(\cos(nt)\varphi c_n(x) + t\left(\sin(nt)\varphi st_n(x)\right)\right), \tag{9.3.13}$$

and similarly but in a sine basis for φ_3^i.

We are left with a finite number of ordinary differential equations for the fields $\varphi c_n(x)$, $\varphi st_n(x)$ and the corresponding ones for φ_3^i. Once these equations are solved analytically we encounter the final solution at third order in perturbation theory. Terms increasing linearly in time (secular terms) appear in the solutions. We can use the correction to frequencies at second order, $\omega_{1,2}$ and $\omega_{2,2}$, in order to cancel some of the secular terms. In particular we obtain

$$\omega_{1,2} = -\frac{248}{3\pi}, \qquad \omega_{2,2} = -\frac{184}{\pi}. \tag{9.3.14}$$

However, there is a further secular term that cannot be removed and is of the form:

$$\frac{176t\cos(6t)\sin(6x)\csc(x)}{3\pi^{3/2}} \tag{9.3.15}$$

for φ_3^r and the same but with $\sin(6t)$ rather than $\cos(6t)$ for φ_3^i.

This term cannot be avoided in our construction and grows in time, thus signalling a break down of perturbation theory when $t\varepsilon^3 \sim \varepsilon$ i.e. when $t \sim \frac{1}{\varepsilon^2}$. The expression of the source terms in (**??**) is useful because it helps to identify the reason for the appearance of secular terms: in the source terms there appear solutions to the homogeneous piece of equation (**??**). It is natural that the two modes that form the initial data appear but the coefficients $\omega_{1,2}$ and $\omega_{2,2}$ can be set to cancel them. This is no longer the case for other modes, whose solution to the homogeneous equation will appear but the resulting secular term will not get cancelled. From the trigonometric structure in the time coordinate one can infer that if there exists a tetrad (j_1, j_2, j_3, j_4) such that

$$a_{j_1} \neq 0,\ a_{j_2} \neq 0,\ a_{j_3} \neq 0,\ a_{j_4} \neq 0, \qquad \Delta\omega_J \equiv \omega_{j_2} + \omega_{j_3} - \omega_{j_1} - \omega_{j_4} = 0, \tag{9.3.16}$$

then secular terms that cannot be cancelled will appear and the spectrum will be *resonant*.

9.4 Nonlinear numerical analysis of the boundary value problem

In order to solve at full nonlinear level the equations as a boundary value problem we use the procedure explained in Chapter 8. We fix the projection onto two normal modes merging at the perturbative level with (9.3.7). Thus our solutions are periodic in two different frequencies. Because the ω_1 periodicity is not manifest in the functions- thanks to the global phase $e^{i\omega_1 t}$ of the ansatz and hence the fields depend on $\omega_2 - \omega_1$- we can find the desired solutions by treating t as a periodic coordinate with period ω_2. The symmetries in the functions along t allow us to use a half Fourier grid. Thus without loss of generality

we use the following expansions

$$f_i(t_2,x) = \sum_k f_i^{(k)}(x)\cos(k\omega_2 t_2) \qquad i \in \{1,2,3,\}\,,$$
$$f_4(t_2,x) = \sum_k f_4^{(k)}(x)\sin(k\omega_2 t_2) \tag{9.4.1}$$

where $f_n^{(k)}$ indicates the k-th Fourier coefficient for the function f_n. In the radial direction we have also used pseudospectral collocation methods with Legendre polynomials.

We consider two-mode-equal-amplitude solutions to the system of Einstein's and Klein Gordon's equations. In particular we consider the amplitude induced by the scalar product (9.3.2). Let f_i (with $i = 3$ or 4) be a solution to the system of equations, we will require that these solutions obey the following properties:

$$(f_3^{(1)}, \hat{e}_1) = (f_3^{(1)}, \hat{e}_2) = (f_4^{(1)}, \hat{e}_1) = \varepsilon. \tag{9.4.2}$$

Notice that this two-mode-equal-amplitude definition is the same that we used in the perturbative analysis of the previous section. When the solution $\hat{e}_0$ exists we will also consider the case with $n = 0$ and $n = 1$. However, we use subscripts $_1$ and $_2$ to refer in general to the two modes. The equations of motion are solved as a boundary value problem using a Newton-Raphson method.

For Dirichlet boundary conditions ($\kappa = 1$) numerical time evolution evidence as well as the perturbative analysis of the previous section suggests that two-mode-equal-amplitude initial data is collapsing. We thus expect that we will not encounter the two-mode-equal-amplitude multi-oscillators when considering Dirichlet boundary conditions. Decreasing the value of κ and thus moving away from the resonant case we expect these solutions to exist. In addition we would expect them to exist for larger values of the amplitude ε the further we move from the resonant case. The perturbative analysis of the previous section may suggest that the quantity $\sqrt{\Delta\omega_J}$ is a reasonable qualitative estimate for the existence of multi-oscillator solutions. We display the quantity $\sqrt{\Delta\omega_J}$ for the case $j_i = i$ for i between 1 and 4 in Fig. 9.4.1.

In Fig. 9.4.2 we display the maximum value of $\mathcal{E}$, defined in (9.2.5), for which we have obtained multi-oscillator solutions with two-mode-equal-amplitude determined by (9.4.2) as a function of the parameter κ that characterises the double-trace deformation. The behaviour of the curve near the Dircihlet case ($\kappa = 1$) is in agreement with expectations: the maximum energy is zero at precisely $\kappa = 1$ and increases as we vary the value of κ and thus move away from the resonant case. However the result in the Neumann side is unexpected. The maximum energy flattens at an energy around 0.24. This is in agreement

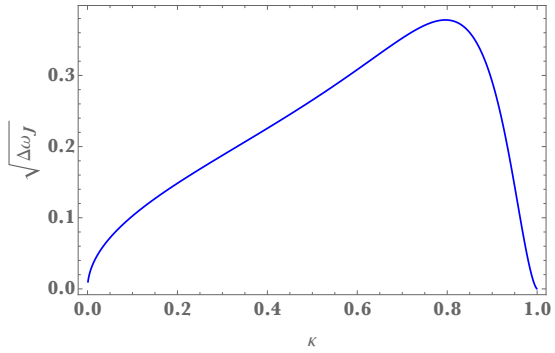

Figure 9.4.1: Value of $\sqrt{\Delta\omega_J}$ as a function of κ. $\kappa = 0$ is the Neumann boundary condition on the scalar field and $\kappa = 1$ a Dirichlet boundary condition. In both these cases, $\Delta\omega_J = 0$ and the spectrum is fully resonant.

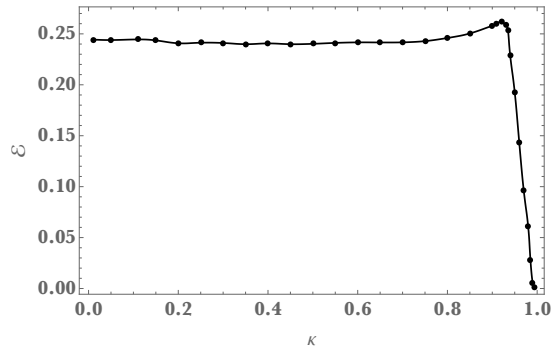

Figure 9.4.2: Maximum value of the energy for which we have encountered multi-oscillators as a function of κ.

with the maximum value of the amplitude ε that flattens at 0.06.

For Neumann boundary conditions the spectrum of frequencies is commensurable and the perturbative construction of double-oscillators breaks down at order ε^3 as we have shown in the previous section. Thus to understand the nature of the multi-oscillator solutions that we have obtained we show Fig. 9.4.3. Using normal modes (9.3.3) as a basis, we project our multi-oscillator solutions onto the basis. The largest coefficients are then given by ε which are the two modes with amplitude ε, see equation (9.4.2). At nonlinear level the projection onto other modes is no longer zero. In particular the largest coefficient other than ε coincides with the projection onto the normal mode $\hat{e}_3$. In Fig. 9.4.3 we display the maximum amplitude for which the projection onto $\hat{e}_3$ is less than 10% the projection onto $\hat{e}_1$. We constructed multi-oscillators such that in the perturbative limit $\varepsilon \to 0$ they reduce to a superposition of the normal modes $\hat{e}_1$ and $\hat{e}_2$. From this figure it is clear that the region for which this assumption is more or less valid qualitatively resembles the curve in Fig. 9.4.1. Thus the multi-oscillators in the Neumann case are solutions that are not close to double-oscillators with just two excited normal modes but rather a larger amount of modes are also excited.

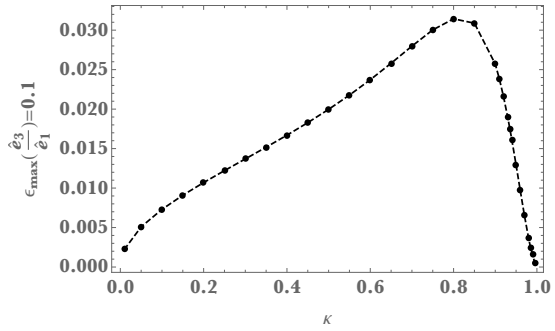

Figure 9.4.3: Maximum value of the energy for which we have encountered multi-oscillators with a ratio of the amplitudes of the projections to $\hat{e}_1$ and $\hat{e}_3$ smaller than 10% as a function of κ.

9.5 Time evolution problem

The results from the previous section point at the existence of islands of stability for Neumann boundary conditions that do not have a counterpart in the Dirichlet case. Indeed, islands of stability have been encountered with initial data that is close to an existing solitonic solution. In fact, in [87] the authors charted islands of stability by changing the ratio of the two leading amplitudes in non-equal-amplitude double-oscillators in the Dirichlet case. In the present case, however, we are encountering solutions that are not at all close to any known solitonic solution but rather resemble multi-oscillating solutions.

In order to confirm the existence of these new islands of stability, we performed a time evolution simulation. As initial data we provided the multi-oscillating solutions at time $t = 0$ and let them evolve. Our objective is to confirm the existence of non-collapsing initial-data that involves more than one dominating mode. We performed the study for different values of ε. In the following we consider the study with $\varepsilon = 0.06$ which corresponds to energy $\mathcal{E} = 0.24$.

The break down of the validity of perturbation theory typically occurs at times of order $t \sim \varepsilon^{-2}$ [64]. We thus let our code evolve until time $t = \varepsilon^{-3} \approx 4630$. As in the boundary value problem, we controlled our numerics through energy conservation and the constraint equation. Both the constraint equation and energy conservation were verified to order 10^{-10}.

The multi-oscillator solutions oscillate in two frequencies. Thus the gauge invariant quantity $\varphi\varphi^*$ should be periodic as the product cancels one of the frequencies. We thus plot the quantity $\varphi\varphi^*$ at the boundary as a function of time in Fig. 9.5.1. The panel above corresponds to the first 50 seconds of the simulation, whereas the panel below to the last 50 seconds. Clearly, the solutions are non-collapsing but rather remain periodic throughout the time of simulation.

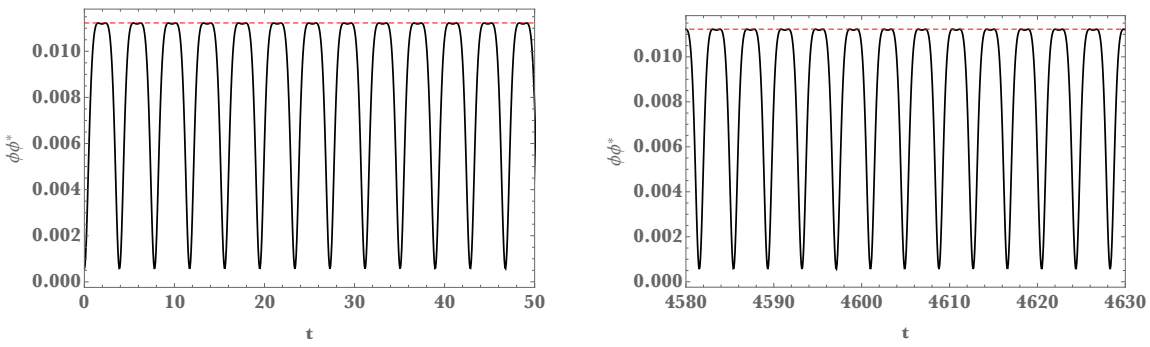

Figure 9.5.1: $\varphi\varphi^*$ at the boundary $x = \pi/2$ as a function of time for initial data consisting of a multi-oscillator with two main amplitudes $\varepsilon = 0.06$. *Top*: The first 50 seconds of the simulation. *Bottom*: The last 50 seconds of the simulation.

CHAPTER 10

Asymptotically flat multioscillators

In this Chapter we present the construction of asymptotically flat multi-oscillators that, in a phase diagram of solutions, merge with an asymptotically flat boson star. This is the first construction of such objects and it appeared in the preprint [4]. The immediate precedents are [161] which hinted at the existence of such objects in a numerical time simulation and similar constructions in asymptotically AdS spacetimes such as those of the previous Chapter.

10.1 Introduction

Boson stars are compact self-gravitating objects made of a massive complex scalar field. They were first introduced by Kaub and also Ruffini and Bonazzola in the late 1960's [91, 92]. (See [93] for a review.) Besides their intrinsic interest as self-gravitating solitonic solutions in general relativity, they are used in models of gravitational collapse, dark matter, and as gravitationally compact objects. Part of their utility stems from the fact that complex scalar fields do not suffer from issues like shocks and discontinuities that affect fluid dynamics. Thus, relative to neutron stars, for example, boson stars are easier to treat computationally, but still remain useful probes of strong field gravity.

The recent success of the gravitational wave observatories LIGO and VIRGO [162, 163]

has led to a growing interest in the merger dynamics of exotic compact objects like boson stars. It is important, therefore, to identify the generic configuration of these compact objects that forms from some dynamical process. In contrast to black holes, there are no uniqueness theorems for boson stars. Indeed, numerical simulations that do not form black holes or disperse to infinity appear to either leave a stable boson star or approach some oscillating solution [164, 165, 161, 166]. Are these oscillating solutions transient or do they remain indefinitely? If they are long-lasting, how large is the space of such oscillating solutions?

We propose that such oscillating solutions constitute an infinite dimensional family. This family includes the usual boson star family, as well as an infinite-parameter space of configurations that oscillate indefinitely on any number of frequencies. By analogy with similar solutions found in anti-deSitter space [51, 74, 79, 167, 86, 87], we call these 'multi-oscillators'. We will explicitly construct such configurations with two oscillations (double-oscillators), but our methods can in principle be used for including more oscillations.

We mention that in [161] strong numerical evidence was presented for the existence of solutions to the Einstein-Klein Gordon system with more than one scalar field. In that case a time evolution with initial data composed of a complex scalar field with the imaginary part phase-shifted was performed and it was found that the system approached a solution that was called a *phase-shifted boson star*. Such solutions should lie within the family of multi-oscillators.

10.2 Boson star and its perturbations

We begin reviewing the phase space and stability of boson stars[168, 169, 170, 171, 172, 173, 174, 175, 176, 164, 165, 161, 166]. For concreteness, we consider the theory of a complex scalar φ with mass μ, minimally coupled to gravity. Boson stars are derived from an ansatz for the scalar field of the form $\varphi = e^{i\omega_1 t}\psi(r)$ for some real function ψ with time coordinate t, and radial coordinate r. That is, the complex scalar is spherically symmetric and has periodic time dependence with frequency ω_1. This time dependence only appears as an overall phase, so the equations of motion are independent of t and reduce to a set of ordinary differential equations (ODEs) in r. Solutions to these equations can be parametrised by the frequency ω_1. Since there is only one periodic oscillation, boson stars are single-oscillators in the multi-oscillator family.

Fig. 10.2.1 shows the energy of boson stars versus the frequency ω_1. We see that there is a maximum energy that divides the solution into two branches. Solutions on the right branch (from arbitrarily small energies up to the maximum energy) are stable, while solutions on

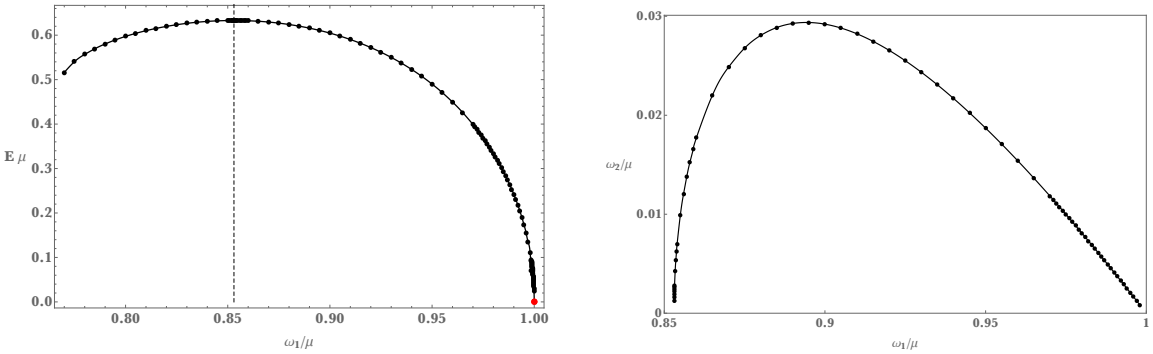

Figure 10.2.1: *Left*: Energy of boson stars versus their frequency. The red dot with zero energy marks Minkowski space. The vertical dashed line separates the solutions into the stable branch (right) and the unstable (left). *Right*: Perturbative frequencies of the stable boson star branch. The zero-frequency at $\omega_1/\mu \approx 0.853$ agrees with the maximum energy in the left panel.

the left branch are unstable.

The spectrum of linear perturbations of solutions on the stable branch consists of an infinite number of normal modes. The lowest normal mode frequency, which we call ω_2, is shown as a function of ω_1 in the right panel of Fig. 10.2.1. The point where ω_2 vanishes (with $\omega_1 \sim 0.85$) coincides with the boson star with maximum energy. That is, at this point, ω_2 corresponds to the zero mode that marks the onset of instability of boson stars.

We will demonstrate that a linear normal mode perturbation of a boson star can in fact be extended to a new nonlinear solution. Nonlinear corrections will modify the perturbative frequency ω_2, so this new solution can be parametrised by ω_1 and ω_2. This solution oscillates on both of those frequencies: a double-oscillator. But the same process can be applied using higher modes than ω_2, as well as any combination of those modes. This generates a family of solutions that oscillate on any number of frequencies ω_i: a multi-oscillator.

10.3 Numerical Construction

The numerical construction for these double-oscillators was generically explained in the Chapter 8. So in this section we will present the details that are particular to this problem.

We use the metric and scalar field ansatz

$$\mathrm{d}s^2 = -\delta\, f \mathrm{d}t^2 + \frac{\mathrm{d}r^2}{f} + r^2 \mathrm{d}\Omega_2, \tag{10.3.1a}$$

$$\varphi = e^{i\omega_1 t}\left(\varphi_r + i\varphi_i\right). \tag{10.3.1b}$$

We use the coordinate ρ given by $r = r_s \frac{\rho\sqrt{2-\rho^2}}{1-\rho^2}$ so that the domain $\rho \in (0,1)$ is compact. Here, r_s is a scaling parameter that can be chosen freely without affecting the physical solution. For convenience, we set

$$\begin{aligned} \delta &= 1 - \left(1-\rho^2\right) f_1, \\ f &= 1 - \rho^2\left(2-\rho^2\right)\left(1-\rho^2\right) f_2, \\ \varphi_r &= \left(1-\rho^2\right)^2 f_3, \\ \varphi_i &= \left(1-\rho^2\right)^2 f_4, \end{aligned} \tag{10.3.2}$$

and take $f_i,\ i = \{1,2,3,4\}$ to be real functions of t and ρ. The equations of motion contain two first-order spatial constraints for f_1 and f_2, and the two second-order Klein-Gordon equations for the scalar fields f_3 and f_4. There is also a first-order temporal constraint equation that we do not solve directly, and use as a measure of numerical accuracy. Note that since ω_1 only appears as an overall phase, the time dependence of the equations of motion lies only in the functions f_i and the derivative ∂_t.

The required boundary conditions are regularity at the origin $\rho = 0$ ($r = 0$) and asymptotic flatness at infinity $\rho \to 1$ ($r \to \infty$). One can also supply initial data for f_3 and f_4 and their time derivatives at a fixed time, say $t = 0$ and solve this system as an initial value problem. For our purposes, however, we wish to find solutions with some specified quasiperiodic behaviour in time. That is, we seek solutions that oscillate with some superposition of periods. We will therefore require additional boundary conditions on t.

Without loss of generality, we can choose the time Fourier series of f_1, f_2, and f_3 to be cosine series, and f_4 to be a sine series.

$$\begin{aligned} f_i(t_2,\rho) &= \sum_k \hat{f}_i^{(k)}(\rho)\cos(k\omega_2 t_2) \qquad i \in \{1,2,3,\}\ , \\ f_4(t_2,\rho) &= \sum_k \hat{f}_4^{(k)}(\rho)\sin(k\omega_2 t_2) \end{aligned} \tag{10.3.3}$$

We introduce the Fourier coefficients

$$\epsilon_1 = \hat{f}_3^{(0)}(0), \qquad \epsilon_2 = \hat{f}_4^{(1)}(0), \tag{10.3.4}$$

which essentially measure the amplitudes of the corresponding fields f_3 and f_4 at the origin. We find ϵ_2 to be more convenient than ω_2 as a parameter since at $\epsilon_2 = 0$ one recovers the boson star. We can therefore treat ϵ_2 as a measure of our deformation from the boson star solution. Thus we use the parameters $\{\omega_1, \epsilon_2\}$ to move numerically in phase space. We take $r_s\mu = 5/\sqrt{\epsilon}_1$ as a convenient choice of scaling parameter r_s.

The main features we extract from our numerical calculation are the frequencies ω_1 and

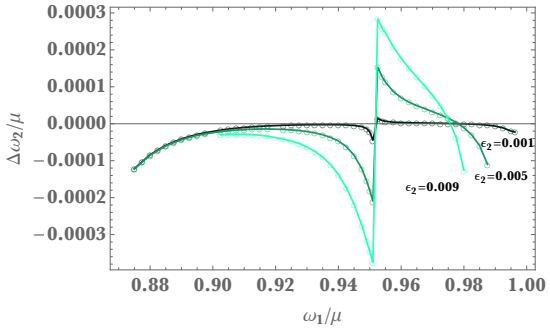

Figure 10.4.1: Change in frequency ω_2 with respect to the normal mode of the boson star as a function of ω_1.

ω_2, as well as the energy E and the mass aspect function M:

$$\frac{E}{\mu} = \frac{r_s}{2}\bar{f}_2(1), \quad \frac{M(\rho)}{\mu} = \frac{r_s\rho^3\left(2-\rho^2\right)^{3/2}}{2}\bar{f}_2(\rho). \tag{10.3.5}$$

Notice that the mass aspect function tends to the energy as $\rho \to 1$. Additionally, since the solutions are periodic in time, we compute these quantities by taking the average over a period in t_2 (which we express using a bar, as in $\bar{f}_2$) at a fixed radius ρ. Though we've taken E to be an average over a period of t_2, energy conservation actually guarantees that $f_2(t_2, 1)$ is constant. We can therefore use the standard deviation of $f_2(t_2, 1)$ as a check on numerics.

We solve the double-oscillator equations numerically using Fourier spectral methods in t_2, and fourth order finite differences in ρ. We use a Newton-Raphson method with the boson star solutions as initial estimates. For our numerical algorithm, we used 31 gridpoints in the time direction and 71 in the radial direction. For data shown here, the temporal constraint and the standard deviation of $f_2(t_2, 1)$ over a period are smaller than 10^{-6}.

10.4 Results

As we have mentioned earlier, solutions with small ϵ_2 are well-approximated by linear perturbation theory about boson stars, where ω_2 is the perturbative normal mode frequency, which have already been shown in Fig. 10.2.1.

In Fig. 10.4.1, we show how ω_2 changes from the perturbative boson star value ($\Delta\omega_2 = \omega_2 - \omega_2^{(\mathrm{BS})}$) as ϵ_2 is increased. Depending on ω_1, ω_2 may either increase or decrease from its perturbative value. Around $\omega_1 \sim 0.952$ there appears to be a divergence in this figure, which arises as a result of a degeneracy of normal modes.

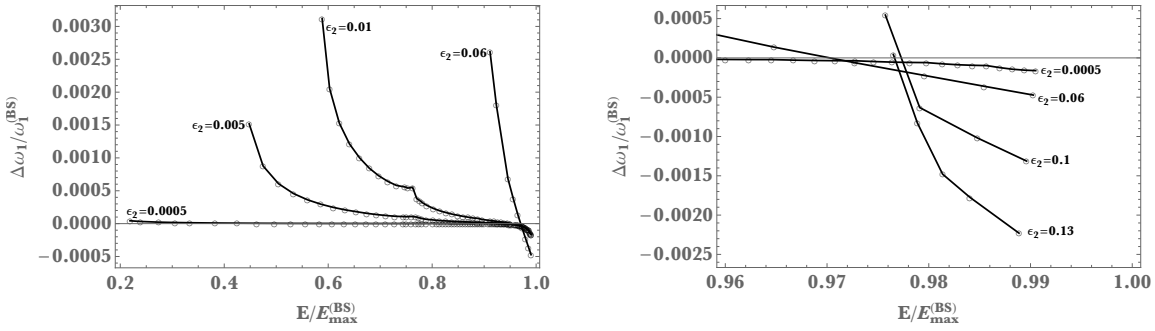

Figure 10.4.2: Difference in principal frequency $\Delta\omega_1 \equiv \omega_1 - \omega_1^{(\mathrm{BS})}$ as a function of the energy. *Top:* larger range of energies, in particular the line with $\epsilon_2 = 0.0005$ goes from frequencies $\omega_1 = 0.997$ to $\omega_1 = 0.875$. *Bottom:* Zoom into the region of larger energies where we have obtained solutions for larger values of ϵ_2.

We mention that a similar divergence has been observed in toroidal perturbations of black branes [177]. In the black brane, this divergence is a consequence of a particular alignment of perturbations. The usual perturbations are ill-defined at this divergence, and are replaced by a special and distinct set of perturbations with different symmetry properties. In the present double-oscillator case, there may likewise be a special double-oscillator generated by a distinct set of perturbations, but such a solution would not be generic.

Despite this feature of a divergence, we conclude from this figure that the secondary frequency ω_2 does not typically differ too far from the perturbative value. This could be anticipated from the fact that corrections to the frequency ω_2 occur at higher orders in perturbation theory.

We now compare various quantities between boson stars and multi-oscillators at fixed energy. We normalize the energy with respect to the maximum energy of the boson star shown in Fig. 10.2.1 using $E/E_{\mathrm{max}}^{(\mathrm{BS})}$. We note that all of the solutions we have found satisfy $E/E_{\mathrm{max}}^{(\mathrm{BS})} \leq 1$. It is conceivable that some multi-oscillators may have higher energy than the maximum boson star energy, but these would most likely exist close to the critical frequency $\omega_1 = 0.853$, where finding such solutions is numerically challenging.

In Fig. 10.4.2 we plot the relative difference between the multi-oscillator primary frequency and the frequency of the boson star $\Delta\omega_1/\omega_1^{(\mathrm{BS})} \equiv \omega_1/\omega_1^{(\mathrm{BS})} - 1$ as a function of the energy. As was seen for ω_2, we find that ω_1 can either decrease or increase from the boson star solution with the same energy, but the difference tends to remain small.

To compare the size of boson stars and double-oscillators, we consider the quantity r_{99}, which is the spherical radius at which the mass aspect function is 99% of the total energy [166]. (We take the usual spherical radius r as defined just below the ansatz (10.3.1) rather than the coordinate ρ.) In Fig. 10.4.3, we again plot a relative radius $\Delta r_{99} = r_{99}/r_{99}^{(\mathrm{BS})} - 1$ as a function of energy. We see from this figure that double-oscillators are larger and

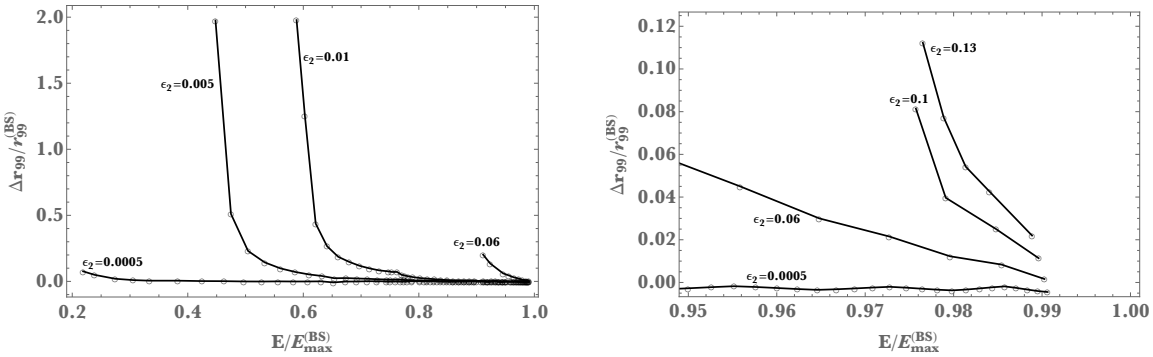

Figure 10.4.3: Position at which the mass aspect function is 99% of the total energy, as a function of the energy. Comparison is made relative to the boson star with the same energy. *Top:* larger range of energies, in particular the line with $\epsilon_2 = 0.0005$ goes from frequencies $\omega_1 = 0.997$ to $\omega_1 = 0.875$. *Bottom:* Zoom into the region of larger energies.

less dense objects than boson stars with the same energy. Among the solutions we have obtained, we find double-oscillators with a radius up to 200% larger than that of the boson star with the same energy.

CHAPTER 11

Discussion

This Part has been focused in the study of multi-oscillator solutions which are horizonless quasiperiodic solutions that oscillate in two or more non-commensurate frequencies. The main technical point we have used to construct these multi-oscillators was given in the general setup of Chapter 8. We made the observation that these solutions can be constructed by solving a boundary value problem. In this setup we promote the unknown functions from a dependence on time and radial direction to a dependence on each period and time direction (8.0.4).

In Chapter 9 we have studied the existence of double-oscillator solutions in asymptotically AdS spacetimes with scalar fields of mass $m^2 = -2$ when introducing a double-trace deformation. We have parametrised the double-trace boundary condition with κ that enables to move away from the resonant case of Dirichlet boundary conditions ($\kappa = 1$) to Neumann boundary conditions ($\kappa = 0$) which also has a commensurate spectrum.

Our results indicate that the study of islands of stability for scalar fields with Dirichlet boundary conditions may not be as universal as one would expect, and indeed we have encountered the existence of islands of stability with Neumann boundary conditions that do not have a counterpart with Dirichlet boundary conditions.

To further confirm the appearance of such islands of stability, we have performed a time evolution simulation. As initial data we have considered the multi-oscillating solutions

found in the boundary value problem. We have allowed the code to run for an order of magnitude longer than the expected time of collapse and confirmed that the multi-oscillator solutions remained during all the time of simulation.

The results we have presented for the multi-oscillators, both in the boundary value problem and in the time evolution, fixed the amplitude of the projection of the solutions onto the normal modes $\hat{e}_1$ and $\hat{e}_2$. We have also studied the lowest excited solutions that for $\kappa \leq \frac{2}{\pi}\tan^{-1}\left(\frac{2}{\pi}\right)$ are $\hat{e}_0$ and $\hat{e}_1$. We have observed that the qualitative results in both cases are equivalent.

The existence of multi-oscillating solutions in the Neumann case that do not have a counterpart in the Dirichlet case, immediately raise the question of the basin of attraction that these multi-oscillator solutions have to different initial data. One should notice that the family of multi-oscillators is an infinite parameter family in the frequencies, thus there should be a big degeneracy of possible end-state multi-oscillating solutions for different types of initial data.

Inspired by the construction of multi-oscillators in AdS and the fact that in asymptotically flat spacetimes there exist boson stars that have perturbations with real frequencies, we have found asymptotically flat multi-oscillators in Chapter 10.

We have shown that boson stars are only a special case of the more general double-oscillator solutions, which we propose are part of an infinite-parameter family of multi-oscillator solutions. The construction comes primarily from extending normal modes of a boson star to fully backreacted configurations. Our construction is general and can be used, in principle, to obtain any multi-oscillator solution with more frequencies. We are also unconstrained by the specific matter content we have considered. So long as there are solitonic configurations with perturbative normal modes, our methods can be used to construct multi-oscillating extensions to them.

While we have not studied the stability of double-oscillators, the apparent stability of boson stars implies that nearby multi-oscillator solutions should also be stable.

We note that there are unstable boson stars as well, whose scalar field has additional nodes in the radial direction. Their linear perturbations include at least one unstable growing mode, along with an infinite number of stable normal modes. Any of these normal modes can be extended to multi-oscillator solutions. When such multi-oscillators are still near the boson star and well approximated by perturbation theory, they should inherit the instability of the boson star. However, their instability remains unclear when the backreaction is much stronger.

Among the properties analysed, we have found that, for a given energy, the primary fre-

quency of double-oscillators remains close to boson stars, but their size can differ significantly. We expect this difference in size to be a distinguishing feature of these compact objects. In particular, the late merger dynamics of multi-oscillators might be noticeably different from those of boson stars which could have a signature in the gravitational waves emitted [178, 179].

Part IV

Appendix

CHAPTER A

Numerical methods

A.1 Collocation methods

Collocation methods consist in splitting the domain where we want to solve a differential equation or perform an integraton into $N+1$ gridpoints x_i. This procedure of discretisation allows to transform the continuous differential or integral operators into matrix operators. Then the task of solving differential equations reduces to finding the values of the unknown functions f_j in all points x_i. One expects that as the number of gridpoints increases and thus the space h between contiguous points decreases, the function will be better approximated between x_i and x_{i+1}. We consider two different types of collocation methods in this thesis: finite differences and pseudospectral methods.

A.1.1 Finite differences

In addition to the number of gridpoints one specifies the order q of the finite difference method. Then one can interpolate the function between points with a polynomial of order q in order to take derivatives. Effectively this translates into using a specific number of contiguous gridpoints in order to calculate the n-th derivative of a function. Clearly there is a restriction in the order of the derivative: $n < q$. In the present thesis I have used central fourth order finite differences. Important properties of the finite difference method

are:

- The grid using N points between x_- and x_+ is distributed uniformly in the domain.

- To compute the derivative at a point, one needs the value of the function in the two previous and two latter points, that is, the value at 5 points in the grid, including the point itself. The derivative at a point i is approximated as:

$$f'(x_i) = \frac{f(x_{i-2}) - 8f(x_{i-1}) + 8f(x_{i+1}) - f(x_{i+2})}{12h} + \mathcal{O}(h^4). \tag{A.1.1}$$

- The derivatives of boundary points may cause more trouble since there is a lack of points in one of the directions. There are two ways to solve the issue.

  1. When the function is known to be even or odd at the boundary it is best to use this property to construct a mirror grid at the other side of the boundary and compute derivatives with the scheme in (A.1.1).

  2. For a general function one can use, for the points $i = 1$ and $i = 2$ at boundary x_- and $i = N$ and $i = N - 1$ at boundary x_+, the scheme:

$$\begin{aligned}
f'(x_1) &= \frac{-25f(x_1) + 48f(x_2) - 36f(x_3) + 16f(x_4) - 3f(x_5)}{12h} + \mathcal{O}(h^4), \\
f'(x_2) &= \frac{-3f(x_1) - 10f(x_2) + 18f(x_3) - 6f(x_4) + f(x_5)}{12h} + \mathcal{O}(h^4), \\
f'(x_{N-1}) &= \frac{3f(x_N) + 10f(x_{N-1}) - 18f(x_{N-2}) + 6f(x_{N-3}) - f(x_{N-4})}{12h} + \mathcal{O}(h^4). \\
f'(x_N) &= \frac{25f(x_N) - 48f(x_{N-1}) + 36f(x_{N-2}) - 16f(x_{N-3}) + 3f(x_{N-4})}{12h} + \mathcal{O}(h^4),
\end{aligned} \tag{A.1.2}$$

- Higher order derivatives $f^{(n)}$ can be computed applying the same scheme to $f^{(n-1)}$.

- Definite integration can be performed using the scheme:

$$\begin{aligned}
F(x_1) &= 0, \\
F(x_2) &= \frac{h}{24}\left(9f(x_1) + 19f(x_2) - 5f(x_3) + f(x_4)\right), \\
F(x_i) &= \frac{h}{24}\left(-f(x_{i-2}) + 13f(x_{i-1}) + 13f(x_i) - f(x_{i+1})\right), \\
F(x_N) &= \frac{h}{24}\left(f(x_{N-3}) - 5f(x_{N-2}) + 19f(x_{N-1}) + 9f(x_N)\right).
\end{aligned} \tag{A.1.3}$$

  and the total definite integral is given by $\sum_{i=1}^{N} F(x_i)$.

In finite differences one obtains sparse matrices and polynomial convergence. This is to be contrasted with pseudospectral methods for which differentiation matrices are dense but have exponential convergence for smooth analytic functions.

We have used finite differences to discretise the radial part in Chapter 10. The reason being that despite the function is smooth, it is not analytic when $r \to \infty$. In fact the behaviour of the scalar field as $r \to \infty$ is $\phi(r) \to e^{-\alpha r}$. Spectral methods converge exponentially with analytic functions but non-analyticity may spoil the convergence, hence our decision.

A.1.2 Pseudospectral methods

Pseudostpectral methods use all points in the grid in order to compute a derivative at point x_i. This yields dense matrices but exponential convergence. The result is that when both finite differentiation and pseudospectral methods can be used, the latter are more efficient.

In order to work with pseudospectral methods one introduces a basis of functions e_k that are dense in the Hilbert space where one is performing the calculations. Then the unknown functions have the form:

$$f_j = \sum_{k \geq 0} a_{jk} e_j, \tag{A.1.4}$$

where a_{jk} are coefficients. For analytic functions, spectral theorems guarantee that one can truncate the sum at a finite integer N with exponential convergence with respect to $N-1$ for the numerical function obtained:

$$f_j = \sum_{k=0}^{N} a_{jk} e_j + \mathcal{O}(e^{-N}). \tag{A.1.5}$$

Pseudospectral methods have the property that one computes the values of the unknown function at the specified gridpoints as opposed to other spectral methods where one does not interpolate in a grid but rather compute directly coefficients of basis functions such as the a_{jk}. In the thesis I have used three different sets of basis functions depending on the particularities of the specific problem in hand. These are: Fourier decomposition, Chebyshev polynomials and Legendre polynomials. In the following I present each basis and its properties separately and comment when it is better to use each of them.

A.1.2.1 Fourier Basis

This method uses the Fourier series that uses trigonometric functions as basis. It is most suited for periodic functions, where one can use either a cosine or a sine expansion. The gridpoints are evenly distributed in the interval $(0, 2\pi]$. I have used this method to expand the time dependence of the multioscillators in Chapters 9 and 10. Given the particular symmetries of the problems, the functions where either even or odd and hence could be expanded either in a cosine or a sine series. The first and second order differentiation matrices ($D^{(1)}$, $D^{(2)}$) for each case are:

$$\begin{aligned}
\left(D^{(1)}\right)_{i,i} &= \pm\frac{(-1)^{i+j}}{2}\csc\left(\alpha_{ij}^{+}\right), \quad \left(D^{(1)}\right)_{i,0} = 0,\\
\left(D^{(1)}\right)_{i,j} &= \frac{(-1)^{i+j}}{2}\left(\csc\left(\alpha_{ij}^{-}\right) \pm \csc\left(\alpha_{ij}^{+}\right)\right),\\
\left(D^{(2)}\right)_{i,i} &= -\frac{(2N+1)^1 - 1}{12},\\
\left(D^{(2)}\right)_{i,j} &= \frac{(-1)^{i+j+1}}{2}\left(\cot\left(\alpha_{ij}^{-}\right)\csc\left(\alpha_{ij}^{-}\right) \pm \cot\left(\alpha_{ij}^{+}\right)\csc\left(\alpha_{ij}^{+}\right)\right)
\end{aligned} \tag{A.1.6}$$

with $\alpha_{ij}^{\pm} = \frac{\pi(i\pm j)}{2N+1}$, and with the positive sign for the cosine expansion and negative sign for the sine expansion.

A.1.2.2 Chebyshev polynomials

Interpolation with higher order polynomials may not work on evenly distributed points due to the Runge phenomenon that leads to large oscillations of the interpolated function near the edges. This is a good reason to introduce the Chebyshev grid (also the Legendre as we will see below) whose collocation points are distributed according to the function $\rho(x) \sim \frac{1}{2\pi\sqrt{x-x^2}}$. The collocation points are distributed according to the Chebyshev polynomials:

$$x_j = \frac{x_- + x_+}{2} + \frac{x_- - x_+}{2}\cos\left(\frac{(j-1)\pi}{N}\right), \quad j = 1, \ldots, N+1. \tag{A.1.7}$$

The differentiation matrix for Chebyshev pseudospectral methods is:

$$\begin{aligned}
\left(D^{(1)}\right)_{i,i} &= \sum_{k=1,k\neq i}^{N+1}\frac{1}{x_i - x_k}, \quad \left(D^{1}\right)_{i,j} = \frac{a_i}{a_j(x_i - x_j)},\\
D^{(q)} &= \left(D^{(1)}\right)^q.
\end{aligned} \tag{A.1.8}$$

In this thesis Chebyshev pseudospectral methods have been used in the numerical parts of Part II, as well as an independent numerical test for the results of Chapter 10.

A.1.2.3 Legendre polynomials

Like Chebyshev pseudospectral methods, Legendre's collocation points are not evenly distributed but rather located in the zeros of the function

$$h(x) = \frac{(N+1)(xP_N(x) - P_{N+1}(x))}{1-x^2}, \tag{A.1.9}$$

where $P_N(x)$ is the Legendre polynomial of order N. The differentiation matrix is given by

$$\begin{aligned}
&\left(D^{(1)}\right)_{1,1} = -\frac{N(N+1)}{2(x_+ - x_-)}, \quad \left(D^{(1)}\right)_{N+1,N+1} = -\frac{N(N+1)}{2(x_+ - x_-)}, \quad \left(D^{(1)}\right)_{i,i} = 0 \\
&\left(D^{1}\right)_{ij} = \frac{2}{x_+ - x_-}\frac{P_N(x_i)}{P_N(x_j)(x_i - x_j)}, \\
&D^{(q)} = \left(D^{(1)}\right)^q.
\end{aligned} \tag{A.1.10}$$

Legendre pseudospectral methods have been used in Chapter 9. The reason is that one needs to project the function into a basis of normal modes of AdS given by solving the Sturm-Liouville problem (9.3.1). The projection is done by taking the scalar product (9.3.2). The problem is solved numerically using spectral methods and hence one expects to have exponential convergence. Integration using spectral methods can be done using Gauss quadrature.

Consider the integral

$$F = \int_{x_-}^{x_+} f(x)\mathrm{d}x. \tag{A.1.11}$$

Given a basis of polynomials (such as Legendre or Chebyshev) an analytic function in an interval (x_-, x_+) can be approximated knowing the functions in the N gridpoints $(f(x_i))$ by a polynomial of degree N as in (A.1.4) where e_j will be the j-th polynomial of the basis. We can use this polynomial to integrate a function over the interval. The integral of the polynomial is in general exactly known and thus the error in the computation only comes from the error of approximating a function by a polynomial which has exponential convergence in pseudospectral methods.

Since the points in the grid are not evenly distributed, the measure of the integral $\mathrm{d}x$ has to be modified to account for the *weight* (ω_i) of each point (notice that one can either talk about the measure in the continuous case or weights for the discretisation). The integral

(A.1.11) can thus be approximated by

$$F = \sum_{i \geq 0} \omega_i f(x_i). \tag{A.1.12}$$

The measure for Chebyshev decomposition is $\frac{1}{\sqrt{1-x^2}}$ which is not smooth precisely at points $x = \pm 1$ which are the extremes of the domain of the Chebyshev polynomials. In spectral methods all points in the grid matter for the computation of each point and thus this measure can spoil the exponential accuracy of spectral methods. The measure for Legendre polynomials is 1 and hence one can preserve spectral accuracy when integrating.

The expression for the weights at position i for Gauss quadrature using Legendre polynomials is:

$$\omega_i = \frac{2}{N(N+1)P_N(x)^2}. \tag{A.1.13}$$

A.1.3 Boundary conditions

In general one may have mixed type boundary conditions that include a relation between the values of the function and its derivatives at the boundary. For derivatives one can take the corresponding row of the differentiation matrix: D_1 or D_{N+1} for the boundaries x_- and x_+ respectively. The value of the function can only appear in the diagonal. The final expression for the boundary conditions is (for simplicity we only consider a second order differential equation so that boundary conditions involve only first derivatives):

$$\begin{aligned} C_1 \left(D_N\right)_{1,1;;N+1} + C_2 \left(I_{N+1}\right)_{1,1;;N+1} = 0, \quad \text{at } x_-, \\ C_1 \left(D_N\right)_{N+1,1;;N+1} + C_2 \left(I_{N+1}\right)_{N+1,1;;N+1} = 0, \quad \text{at } x_+, \end{aligned} \tag{A.1.14}$$

where $\left(D_N\right)_{1,1;;N+1}$ is the first row of the matrix D_N and I_{N+1} the identity matrix of dimension $N+1$.

A.1.4 PDE's

To solve PDE's, we use a tensor product grid. In Part III we have solved PDE's with dependence on the time and radial coordinate. Since the time coordinate is periodic we have used Fourier decomposition whereas for the radial coordinate we have used finite differences in Chapter 10 and Legendre polynomials in Chapter 9. A function depending on time and space is discretised in both directions giving the discrete matrix $f \to f_I$ with I standing for the grid of points $time \times space$. One can then use co-lexicographic ordering

to map the function f_I to the matrix f_{ij} as

$$I = (i-1)N_x + j, \qquad (i,j) = \left(\text{ceil}\left[\frac{I}{N_x}\right], (I-1)\text{mod}N_x + 1\right) \tag{A.1.15}$$

with N_x the number of grid points in the radial direction and N_t in the time direction.

The function f_{ij} then takes the vector form

$$\begin{pmatrix} f_{10} \\ \vdots \\ f_{1N} \\ f_{20} \\ \vdots \\ f_{nN} \end{pmatrix}, \tag{A.1.16}$$

and the following matrix form for the derivatives matrices:

$$\partial_{x_1} \to D_N^{(x_1)} \otimes I_N^{(x_2)} \otimes \cdots \otimes I_N^{(x_n)}, \tag{A.1.17}$$

with I_N the identity matrix of size N.

A.2 Solving quadratic eigenvalue problems

In general a solution $\phi(t, \vec{x})$ to any equation (can be Klein-Gordon equation, but also Einstein, Maxwell, Dirac equations) defined in a stationary background can be Fourier decomposed:

$$\phi(t, \vec{x}) = e^{-i\omega t}\phi(\vec{x}). \tag{A.2.1}$$

If the initial equation is a second order linear differential equation, the resulting equation after using this decomposition will necessarily have the form:

$$\Big[H_0(\vec{x}) - H_1(\vec{x})\omega - H_2(\vec{x})\omega^2\Big]\phi(\vec{x}) = 0, \quad B_0^{(1)}(\vec{x}^1) - B_1^{(1)}(\vec{x}^1)\omega = 0, \tag{A.2.2}$$

$$B_0^{(2)}(\vec{x}^2) - B_1^{(2)}(\vec{x}^2)\omega = 0 \tag{A.2.3}$$

where $H_i,\ B_j^{(k)}$ are differential operators of order i and j respectively, and the B's refer to the boundary conditions. Now we can introduce the eigenfunction $Q(\vec{x}) = (\omega\phi(\vec{x}), \phi(\vec{x}))$

in order to write the equation in the form of the usual eigenvalue problem:

$$\left[\begin{pmatrix} -H_1 & H_0 \\ 1 & 0 \end{pmatrix} - \omega \begin{pmatrix} H_2 & 0 \\ 0 & 1 \end{pmatrix} \right] Q(x) = 0. \tag{A.2.4}$$

Notice that the equation from the first line is (A.2.2) and the second equation is $\omega\phi(\vec{x}) - \omega\phi(\vec{x}) = 0$ which is an identity.

One can now use the discretisation procedure explained in A.1 to write the system of equations in a matrix form and solve the generalised eigenvalue problem

$$AQ = \omega BQ. \tag{A.2.5}$$

This method is valid in order to solve eigenvalue linear differential equations that are quadratic in the eigenvalue. In general the first eigenvalues and eigenvectors of the discrete problem (A.2.5) are approximated with high accuracy depending on N, but higher ones are not well resolved by the grid. This is natural since one expects to have more ripples, separated by one wavelength for eigenvectors of higher eigenvalues. When the wavelength becomes of the order of the distance between points in the grid, the function cannot be well resolved.

In this method one obtains many spurious solutions. These are eigenvalues and eigenvectors of the matrix that do not correspond to solutions of the differential equation. In general when one varies N, these spurious solutions change whereas the correct solutions remain unchanged.

A.3 Newton-Raphson algorithm

We present a general overview of the Newton-Raphson method to find solutions to differential equations and in the end of the section we will apply the method to the eigenvalue problem.

Consider a set of differential equations written in generic form as $F[\vec{x}, \vec{f}] = 0$ with $\vec{x}$ the coordinate variables and $\vec{f}$ the M functions, and the dependence of F on $\vec{f}$ also includes its derivatives. Consider guess functions $\vec{f}^{(1)}$ and expand the equation around them to linear order:

$$F[\vec{x}, \vec{f}] = F[\vec{x}, \vec{f}^{(1)}] + \sum_{j=1}^{M} \frac{\delta F}{\delta f_j}[\vec{x}, \vec{f}^{(1)}]\delta f_j + \mathcal{O}(\delta f^2) \tag{A.3.1}$$

with $\delta f_j = f_j - f_j^{(1)}$. If the set of functions $\vec{f}^{(1)}$ are close enough to a solution, then we have that $F[\vec{x}, \vec{f}] = 0$ and

$$\sum_{j=1}^{M} \frac{\delta F}{\delta f_j}[\vec{x}, \vec{f}^{(1)}]\delta f_j = -F[\vec{x}, \vec{f}^{(1)}]. \tag{A.3.2}$$

The above equation is a linear equation that can be discretised and solved as a common problem $AX = b$. The solution to this system is $\vec{\delta} f$, that we can use to approach the solution:

$$\vec{f}^{(2)} = \vec{f}^{(1)} + \vec{\delta} f. \tag{A.3.3}$$

The procedure can be repeated now with $f^{(2)}$ until achieving the desired convergence error ϵ given by $|\vec{f}^{(n)} - \vec{f}^{(n+1)}|_{L^\infty} < \epsilon$.

The speed of convergence of the method is quadratic. To see this, consider the function f and apply the Newton Raphson method to find a root of f starting with the guess $x^{(1)}$:

$$f(x) = f(x^{(1)}) + f'(x^{(1)})(x - x^{(1)}) + ((x - x^{(1)})^2). \tag{A.3.4}$$

The new solution is

$$x^{(2)} = x^{(1)} - \frac{f(x^{(1)})}{f'(x^{(1)})}. \tag{A.3.5}$$

Now consider a real root x of the function f, and the error after the n-th iteration $\epsilon_n = x - x_n$. Taylor expanding around x_n:

$$f(x_n + \epsilon_n) = f(x_n) + \epsilon_n f'(x_n) + \frac{\epsilon_n^2}{2} f''(x_n) + \mathcal{O}(\epsilon_n^3) = 0. \tag{A.3.6}$$

We apply the Newton Raphson method again to the function f:

$$\epsilon_{n+1} = x_s - x_{n+1} = x_s - \left(x_n - \frac{f(x_n)}{f'(x_n)}\right) = -\frac{\epsilon_n^2}{2} f''(x_n) + \mathcal{O}(\epsilon_n^3) \tag{A.3.7}$$

Which shows that the convergence is quadratic.

The main drawback of the Newton-Raphson method is the initial guess solution wich is usually called seed. If the seed is not carefully chosen, the error may grow unboundedly, or enter an infinite cycle. Also, if more than one solution exists, as in an eigenvalue problem with an infinite number of eigenvalues, each solution has its basin of attraction. If the seed is not chosen close enough to the desired solution, it may fall in the basin of attraction of a different solution. Hence the algorithm would converge but not to the desired solution.

Different approaches may be taken to give a proper seed. If one is looking for a solution that is continuously connected through some parameters to a known solution, then a good strategy is to start with the known solution and solve the equations along the flow of the parameters. In the particular case of searching for eigenvalues and eigenvectors, a good strategy is to use the method described in A.2 to obtain a good guess that one uses as seed, and then hunt for the desired accuracy with the Newton-Raphson method.

The Newton-Raphson method, in general, is useful for non-linear equations, as it first linearises them. If the equation is linear, then one can readily iterate. The general eigenvalue problem (A.2.2) is a linear differential equation but it is quadratic in the eigenvalue. The Newton-Raphson method applied to this case consists in considering a seed formed of a vector with the eigenvector and the eigenvalue, linearise the equation and iterate as explained previously. Consider, then the equation (A.2.2) written in the form:

$$\mathcal{H}(x,\omega)\phi(x) = 0, \tag{A.3.8}$$

where the differential operator $\mathcal{H}$ includes all H_i from (A.2.2). Then the structure of the problem is:

$$\begin{pmatrix} \mathcal{H}(x,\omega^{(n)}) & \frac{\partial\mathcal{H}}{\partial\omega}(x,\omega^{(n)})\phi^{(n)} \\ \frac{\partial N}{\partial\phi}(\phi^{(n)}) & 0 \end{pmatrix} \begin{pmatrix} \delta\phi^{(n)} \\ \delta\omega^{(n)} \end{pmatrix} = - \begin{pmatrix} \mathcal{H}(x,\omega^{(n)})\phi^{(n)} \\ N(\phi^{(n)}) \end{pmatrix}, \tag{A.3.9}$$

where $N(\phi^{(n)})$ is a normalisation condition that one can choose conveniently, for example by demanding that the value of the eigenvector at the left boundary is 1. This is already a discrete condition:

$$N(f) = (0,\ldots,0,f_N). \tag{A.3.10}$$

The term $\frac{\partial\mathcal{H}}{\partial\omega}(x,\omega^{(n)})$ will give for the case (A.2.2)

$$-H_1(\vec{x}) - 2H_2\omega^{(n)}(\vec{x}). \tag{A.3.11}$$

Finally, notice that the first row and column in the LHS of (A.3.9) is the operator itself. This is a consequence of the differential equation being linear.

Bibliography

[1] O. J. C. Dias and R. Masachs, *Hairy black holes and the endpoint of AdS_4 charged superradiance*, 1610.03496.

[2] O. J. C. Dias and R. Masachs, *Charged black hole bombs in a Minkowski cavity*, 1801.10176.

[3] O. J. C. Dias and R. Masachs, *Evading no-hair theorems: hairy black holes in a Minkowski box*, 1802.01603.

[4] M. Choptuik, R. Masachs and B. Way, *Multi-oscillating Boson Stars*, 1904.02168.

[5] G. 't Hooft, *Dimensional reduction in quantum gravity*, *Conf. Proc.* **C930308** (1993) 284–296, [gr-qc/9310026].

[6] L. Susskind, *The World as a hologram*, *J. Math. Phys.* **36** (1995) 6377–6396, [hep-th/9409089].

[7] C. B. Thorn, *Reformulating string theory with the 1/N expansion*, in *The First International A.D. Sakharov Conference on Physics Moscow, USSR, May 27-31, 1991*, pp. 0447–454, 1991. hep-th/9405069.

[8] I. R. Klebanov and L. Susskind, *Continuum Strings From Discrete Field Theories*, *Nucl. Phys.* **B309** (1988) 175–187.

[9] J. D. Bekenstein, *Black holes and the second law*, *Lett. Nuovo Cim.* **4** (1972)

737–740.

[10] S. W. Hawking, *Particle Creation by Black Holes*, *Commun. Math. Phys.* **43** (1975) 199–220.

[11] J. M. Maldacena, *The Large N limit of superconformal field theories and supergravity*, *Int. J. Theor. Phys.* **38** (1999) 1113–1133, [hep-th/9711200].

[12] E. Witten, *Anti-de Sitter space and holography*, *Adv. Theor. Math. Phys.* **2** (1998) 253–291, [hep-th/9802150].

[13] S. S. Gubser, I. R. Klebanov and A. M. Polyakov, *Gauge theory correlators from noncritical string theory*, *Phys. Lett.* **B428** (1998) 105–114, [hep-th/9802109].

[14] O. Aharony, O. Bergman, D. L. Jafferis and J. Maldacena, *N=6 superconformal Chern-Simons-matter theories, M2-branes and their gravity duals*, *JHEP* **10** (2008) 091, [0806.1218].

[15] G. Policastro, D. T. Son and A. O. Starinets, *The Shear viscosity of strongly coupled N=4 supersymmetric Yang-Mills plasma*, *Phys. Rev. Lett.* **87** (2001) 081601, [hep-th/0104066].

[16] P. Kovtun, D. T. Son and A. O. Starinets, *Viscosity in strongly interacting quantum field theories from black hole physics*, *Phys. Rev. Lett.* **94** (2005) 111601, [hep-th/0405231].

[17] J. Casalderrey-Solana, H. Liu, D. Mateos, K. Rajagopal and U. A. Wiedemann, *Gauge/String Duality, Hot QCD and Heavy Ion Collisions*, 1101.0618.

[18] S. A. Hartnoll, C. P. Herzog and G. T. Horowitz, *Building a Holographic Superconductor*, *Phys. Rev. Lett.* **101** (2008) 031601, [0803.3295].

[19] S. A. Hartnoll, C. P. Herzog and G. T. Horowitz, *Holographic Superconductors*, *JHEP* **12** (2008) 015, [0810.1563].

[20] P. McFadden and K. Skenderis, *Holography for Cosmology*, *Phys. Rev.* **D81** (2010) 021301, [0907.5542].

[21] N. Afshordi, C. Coriano, L. Delle Rose, E. Gould and K. Skenderis, *From Planck data to Planck era: Observational tests of Holographic Cosmology*, *Phys. Rev. Lett.* **118** (2017) 041301, [1607.04878].

[22] O. Aharony, S. S. Gubser, J. M. Maldacena, H. Ooguri and Y. Oz, *Large N field theories, string theory and gravity*, *Phys. Rept.* **323** (2000) 183–386, [hep-th/9905111].

[23] M. T. Anderson, *Geometric aspects of the AdS / CFT correspondence*, *IRMA Lect. Math. Theor. Phys.* **8** (2005) 1–31, [hep-th/0403087].

[24] K. Skenderis, *Lecture notes on holographic renormalization*, *Class. Quant. Grav.* **19** (2002) 5849–5876, [hep-th/0209067].

[25] A. Ashtekar and S. Das, *Asymptotically Anti-de Sitter space-times: Conserved quantities*, *Class. Quant. Grav.* **17** (2000) L17–L30, [hep-th/9911230].

[26] V. Balasubramanian and P. Kraus, *A Stress tensor for Anti-de Sitter gravity*, *Commun. Math. Phys.* **208** (1999) 413–428, [hep-th/9902121].

[27] S. de Haro, S. N. Solodukhin and K. Skenderis, *Holographic reconstruction of space-time and renormalization in the AdS / CFT correspondence*, *Commun. Math. Phys.* **217** (2001) 595–622, [hep-th/0002230].

[28] K. Skenderis, *Asymptotically Anti-de Sitter space-times and their stress energy tensor*, *Int. J. Mod. Phys.* **A16** (2001) 740–749, [hep-th/0010138].

[29] M. Henningson and K. Skenderis, *The Holographic Weyl anomaly*, *JHEP* **07** (1998) 023, [hep-th/9806087].

[30] V. Cardoso, O. J. C. Dias, G. S. Hartnett, L. Lehner and J. E. Santos, *Holographic thermalization, quasinormal modes and superradiance in Kerr-AdS*, *JHEP* **04** (2014) 183, [1312.5323].

[31] P. Breitenlohner and D. Z. Freedman, *Stability in Gauged Extended Supergravity*, *Annals Phys.* **144** (1982) 249.

[32] P. Breitenlohner and D. Z. Freedman, *Positive Energy in anti-De Sitter Backgrounds and Gauged Extended Supergravity*, *Phys. Lett.* **115B** (1982) 197–201.

[33] E. Witten, *Multitrace operators, boundary conditions, and AdS / CFT correspondence*, hep-th/0112258.

[34] S. S. Gubser and I. Mitra, *Double trace operators and one loop vacuum energy in AdS / CFT*, *Phys. Rev.* **D67** (2003) 064018, [hep-th/0210093].

[35] M. Henneaux, C. Martinez, R. Troncoso and J. Zanelli, *Asymptotically anti-de Sitter spacetimes and scalar fields with a logarithmic branch*, *Phys. Rev.* **D70** (2004) 044034, [hep-th/0404236].

[36] M. Henneaux, C. Martinez, R. Troncoso and J. Zanelli, *Asymptotic behavior and Hamiltonian analysis of anti-de Sitter gravity coupled to scalar fields*, *Annals Phys.* **322** (2007) 824–848, [hep-th/0603185].

[37] D. T. Son and A. O. Starinets, *Viscosity, Black Holes, and Quantum Field Theory*, *Ann. Rev. Nucl. Part. Sci.* **57** (2007) 95–118, [0704.0240].

[38] K. Skenderis and B. C. van Rees, *Real-time gauge/gravity duality: Prescription, Renormalization and Examples*, *JHEP* **05** (2009) 085, [0812.2909].

[39] K. Skenderis and B. C. van Rees, *Real-time gauge/gravity duality*, *Phys. Rev. Lett.* **101** (2008) 081601, [0805.0150].

[40] C. P. Herzog and D. T. Son, *Schwinger-Keldysh propagators from AdS/CFT correspondence*, *JHEP* **03** (2003) 046, [hep-th/0212072].

[41] B. C. van Rees, *Real-time gauge/gravity duality and ingoing boundary conditions*, *Nucl. Phys. Proc. Suppl.* **192-193** (2009) 193–196, [0902.4010].

[42] M. Bianchi, D. Z. Freedman and K. Skenderis, *How to go with an RG flow*, *JHEP* **08** (2001) 041, [hep-th/0105276].

[43] M. Bianchi, D. Z. Freedman and K. Skenderis, *Holographic renormalization*, *Nucl. Phys.* **B631** (2002) 159–194, [hep-th/0112119].

[44] I. Papadimitriou and K. Skenderis, *AdS / CFT correspondence and geometry*, *IRMA Lect. Math. Theor. Phys.* **8** (2005) 73–101, [hep-th/0404176].

[45] S. W. Hawking, *Black holes in general relativity*, *Commun. Math. Phys.* **25** (1972) 152–166.

[46] R. Ruffini and J. A. Wheeler, *Introducing the black hole*, *Phys. Today* **24** (1971) 30.

[47] J. D. Bekenstein, *Black hole hair: 25 - years after*, in *Physics. Proceedings, 2nd International A.D. Sakharov Conference, Moscow, Russia, May 20-24, 1996*, 1996. gr-qc/9605059.

[48] B. F. Whiting, *Mode Stability of the Kerr Black Hole*, *J. Math. Phys.* **30** (1989)

1301.

[49] O. J. C. Dias, M. Godazgar and J. E. Santos, *Linear Mode Stability of the Kerr-Newman Black Hole and Its Quasinormal Modes*, *Phys. Rev. Lett.* **114** (2015) 151101, [1501.04625].

[50] O. J. C. Dias, J. E. Santos and B. Way, *Numerical Methods for Finding Stationary Gravitational Solutions*, *Class. Quant. Grav.* **33** (2016) 133001, [1510.02804].

[51] P. Basu, J. Bhattacharya, S. Bhattacharyya, R. Loganayagam, S. Minwalla and V. Umesh, *Small Hairy Black Holes in Global AdS Spacetime*, *JHEP* **10** (2010) 045, [1003.3232].

[52] O. J. C. Dias, P. Figueras, R. Monteiro, H. S. Reall and J. E. Santos, *An instability of higher-dimensional rotating black holes*, *JHEP* **05** (2010) 076, [1001.4527].

[53] O. J. C. Dias, G. T. Horowitz and J. E. Santos, *Black holes with only one Killing field*, *JHEP* **07** (2011) 115, [1105.4167].

[54] S. W. Hawking and H. S. Reall, *Charged and rotating AdS black holes and their CFT duals*, *Phys. Rev.* **D61** (2000) 024014, [hep-th/9908109].

[55] V. Cardoso and O. J. C. Dias, *Small Kerr-anti-de Sitter black holes are unstable*, *Phys. Rev.* **D70** (2004) 084011, [hep-th/0405006].

[56] S. S. Gubser, *Breaking an Abelian gauge symmetry near a black hole horizon*, *Phys. Rev.* **D78** (2008) 065034, [0801.2977].

[57] W. H. Press and S. A. Teukolsky, *Floating Orbits, Superradiant Scattering and the Black-hole Bomb*, *Nature* **238** (1972) 211–212.

[58] T. J. M. Zouros and D. M. Eardley, *Instabilities of massive scalar perturbations of a rotating black hole*, *Annals Phys.* **118** (1979) 139–155.

[59] S. Detweiler, *Klein-gordon equation and rotating black holes*, *Phys. Rev. D* **22** (Nov, 1980) 2323–2326.

[60] C. A. R. Herdeiro and E. Radu, *Kerr black holes with scalar hair*, *Phys. Rev. Lett.* **112** (2014) 221101, [1403.2757].

[61] D. Christodoulou and S. Klainerman, *The Global nonlinear stability of the Minkowski space*, .

[62] H. Friedrich, *On the global existence and the asymptotic behavior ofsolutions to the Einstein-Maxwell-Yang-Mills equations*, *J. Diff. Geom.* **34** (1991) 275–345.

[63] M. Dafermos and G. Holzegel, *Dynamic instability of solitons in 4 + 1-dimensional gravity with negative cosmological constant*, *(University of Cambridge, 2006)* (2006) , [Available at: https://www.dpmms.cam.ac.uk/?md384/ADSinstability.pdf].

[64] P. Bizon and A. Rostworowski, *On weakly turbulent instability of anti-de Sitter space*, *Phys. Rev. Lett.* **107** (2011) 031102, [1104.3702].

[65] Y. B. Zel'dovich, *Generation of Waves by a Rotating Body*, *JETP Lett.* **14** (1971) 180.

[66] A. A. Starobinsky and S. M. Churilov, *Amplification of electromagnetic and gravitational waves scattered by a rotating black hole*, *Sov. Phys. JETP* **38** (1973) 1.

[67] S. Teukolsky and W. Press, *Perturbations of a rotating black hole. III - Interaction of the hole with gravitational and electromagnetic radiation*, *Astrophys.J.* **193** (1974) 443–461.

[68] R. Brito, V. Cardoso and P. Pani, *Superradiance*, 1501.06570.

[69] B. Ganchev, *Superradiant instability in AdS*, 1608.01798.

[70] O. J. C. Dias and J. E. Santos, *Boundary Conditions for Kerr-AdS Perturbations*, *JHEP* **10** (2013) 156, [1302.1580].

[71] I. R. Klebanov and E. Witten, *AdS / CFT correspondence and symmetry breaking*, *Nucl.Phys.* **B556** (1999) 89–114, [hep-th/9905104].

[72] O. J. C. Dias, R. Monteiro, H. S. Reall and J. E. Santos, *A Scalar field condensation instability of rotating anti-de Sitter black holes*, *JHEP* **11** (2010) 036, [1007.3745].

[73] A. J. Amsel, G. T. Horowitz, D. Marolf and M. M. Roberts, *Uniqueness of Extremal Kerr and Kerr-Newman Black Holes*, *Phys. Rev.* **D81** (2010) 024033, [0906.2367].

[74] O. J. C. Dias, G. T. Horowitz and J. E. Santos, *Gravitational Turbulent Instability of Anti-de Sitter Space*, *Class. Quant. Grav.* **29** (2012) 194002, [1109.1825].

[75] G. Moschidis, *A proof of the instability of AdS for the Einstein–null dust system with an inner mirror*, 1704.08681.

[76] G. Moschidis, *The Einstein–null dust system in spherical symmetry with an inner mirror: structure of the maximal development and Cauchy stability*, 1704.08685.

[77] G. Moschidis, *A proof of the instability of AdS for the Einstein–massless Vlasov system*, 1812.04268.

[78] O. J. C. Dias, G. T. Horowitz, D. Marolf and J. E. Santos, *On the Nonlinear Stability of Asymptotically Anti-de Sitter Solutions*, *Class. Quant. Grav.* **29** (2012) 235019, [1208.5772].

[79] M. Maliborski and A. Rostworowski, *Time-Periodic Solutions in an Einstein AdS?Massless-Scalar-Field System*, *Phys. Rev. Lett.* **111** (2013) 051102, [1303.3186].

[80] A. Buchel, S. L. Liebling and L. Lehner, *Boson stars in AdS spacetime*, *Phys. Rev.* **D87** (2013) 123006, [1304.4166].

[81] V. Balasubramanian, A. Buchel, S. R. Green, L. Lehner and S. L. Liebling, *Holographic Thermalization, Stability of Anti-de Sitter Space, and the Fermi-Pasta-Ulam Paradox*, *Phys. Rev. Lett.* **113** (2014) 071601, [1403.6471].

[82] P. Bizon and A. Rostworowski, *Comment on Holographic Thermalization, Stability of Anti-de Sitter Space, and the Fermi-Pasta-Ulam Paradox?*, *Phys. Rev. Lett.* **115** (2015) 049101, [1410.2631].

[83] V. Balasubramanian, A. Buchel, S. R. Green, L. Lehner and S. L. Liebling, *Reply to Comment on Holographic Thermalization, Stability of Anti-de Sitter Space, and the Fermi-Pasta-Ulam Paradox?*, *Phys. Rev. Lett.* **115** (2015) 049102, [1506.07907].

[84] F. Dimitrakopoulos and I.-S. Yang, *Conditionally extended validity of perturbation theory: Persistence of AdS stability islands*, *Phys. Rev.* **D92** (2015) 083013, [1507.02684].

[85] S. R. Green, A. Maillard, L. Lehner and S. L. Liebling, *Islands of stability and recurrence times in AdS*, *Phys. Rev.* **D92** (2015) 084001, [1507.08261].

[86] M. W. Choptuik, O. J. C. Dias, J. E. Santos and B. Way, *Collapse and Nonlinear Instability of AdS Space with Angular Momentum*, *Phys. Rev. Lett.* **119** (2017) 191104, [1706.06101].

[87] M. Choptuik, J. E. Santos and B. Way, *Charting Islands of Stability with Multioscillators in anti?de Sitter space*, *Phys. Rev. Lett.* **121** (2018) 021103,

[1803.02830].

[88] A. Buchel, S. R. Green, L. Lehner and S. L. Liebling, *Conserved quantities and dual turbulent cascades in anti?de Sitter spacetime*, *Phys. Rev.* **D91** (2015) 064026, [1412.4761].

[89] B. Craps, O. Evnin and J. Vanhoof, *Renormalization group, secular term resummation and AdS (in)stability*, *JHEP* **10** (2014) 48, [1407.6273].

[90] B. Craps, O. Evnin and J. Vanhoof, *Renormalization, averaging, conservation laws and AdS (in)stability*, *JHEP* **01** (2015) 108, [1412.3249].

[91] D. J. Kaup, *Klein-Gordon Geon*, *Phys. Rev.* **172** (1968) 1331–1342.

[92] R. Ruffini and S. Bonazzola, *Systems of selfgravitating particles in general relativity and the concept of an equation of state*, *Phys. Rev.* **187** (1969) 1767–1783.

[93] S. L. Liebling and C. Palenzuela, *Dynamical Boson Stars*, *Living Rev. Rel.* **15** (2012) 6, [1202.5809].

[94] P. M. Chesler and D. A. Lowe, *Nonlinear evolution of the AdS_4 black hole bomb*, 1801.09711.

[95] H. S. Reall, *Higher dimensional black holes and supersymmetry*, *Phys.Rev.* **D68** (2003) 024024, [hep-th/0211290].

[96] H. K. Kunduri, J. Lucietti and H. S. Reall, *Gravitational perturbations of higher dimensional rotating black holes: Tensor perturbations*, *Phys.Rev.* **D74** (2006) 084021, [hep-th/0606076].

[97] S. Stotyn, M. Park, P. McGrath and R. B. Mann, *Black Holes and Boson Stars with One Killing Field in Arbitrary Odd Dimensions*, *Phys. Rev.* **D85** (2012) 044036, [1110.2223].

[98] O. J. C. Dias, J. E. Santos and B. Way, *Black holes with a single Killing vector field: black resonators*, *JHEP* **12** (2015) 171, [1505.04793].

[99] S. R. Green, S. Hollands, A. Ishibashi and R. M. Wald, *Superradiant instabilities of asymptotically anti-de Sitter black holes*, *Class. Quant. Grav.* **33** (2016) 125022, [1512.02644].

[100] B. E. Niehoff, J. E. Santos and B. Way, *Towards a violation of cosmic censorship*,

1510.00709.

[101] L. Lehner and F. Pretorius, *Black Strings, Low Viscosity Fluids, and Violation of Cosmic Censorship*, *Phys. Rev. Lett.* **105** (2010) 101102, [1006.5960].

[102] P. Figueras, M. Kunesch and S. Tunyasuvunakool, *End Point of Black Ring Instabilities and the Weak Cosmic Censorship Conjecture*, *Phys. Rev. Lett.* **116** (2016) 071102, [1512.04532].

[103] T. Crisford and J. E. Santos, *Violating the Weak Cosmic Censorship Conjecture in Four-Dimensional Anti?de Sitter Space*, *Phys. Rev. Lett.* **118** (2017) 181101, [1702.05490].

[104] T. Crisford, G. T. Horowitz and J. E. Santos, *Testing the Weak Gravity - Cosmic Censorship Connection*, *Phys. Rev.* **D97** (2018) 066005, [1709.07880].

[105] T. Crisford, G. T. Horowitz and J. E. Santos, *Attempts at vacuum counterexamples to cosmic censorship in AdS*, *JHEP* **02** (2019) 092, [1805.06469].

[106] P. Bosch, S. R. Green and L. Lehner, *Nonlinear Evolution and Final Fate of Charged Anti-de Sitter Black Hole Superradiant Instability*, *Phys. Rev. Lett.* **116** (2016) 141102, [1601.01384].

[107] N. Sanchis-Gual, J. C. Degollado, P. J. Montero, J. A. Font and C. Herdeiro, *Explosion and Final State of an Unstable Reissner-Nordstrm̈ Black Hole*, *Phys. Rev. Lett.* **116** (2016) 141101, [1512.05358].

[108] C. A. R. Herdeiro, J. C. Degollado and H. F. Rúnarsson, *Rapid growth of superradiant instabilities for charged black holes in a cavity*, *Phys. Rev.* **D88** (2013) 063003, [1305.5513].

[109] S. Hod, *Analytic treatment of the charged black-hole-mirror bomb in the highly explosive regime*, *Phys. Rev.* **D88** (2013) 064055, [1310.6101].

[110] J. C. Degollado and C. A. R. Herdeiro, *Time evolution of superradiant instabilities for charged black holes in a cavity*, *Phys. Rev.* **D89** (2014) 063005, [1312.4579].

[111] S. Hod, *Resonance spectra of caged black holes*, *Eur. Phys. J.* **C74** (2014) 3137, [1410.4567].

[112] R. Li, J.-K. Zhao and Y.-M. Zhang, *Superradiant Instability of D-Dimensional Reissner-Nordstrm̈ Black Hole Mirror System*, *Commun. Theor. Phys.* **63** (2015)

569–574, [1404.6309].

[113] S. R. Dolan, S. Ponglertsakul and E. Winstanley, *Stability of black holes in Einstein-charged scalar field theory in a cavity*, *Phys. Rev.* **D92** (2015) 124047, [1507.02156].

[114] P. Basu, C. Krishnan and P. N. B. Subramanian, *Hairy Black Holes in a Box*, *JHEP* **11** (2016) 041, [1609.01208].

[115] S. Ponglertsakul, E. Winstanley and S. R. Dolan, *Stability of gravitating charged-scalar solitons in a cavity*, *Phys. Rev.* **D94** (2016) 024031, [1604.01132].

[116] S. Ponglertsakul and E. Winstanley, *Effect of scalar field mass on gravitating charged scalar solitons and black holes in a cavity*, *Phys. Lett.* **B764** (2017) 87–93, [1610.00135].

[117] N. Sanchis-Gual, J. C. Degollado, C. Herdeiro, J. A. Font and P. J. Montero, *Dynamical formation of a Reissner-Nordstr?m black hole with scalar hair in a cavity*, *Phys. Rev.* **D94** (2016) 044061, [1607.06304].

[118] N. Sanchis-Gual, J. C. Degollado, J. A. Font, C. Herdeiro and E. Radu, *Dynamical formation of a hairy black hole in a cavity from the decay of unstable solitons*, *Class. Quant. Grav.* **34** (2017) 165001, [1611.02441].

[119] S. Hod, *The charged black-hole bomb: A lower bound on the charge-to-mass ratio of the explosive scalar field*, *Phys. Lett.* **B755** (2016) 177–182, [1606.00444].

[120] O. Fierro, N. Grandi and J. Oliva, *Superradiance of charged black holes in Einstein-Gauss-Bonnet Gravity*, 1708.06037.

[121] R. Li and J. Zhao, *Superradiant instability of charged scalar field in stringy black hole mirror system*, *Eur. Phys. J.* **C74** (2014) 3051, [1403.7279].

[122] R. Li and J. Zhao, *Numerical study of superradiant instability for charged stringy black hole mirror system*, *Phys. Lett.* **B740** (2015) 317–321, [1412.1527].

[123] R. Li, Y. Tian, H.-b. Zhang and J. Zhao, *Time domain analysis of superradiant instability for the charged stringy black hole mirror system*, *Phys. Lett.* **B750** (2015) 520–527, [1506.04267].

[124] R. Li, J. Zhao, X. Wu and Y. Zhang, *Scalar clouds in charged stringy black hole-mirror system*, *Eur. Phys. J.* **C75** (2015) 142, [1501.07358].

[125] S. Bhattacharyya, S. Minwalla and K. Papadodimas, *Small Hairy Black Holes in $AdS_5 x S^5$*, *JHEP* **11** (2011) 035, [1005.1287].

[126] O. J. C. Dias, P. Figueras, S. Minwalla, P. Mitra, R. Monteiro and J. E. Santos, *Hairy black holes and solitons in global AdS_5*, *JHEP* **08** (2012) 117, [1112.4447].

[127] S. A. Gentle, M. Rangamani and B. Withers, *A Soliton Menagerie in AdS*, *JHEP* **05** (2012) 106, [1112.3979].

[128] J. Markeviciute and J. E. Santos, *Hairy black holes in $AdS_5 \times S^5$*, *JHEP* **06** (2016) 096, [1602.03893].

[129] B. Ganchev and J. E. Santos, *Scalar hairy black holes in four dimensions are unstable*, 1711.08464.

[130] J. C. Degollado, C. A. R. Herdeiro and E. Radu, *Effective stability against superradiance of Kerr black holes with synchronised hair*, 1802.07266.

[131] R. Arias, J. Mas and A. Serantes, *Stability of charged global AdS_4 spacetimes*, *JHEP* **09** (2016) 024, [1606.00830].

[132] P. T. Chrusciel, *'No hair' theorems: Folklore, conjectures, results*, *Contemp. Math.* **170** (1994) 23–49, [gr-qc/9402032].

[133] M. Heusler, *Stationary black holes: Uniqueness and beyond*, *Living Rev. Rel.* **1** (1998) 6.

[134] C. A. R. Herdeiro and E. Radu, *Asymptotically flat black holes with scalar hair: a review*, *Int. J. Mod. Phys.* **D24** (2015) 1542014, [1504.08209].

[135] A. E. Mayo and J. D. Bekenstein, *No hair for spherical black holes: Charged and nonminimally coupled scalar field with selfinteraction*, *Phys. Rev.* **D54** (1996) 5059–5069, [gr-qc/9602057].

[136] L. Mezincescu and P. K. Townsend, *Stability at a Local Maximum in Higher Dimensional Anti-de Sitter Space and Applications to Supergravity*, *Annals Phys.* **160** (1985) 406.

[137] N. Uchikata and S. Yoshida, *Quasinormal modes of a massless charged scalar field on a small Reissner-Nordstrom-anti-de Sitter black hole*, *Phys. Rev.* **D83** (2011) 064020, [1109.6737].

[138] R. Li, H. Zhang and J. Zhao, *Time evolutions of scalar field perturbations in D-dimensional Reissner-Nordström Anti-de Sitter black holes*, *Phys. Lett.* **B758** (2016) 359–364, [1604.01267].

[139] S. Chandrasekhar, *The mathematical theory of black holes*, in *Oxford, UK: Clarendon (1992) 646 p., OXFORD, UK: CLARENDON (1985) 646 P.*, 1985.

[140] V. Cardoso, O. J. C. Dias, J. P. S. Lemos and S. Yoshida, *The Black hole bomb and superradiant instabilities*, *Phys. Rev.* **D70** (2004) 044039, [hep-th/0404096].

[141] S. Hod, *The spinning Kerr-black-hole-mirror bomb: A lower bound on the radius of the reflecting mirror*, *Phys. Lett.* **B761** (2016) 326–332, [1612.02819].

[142] W. Israel, *Singular hypersurfaces and thin shells in general relativity*, *Nuovo Cim.* **B44S10** (1966) 1.

[143] W. Israel, *Discontinuities in spherically symmetric gravitational fields and shells of radiation*, *Proceedings of the Royal Society of London A: Mathematical, Physical and Engineering Sciences* **248** (1958) 404–414, [http://rspa.royalsocietypublishing.org/content/248/1254/404.full.pdf].

[144] K. Kuchar, *Charged shells in general relativity and their gravitational collapse*, *Czech. J. Phys. B* **B18** (1968) 435.

[145] C. Barrabes and W. Israel, *Thin shells in general relativity and cosmology: The Lightlike limit*, *Phys. Rev.* **D43** (1991) 1129–1142.

[146] J. D. Brown and J. W. York, Jr., *Quasilocal energy and conserved charges derived from the gravitational action*, *Phys. Rev.* **D47** (1993) 1407–1419, [gr-qc/9209012].

[147] Ó. Dias and J. E. Santos, *AdS nonlinear instability: moving beyond spherical symmetry*, *Class. Quant. Grav.* **33** (2016) 23LT01, [1602.03890].

[148] C. Fefferman and C. R. Graham, *Conformal invariants, in The Mathematical Heritage of Élie Cartan (Lyon, 1984)*, *Astérisque* **98** (1985) 95–116.

[149] C. R. Graham, *Volume and area renormalizations for conformally compact Einstein metrics*, in *Proceedings, 19th Winter School on Geometry and Physics*, 1999. math/9909042.

[150] A. Chamblin, R. Emparan, C. V. Johnson and R. C. Myers, *Charged AdS black holes and catastrophic holography*, *Phys. Rev.* **D60** (1999) 064018,

[hep-th/9902170].

[151] A. Chamblin, R. Emparan, C. V. Johnson and R. C. Myers, *Holography, thermodynamics and fluctuations of charged AdS black holes*, *Phys. Rev.* **D60** (1999) 104026, [hep-th/9904197].

[152] G. W. Gibbons and M. J. Perry, *Black Holes and Thermal Green's Functions*, *Proc. Roy. Soc. Lond.* **A358** (1978) 467–494.

[153] S. W. Hawking and D. N. Page, *Thermodynamics of Black Holes in anti-De Sitter Space*, *Commun. Math. Phys.* **87** (1983) 577.

[154] H. W. Braden, J. D. Brown, B. F. Whiting and J. W. York, Jr., *Charged black hole in a grand canonical ensemble*, *Phys. Rev.* **D42** (1990) 3376–3385.

[155] T. Andrade, W. R. Kelly, D. Marolf and J. E. Santos, *On the stability of gravity with Dirichlet walls*, *Class. Quant. Grav.* **32** (2015) 235006, [1504.07580].

[156] C. W. Misner, K. S. Thorne and J. A. Wheeler, *Gravitation*. W.H. Freeman and Co., San Francisco, 1973.

[157] R. L. Arnowitt, S. Deser and C. W. Misner, *The Dynamics of general relativity*, *Gen. Rel. Grav.* **40** (2008) 1997–2027, [gr-qc/0405109].

[158] E. Poisson, *A Relativist's Toolkit: The Mathematics of Black-Hole Mechanics*. Cambridge University Press, 2004, 10.1017/CBO9780511606601.

[159] R. M. Wald, *General relativity*. Chicago Univ. Press, Chicago, IL, 1984.

[160] A. Buchel, L. Lehner and S. L. Liebling, *Scalar Collapse in AdS*, *Phys. Rev.* **D86** (2012) 123011, [1210.0890].

[161] S. H. Hawley and M. W. Choptuik, *Numerical evidence for 'multi - scalar stars'*, *Phys. Rev.* **D67** (2003) 024010, [gr-qc/0208078].

[162] LIGO Scientific, Virgo collaboration, B. P. Abbott et al., *Observation of Gravitational Waves from a Binary Black Hole Merger*, *Phys. Rev. Lett.* **116** (2016) 061102, [1602.03837].

[163] LIGO Scientific, Virgo collaboration, B. P. Abbott et al., *GWTC-1: A Gravitational-Wave Transient Catalog of Compact Binary Mergers Observed by LIGO and Virgo during the First and Second Observing Runs*, 1811.12907.

[164] J. Balakrishna, E. Seidel and W.-M. Suen, *Dynamical evolution of boson stars. 2. Excited states and selfinteracting fields*, *Phys. Rev.* **D58** (1998) 104004, [gr-qc/9712064].

[165] S. H. Hawley and M. W. Choptuik, *Boson stars driven to the brink of black hole formation*, *Phys. Rev.* **D62** (2000) 104024, [gr-qc/0007039].

[166] C. W. Lai and M. W. Choptuik, *Final fate of subcritical evolutions of boson stars*, 0709.0324.

[167] G. T. Horowitz and J. E. Santos, *Geons and the Instability of Anti-de Sitter Spacetime*, *Surveys Diff. Geom.* **20** (2015) 321–335, [1408.5906].

[168] T. D. Lee, *Soliton Stars and the Critical Masses of Black Holes*, *Phys. Rev.* **D35** (1987) 3637.

[169] R. Friedberg, T. D. Lee and Y. Pang, *MINI - SOLITON STARS*, *Phys. Rev.* **D35** (1987) 3640.

[170] T. D. Lee and Y. Pang, *Stability of Mini - Boson Stars*, *Nucl. Phys.* **B315** (1989) 477.

[171] M. Gleiser, *Stability of Boson Stars*, *Phys. Rev.* **D38** (1988) 2376.

[172] M. Gleiser and R. Watkins, *Gravitational Stability of Scalar Matter*, *Nucl. Phys.* **B319** (1989) 733–746.

[173] R. Ferrell and M. Gleiser, *Gravitational Atoms. 1. Gravitational Radiation From Excited Boson Stars*, *Phys. Rev.* **D40** (1989) 2524.

[174] P. Jetzer, *Boson stars*, *Phys. Rept.* **220** (1992) 163–227.

[175] T. D. Lee and Y. Pang, *Nontopological solitons*, *Phys. Rept.* **221** (1992) 251–350.

[176] E. Seidel and W.-M. Suen, *Dynamical Evolution of Boson Stars. 1. Perturbing the Ground State*, *Phys. Rev.* **D42** (1990) 384–403.

[177] Ó. J. C. Dias, J. E. Santos and B. Way, *Lattice Black Branes: Sphere Packing in General Relativity*, *JHEP* **05** (2018) 111, [1712.07663].

[178] M. Bezares, C. Palenzuela and C. Bona, *Final fate of compact boson star mergers*, *Phys. Rev.* **D95** (2017) 124005, [1705.01071].

[179] C. Palenzuela, P. Pani, M. Bezares, V. Cardoso, L. Lehner and S. Liebling, *Gravitational Wave Signatures of Highly Compact Boson Star Binaries*, *Phys. Rev.* **D96** (2017) 104058, [1710.09432].